5. SITE 660[1]

Shipboard Scientific Party[2]

HOLE 660A

Date occupied: 15 March 1986, 0030 UTC

Date departed: 16 March 1986, 1030 UTC

Time on hole: 34 hr

Position: 10°00.809′N, 19°14.738′W

Water depth (sea level; corrected m, echo-sounding): 4327.8

Water depth (rig floor; corrected m, echo-sounding): 4338.3

Bottom felt (rig floor; m, drill pipe measurement): 4342.7

Distance between rig floor and sea level (m): 10.5

Total depth (rig floor, m): 4507.6

Penetration (m): 164.9

Number of cores (including cores with no recovery): 19

Total length of cored section (m): 164.9

Total core recovered (m): 163.74

Core recovery (%): 99.3

Oldest sediment cored:
Depth (mbsf): 163.74
Nature: radiolarian ooze and chert
Age: middle Eocene
Measured velocity (km/s): 1.6

HOLE 660B

Date occupied: 16 March 1986, 1030 UTC

Date departed: 17 March 1986, 1215 UTC

Time on hole: 25.75 hr

Position: 10°00.809′N, 19°14.738′W

Water depth (sea level; corrected m, echo-sounding): 4327.8

Water depth (rig floor; corrected m, echo-sounding): 4338.3

Bottom felt (rig floor; m, drill pipe measurement): 4342.8

Distance between rig floor and sea level (m): 10.5

Total depth (rig floor, m): 4491.6

Penetration (m): 148.8

Number of cores (including cores with no recovery): 16

Total length of cored section (m): 148.8

Total core recovered (m): 141.97

Core recovery (%): 95.41

Oldest sediment cored:
Depth (mbsf): 148.8
Nature: green radiolarian ooze
Age: middle Eocene
Measured velocity (km/s): approximately 1.6

Principal results: Site 660 is located near the northern end of the Kane Gap, the major deep-water passage through the Sierra Leone Rise between the southern and northern east Atlantic. The site lies at 10°00.809′N, 19°14.738′W, at a water depth of 4332.2 m. The upper part of the seismic record for this site is a layered unit of standing-sediment waves on top of a rather transparent zone. This middle unit is underlain by another layered seismic unit, the top of which pinches out in the Kane Gap.

Site 660 was the deeper of two closely spaced ODP sites selected to investigate bottom-current action and deep-water stagnation near the upper boundary of a water mass mixed with Antarctic Bottom Water (AABW). Other important objectives were to monitor the Cenozoic history of equatorial surface-water oceanography and productivity and the advection of the dust recording African aridity. From Holes 660A and 660B, we recovered a total of 30 advance piston corer (APC) and 5 extended-core barrel (XCB) cores to depths of 164.9 and 148.8 meters below seafloor (mbsf), respectively. Both holes were cored continuously.

The Cenozoic sediment sections recovered at Site 660 comprise three major lithologic units (Fig. 1). Units I and III have good-to-excellent biostratigraphic time control; in contrast, Unit II has little. Magnetostratigraphy is good for the last 4 m.y. Continuous magnetic-susceptibility and *P*-wave-velocity curves enabled us to establish a mostly complete composite-depth (c.d.) section for both holes, which in turn allowed us to increase accumulated penetration depth downhole by 4 to 5 mbsf.

Unit I (0–75 mbsf) consists of uppermost Miocene through Holocene cycles of dark gray silty clay and olive light gray (muddy) nannofossil ooze, with up to 1.6% organic carbon in the dark layers. Below Subunit IA (0–20.8 mbsf), near 0.82 Ma, carbonate content and foraminifer preservation increased markedly in Subunit IB (20.8–58.8 mbsf) and gradually decreased below 68 mbsf (near 3.9 Ma) in Subunit IC (58.8–75.0 mbsf). *Unit II* (75.0–115.8 mbsf) is composed of cyclic yellowish brown clay, which is barren of fossils below 76.8 mbsf (5.6–6.5 Ma). *Unit III* (115.8–164.9 mbsf) consists of middle Eocene, massive, relatively coarse-grained yellowish radiolarian ooze with common pale brown to dark gray laminations and chips of chert near the base of the hole.

Deposition rates varied from 25.1 m/m.y. (27.2 m/m.y., based on composite depth) during the last 0.98 m.y. to 16.1 m/m.y. (16.75 m/m.y., based on composite depth) from 0.98 to 3.9 Ma. These

---

[1] Ruddiman, W., Sarnthein, M., Baldauf, J., et al., 1988. *Proc., Init. Repts. (Pt. A), ODP*, 108.

[2] William Ruddiman (Co-Chief Scientist), Lamont-Doherty Geological Observatory, Palisades, NY 10964; Michael Sarnthein (Co-Chief Scientist), Geologisch-Paläontologisches Institut, Universität Kiel, Olshausenstrasse 40, D-2300 Kiel, Federal Republic of Germany; Jack Baldauf, ODP Staff Scientist, Ocean Drilling Program, Texas A&M University, College Station, TX 77843; Jan Backman, Department of Geology, University of Stockholm, S-106 91 Stockholm, Sweden; Jan Bloemendal, Graduate School of Oceanography, University of Rhode Island, Narragansett, RI 02882-1197; William Curry, Woods Hole Oceanographic Institution, Woods Hole, MA 02543; Paul Farrimond, School of Chemistry, University of Bristol, Cantocks Close, Bristol BS8 1TS, United Kingdom; Jean Claude Faugeres, Laboratoire de Géologie-Océanographie, Université de Bordeaux I, Avenue des Facultés Talence 33405, France; Thomas Janacek, Lamont-Doherty Geological Observatory, Palisades, NY 10964; Yuzo Katsura, Institute of Geosciences, University of Tsukuba, Ibaraki 305, Japan; Hélène Manivit, Laboratoire de Stratigraphie des Continents et Océans, (UA 319) Université Paris VI, 4 Place Jussieu, 75230 Paris Cedex, France; James Mazzullo, Department of Geology, Texas A&M University, College Station, TX 77843; Jürgen Mienert, Geologisch-Paläontologisches Institut, Universität Kiel, Olshausenstrasse 40, D-2300 Kiel, Federal Republic of Germany, and Woods Hole Oceanographic Institution, Woods Hole, MA 02543; Edward Pokras, Lamont-Doherty Geological Observatory, Palisades, NY 10964; Maureen Raymo, Lamont-Doherty Geological Observatory, Palisades, NY 10964; Peter Schultheiss, Institute of Oceanographic Sciences, Brook Road, Wormley, Godalming, Surrey GU8 5UG, United Kingdom; Rüdiger Stein, Geologisch-Paläontologisches Institut, Universität Giessen, Senckenbergstrasse 3, 6300 Giessen, Federal Republic of Germany; Lisa Tauxe, Scripps Institution of Oceanography, La Jolla, CA 92093; Jean-Pierre Valet, Centre des Faibles Radioactivités, CNRS, Avenue de la Terrasse, 91190 Gif-sur-Yvette, France; Philip Weaver, Institute of Oceanographic Sciences, Brook Road, Wormley, Godalming, Surrey GU8 5UG, United Kingdom; Hisato Yasuda, Department of Geology, Kochi University, Kochi 780, Japan.

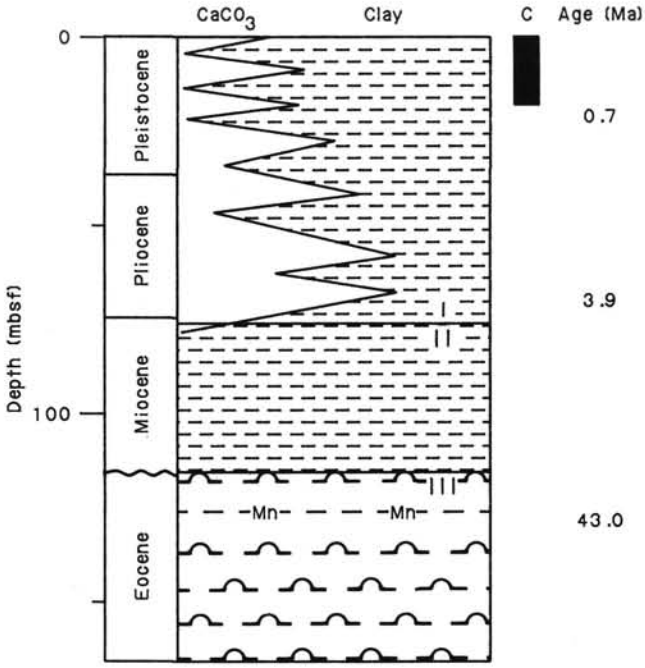

Figure 1. Lithostratigraphic and biostratigraphic summary for Site 660. Schematic $CaCO_3$ cycles show general range of $CaCO_3$ fluctuations. I, II, and III are lithologic units. C = >0.5% organic carbon.

rates decreased to 2.5 m/m.y. from 3.9 to ~6.0 Ma and are unknown before that time.

The almost pure radiolarian ooze from 129.8 to 148.8 mbsf, and probably up to the manganese-rich layer at 126 mbsf, formed during the radiolarian zones *Podocyrtis mitra* through *Podocyrtis geotheana*, i.e., during a very short time interval of less than 2 m.y. (about 41 to 42.8 Ma). This rapid deposition, the laminations free of bioturbation, the absence of organic matter, and a mound-like seismic structure all may reveal the ooze as displaced sediment reflecting cyclic bottom-current activity.

The drastic change in $CaCO_3$ between 3.9 and 4.6 Ma matches changes at Sites 657, 659, and 661 and indicates a major event of deep-water paleoceanography in the east Atlantic. Enhanced sedimentation rates and increased abundance of biogenic opal and organic carbon in the uppermost 21 mbsf imply increased upwelling and productivity at the Northern Equatorial Divergence and phases of enhanced bottom-water stagnation during the last 0.8 m.y.

BACKGROUND AND SCIENTIFIC OBJECTIVES

Introduction

Three major boundaries, the Intertropical Convergence Zone (ITCZ), the thermal equator, and the east/west-running topographic barrier of the Sierra Leone Rise (Fig. 2) make the eastern equatorial Atlantic a critical boundary zone of surface- and deep-water oceanography, the variations of which are tightly linked to global climate history. Seasonal and mean annual positions of the ITCZ and thermal equator in part reflect (1) local forcing by trade winds from both the northeast and southeast, (2) monsoonal winds from the southwest during northern summer, (3) the configuration of the African coastal outlines vs. the geographical equator resulting in differential Coriolis influence, and (4) low-latitude insolation.

This large number of climatic controls is reflected by a vast oceanographic complexity (Fig. 3) and suggests a complicated response of the equatorial Atlantic Ocean over the time scales available for paleoceanographic studies. However, first spectral analyses of time series of Quaternary sea-surface-temperature fluctuations (McIntyre et al., 1982) show that a 23,000-yr periodicity (i.e., the low-latitude signal of orbital precession) dominates the equatorial sediment record.

Monitoring variations of the ITCZ is vital for understanding the evolution of the tropical Hadley Cell during the past. In the eastern equatorial Atlantic, the ITCZ can be documented by a variety of windblown sediment components supplied late in northern winter by a combination of midtropospheric zonal and meridional surface winds (see Fig. 4, Site 657 chapter, this volume). These components record the history of both atmospheric circulation and continental aridity in Africa (Hooghiemstra and Agwu, in press; Pokras and Mix, 1985; Sarnthein et al., 1981 and 1982; Stein, 1985; Tetzlaff and Wolter, 1980). For Leg 108, Sites 660 and 661 provide the southern end members of a north-south transect across the center of an area of eolo-marine dust deposition in the northeastern Atlantic.

The deep-water oceanography of the eastern Atlantic also is marked by a major boundary zone near the equator, the barrier of the (tectonically passive) Sierra Leone Rise, which separates the Sierra Leone Basin in the south from the Cape Verde Basin in the north. The deep basins of the northeastern Atlantic are filled by a mixture of North Atlantic Deep Water (NADW) and AABW. The latter originates in the western Atlantic and enters the eastern basins both north and south of the Sierra Leone Rise through two low-latitude fracture zones, the Vema and the Romanche, respectively (Mantyla and Reid, 1983). In both places, the AABW flows eastward, driven in part by the (weak) Coriolis force in low latitudes of the Northern Hemisphere. Subsequently, it flows around the eastern end of the Sierra Leone Rise in a northerly direction through a passage with a sill depth of 4570 m—the Kane Gap (Mienert, 1985; Sarnthein et al., 1985) (Fig. 4). The upper boundary of this mixed bottom water lies near a 4350-m depth in the Kane Gap and gradually rises northward to about 3900 m south of the Canary Islands (Fig. 5) as a result of the northward-increasing Coriolis force.

Differences in the bathymetric distribution of calcium-carbonate dissolution and of $\delta^{13}C$ (Curry and Lohmann, 1983 and 1984) indicate that dramatic changes occurred during the exchange of deep water and oxygen between the western and eastern Atlantic from glacial to interglacial time. Furthermore, a number of erosional reflectors, various echo characters, and differential growth rates of manganese nodules in the Kane Gap (Mienert, 1985) suggest that the exchange of bottom water between the eastern North and South Atlantic was subject to long-term conspicuous changes superimposing with the outlined short-term fluctuations during late Neogene time. However, these events have remained mostly undated and their paleoclimatic context unexplained, despite recent efforts to model the late Neogene deep-water paleocirculation patterns (Stein et al., 1986a).

ODP Leg 108 was undertaken to investigate some of these objectives at companion Sites 660 and 661 along a depth transect directly east of the Kane Gap deep-water passage. Site 660 (target Site SLR-1) was selected as the deeper companion site near the present upper boundary of the AABW (Fig. 5) to investigate the following objectives:

1. To analyze accumulation rates of organic-carbon and various other sediment components indicative of oceanic productivity so as to record the productivity history of the Guinea Dome upwelling at the eastern end of the North Equatorial Divergence Zone.
2. To reconstruct a bathymetric profile of sediment parameters (organic-carbon accumulation, carbonate dissolution and accumulation, benthic-stable isotopes) that record the history of deep-water circulation, hydrography and chemistry, and, particularly, to monitor the Tertiary history of the exchange of deep water and oxygen among different basins of the Atlantic.

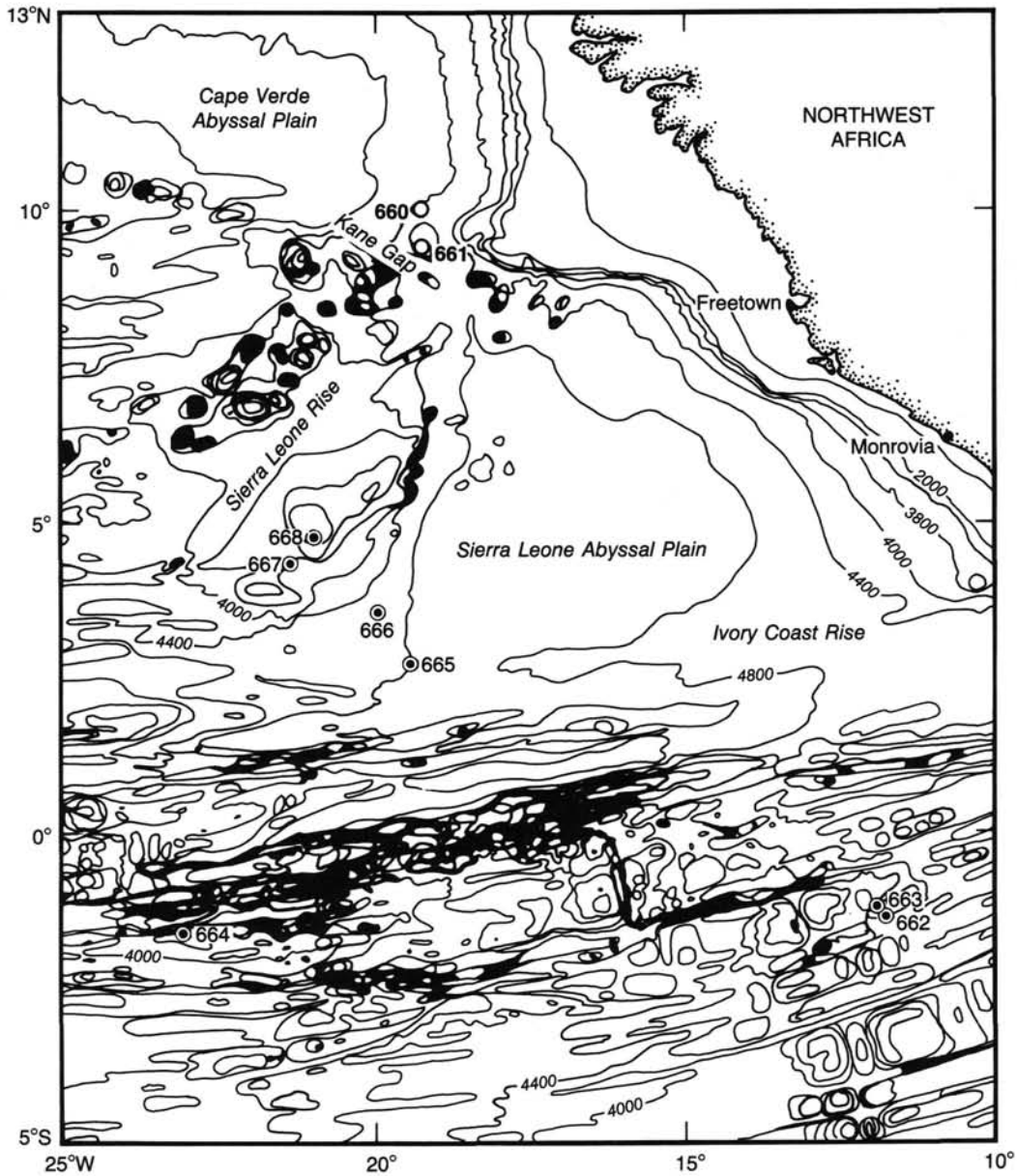

Figure 2. Bathymetry of the eastern equatorial Atlantic in the vicinity of the southern sites of ODP Leg 108.

3. To investigate at the critical "watchdog" position of Site 660 sediment structures related to bottom-current activity (e.g., contourites) and to identify and date seismic reflectors that may document major events of bottom-water circulation.

4. To study eolian-dust sediments so as to monitor the history of atmospheric paleocirculation during northern winter and the history of African aridity in the Sahel zone and to decipher the dominant mode of Milankovitch cycles controlling their long-term fluctuations.

Geologic and Topographic Setting

Site 660 (10°00.809′N, 19°14.738′W) lies 80 km northeast of the northern end of the Kane Gap, about 400 km west of Guinea-Bissau, at a water depth of 4332.2 m on the lower slope of a rise that is an extension of the Sierra Leone Rise toward the northeast (Fig. 4).

This position was selected on the basis of (1) nearby *Meteor* cruise 3.5-kHz echogram lines 65-36a and from an unpublished seismic air-gun record of Jones and Mbgatogu (1982), (2) the juncture of three GEOTROPEX'85 seismic air-gun records of 15 October 1985, and (3) the 11.5-m-long *Meteor* core 16414 (9°58.9′W, 19°15.3′W) (Sarnthein et al., 1983 and 1985). During the approach to Site 660, *JOIDES Resolution* obtained a seismic water-gun record and a 3.5-kHz echogram between Points 1 and B across the site position (Figs. 6 and 7). On the *Meteor* 3.5-kHz record, the top 0.05 s of two-way traveltime below seafloor (sbsf) is characterized by five parallel strong reflectors that form standing-sediment waves. Below this is a layered, rather transparent zone down to 0.12 sbsf, which lies on top of a marked double reflector with a base at 0.13 sbsf. The double reflector pinches out in the Kane Gap as reddish brown clay covered with manganese nodules (Sarnthein et al., 1983). The processed air-gun seismic record of Jones and Mbgatogu (1982) shows a first double reflector between 0.07 and 0.08 sbsf, with a second double reflector at 0.12/0.15 sbsf. Below this is a dark, finely laminated zone that grades into a more transparent seis-

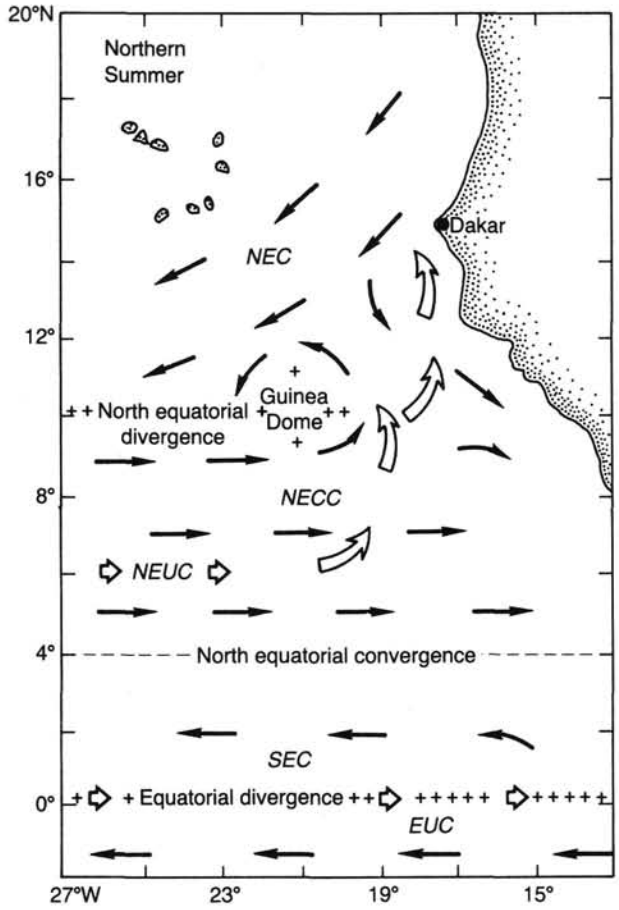

Figure 3. Surface currents in the eastern equatorial Atlantic during northern summer. Hatched area = seasonal coastal upwelling; *NEC* = North Equatorial Current; *NECC* = North Equatorial Counter Current; *NEUC* = Northern Equatorial Undercurrent; *SEC* = South Equatorial Current; *EUC* = Equatorial Undercurrent (compiled from various sources by Tiedemann, 1985).

mic character below 0.4 sbsf and that continues down to 0.6 sbsf. This zone lies on top of another well-layered seismic section 0.5 s thick (Fig. 7B).

OPERATIONS

From Site 659, we steamed southward for approximately 1.5 days, toward Site 660 (target Site SLR-1). *JOIDES Resolution* entered the region of Site 660 at approximately 2000 UTC on 14 March 1986. (All times are UTC, Universal Time Coordinated, formerly GMT, Greenwich Mean Time.) Because of a slump escarpment and some irregular sub-bottom reflectors close to the target site, revealed by the GEOTROPEX'85 pre-site survey (see "Background and Scientific Objectives" section, this chapter), we obtained an additional seismic survey line running along the slope at 5.5 kt from Point 1 to Point B across the proposed site and, after turning at Point B, back to the proposed Site 660 position (Fig. 6; Table 1). This survey deployed 80-in.^{3} water-guns, a 3.5-kHz sub-bottom profiler, and a magnetometer. A beacon was dropped at 0030 on 15 March, and the survey gear retrieved until 0045. Then, the ship stopped over the beacon, and we began tripping drill pipe into the hole. Because navigation satellites were scarce during this time, we found that the site selected from the seismic record was approximately 2 km north of our originally proposed position. The mud line for Hole 660A was established by drill pipe length at 4332.2 m.

The first APC core was brought on deck at 1005 on 15 March, and coring continued successfully (99.3% recovery with excellent preservation; Table 2) for 16 cores until 0427 on 16 March, when we changed to XCB coring. We continued coring until Core 108-660A-19X came on deck from 164.9 mbsf at 1140, when further core recovery and penetration ceased because of chips of chert below 160 mbsf. We began tripping out of Hole 660A, cleared the mud line, and finished a 15-m offset to Hole 660B at 1030.

The first of 15 APC cores from Hole 660B was brought on deck at 1238 on 16 March, and the last core came on deck at 0115 on 17 March. One final XCB core (Core 108-660B-16X; Table 2) penetrated down to 148.8 mbsf. We began tripping out of Hole 660B at 0435, brought the drill string on deck, and were under way to Site 661 at 1215 on 17 March. On our way to Site 661, we again surveyed Site 660 with a seismic water-gun line.

Continuous downcore sound-velocity and susceptibility logs provided an excellent basis for between-hole correlations to verify that a complete record was cored at this two-hole site.

LITHOSTRATIGRAPHY AND SEDIMENTOLOGY

Introduction

Three major sedimentary units are recognized at Site 660 (Fig. 8). Unit I is composed of silty clay, nannofossil ooze, muddy nannofossil ooze, and nannofossil silty clay, and ranges in age from early Pliocene through Holocene. Unit II is composed of unfossiliferous red clay, which is possibly Miocene in age. Unit III is composed of radiolarian ooze and rare amounts of chert and is middle to late Eocene in age. Each sedimentary unit is described in detail in the following sections.

Unit I

Cores 108-660A-1H through -660A-9H-6, 120 cm; depth, 0–75.0 mbsf; thickness, 75.0 m; age, early Pliocene through Holocene.
Cores 108-660B-1H through -660B-8H-5, 90 cm; depth, 0–70.2 mbsf; thickness, 70.2 m; age, early Pliocene through Holocene.

Unit I is composed primarily of interbedded silty clay and nannofossil ooze, with lesser amounts of muddy nannofossil ooze and nannofossil silty clay. Unit I can be subdivided into three distinct units, based on detailed carbonate and organic-carbon analyses of Hole 660A (Fig. 9):

Hole 660A

Subunit IA	0–20.8 mbsf
Subunit IB	20.8–58.8 mbsf
Subunit IC	58.8–75.0 mbsf

Subunit IA is composed predominantly of beds of silty clay that grade upward into thinner beds of muddy nannofossil ooze or nannofossil silty clay. This unit is characterized by a measured carbonate content that ranges from 0% to 49%, by a high organic-carbon content (0.4% to 1.6%; see "Organic Geochemistry" section, this chapter), and by a high quartz content (Fig. 10). The silty clay is generally gray to very dark gray, is moderately bioturbated (i.e., has a moderate density of preserved bioturbation traces), and contains greenish-gray laminae of silty clay. The nannofossil-rich sediment is generally olive gray to light gray and is moderately bioturbated to massive (i.e., presumably has been homogenized by extensive bioturbation, but contains no visible trace of bioturbation).

Subunit IB is composed of interbedded silty clay, muddy nannofossil ooze, and nannofossil ooze, which commonly are massive to moderately bioturbated. This subunit is characterized by a general downward increase in carbonate content that distinguishes it from the over- and underlying subunits. The top

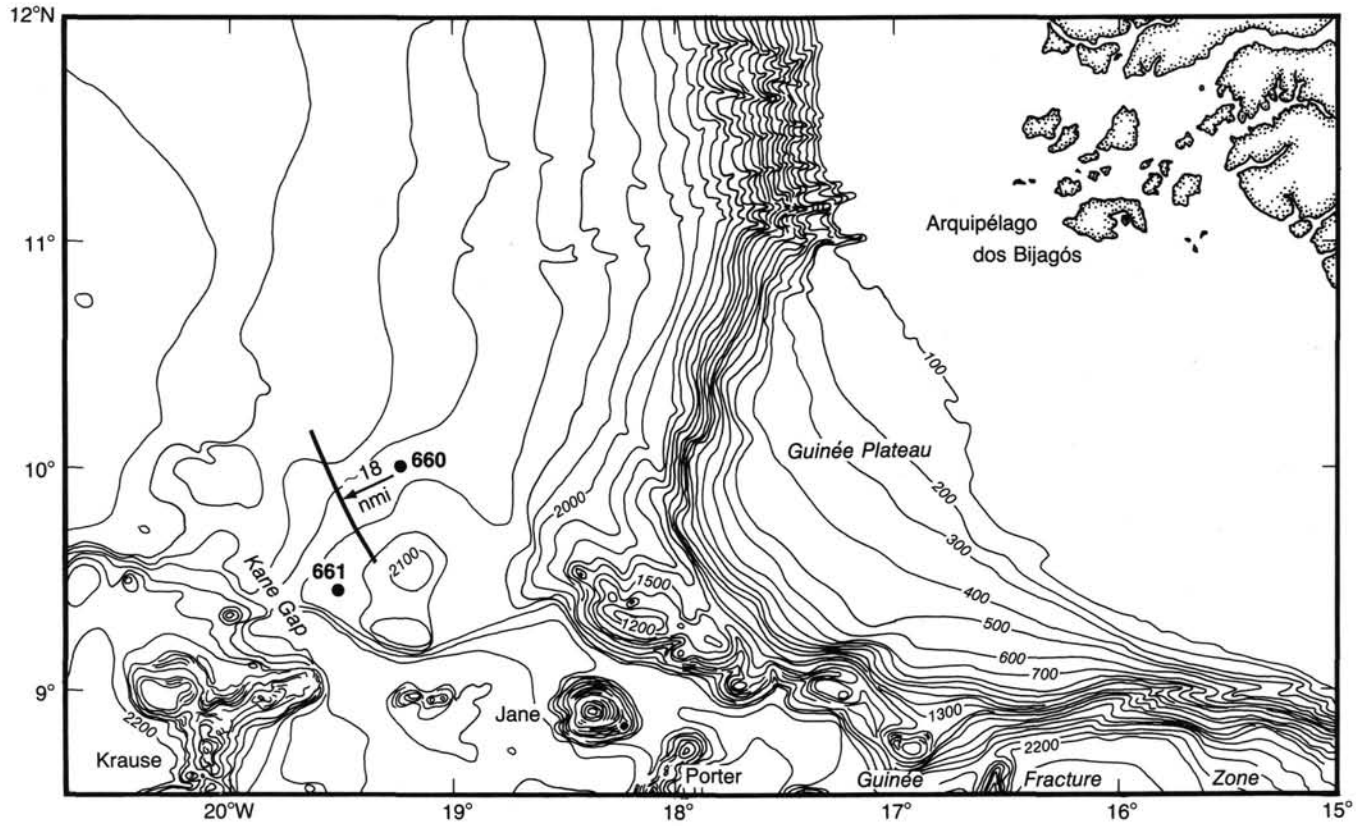

Figure 4. Bathymetry in the vicinity of Sites 660 and 661 (depths in fathoms; from Jones and Mgbatogu, 1982).

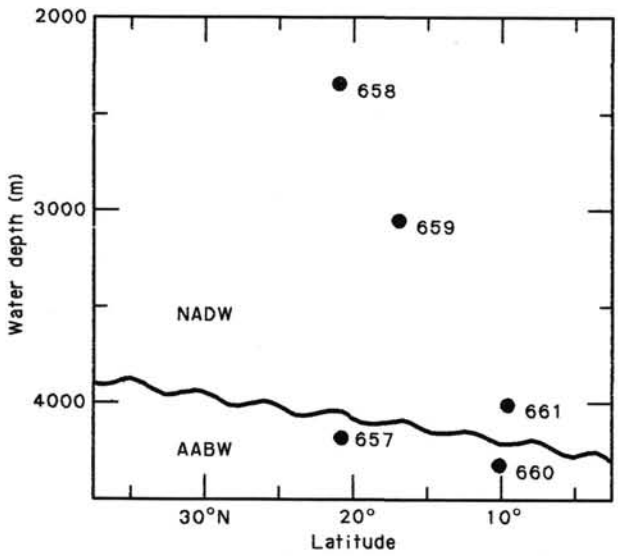

Figure 5. Site positions in a north-south transect of latitude vs. water depth along the west African continental margin. *AABW* = Antarctic Bottom Water mixed with North Atlantic Deep Water (*NADW*). Boundary line after Hobart et al. (1975) at 9°30′N and after Lonsdale (1978) at 27°N.

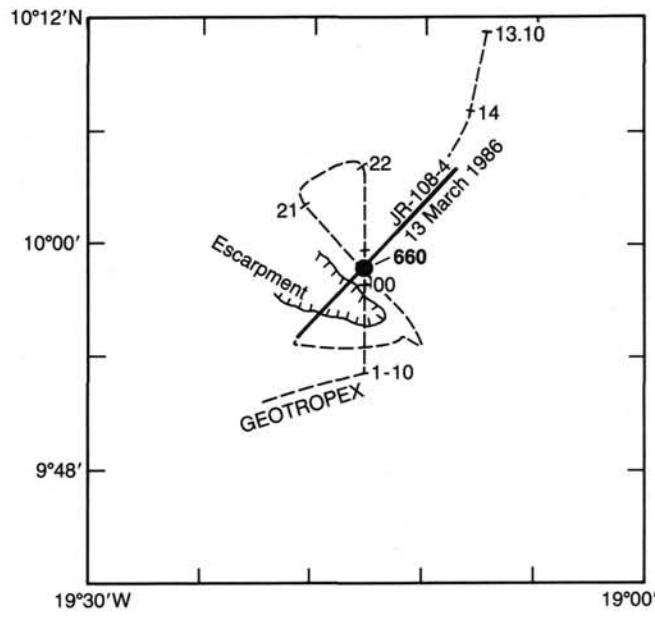

Figure 6. Map of seismic tracks available in the vicinity of Site 660.

of Subunit IB (e.g., Core 108-660A-4H) is composed of beds of gray to very dark gray silty clay that grade upward into beds of light olive gray to light gray mud- and foraminifer-bearing nannofossil ooze, with a measured carbonate content that varies from 0% to 40%. The base of the subunit (e.g., Core 108-660A-7H) is composed of beds of white to light gray muddy nannofossil ooze that grade upward into beds of foraminifer- and mud-bearing nannofossil ooze, with a measured carbonate content that varies from 40% to 70%.

Subunit IC is composed of interbedded silty clay and nannofossil ooze and is characterized by a downward decrease in carbonate content. The silty clay is olive and light olive gray, contains minor amounts of nannofossils, and is slightly to moder-

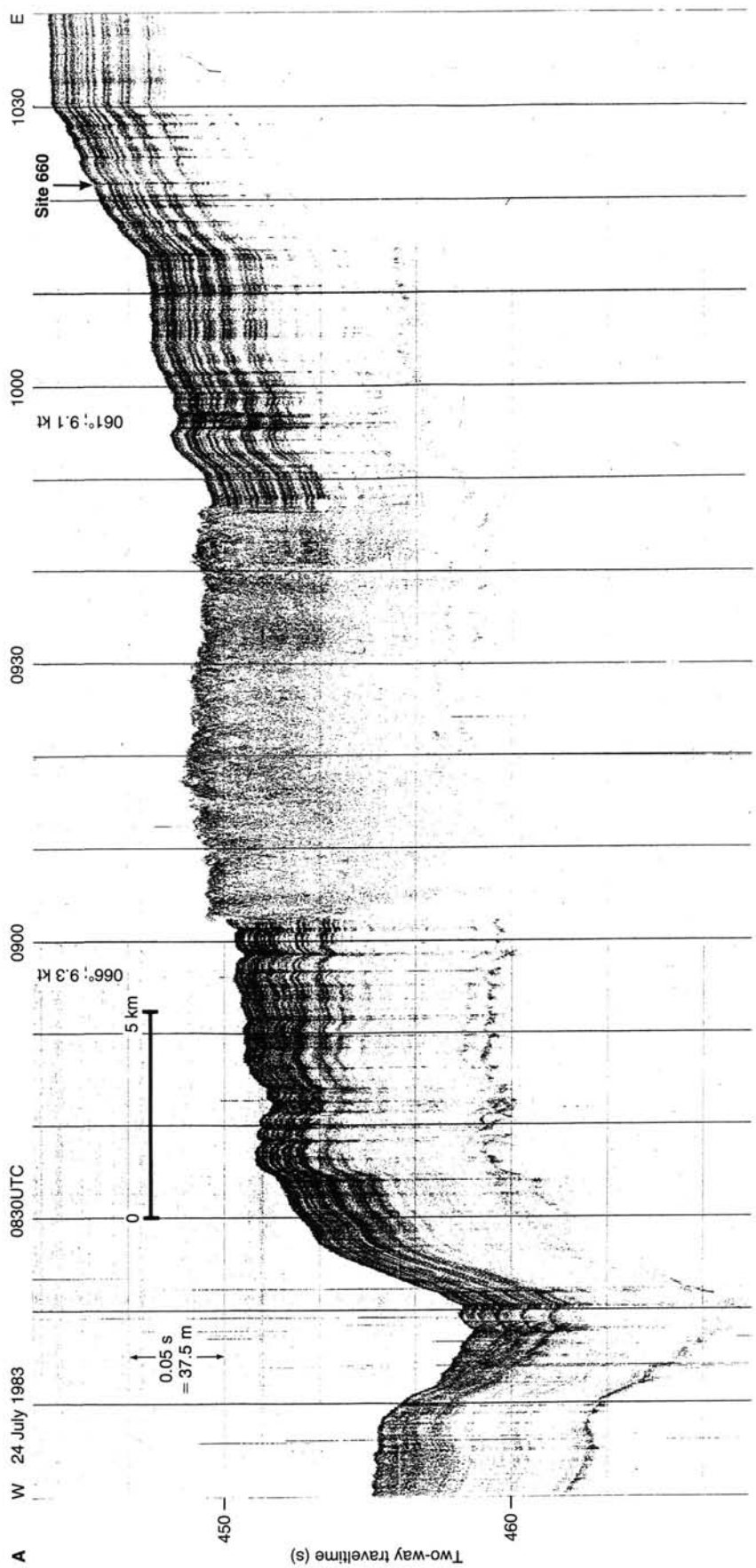
A
W
24 July 1983
0830UTC
0900
0930
1000
1030
E
Site 660
066°; 9.3 kt
061°; 9.1 kt
5 km
0
0.05 s
= 37.5 m
450
460
Two-way traveltime (s)

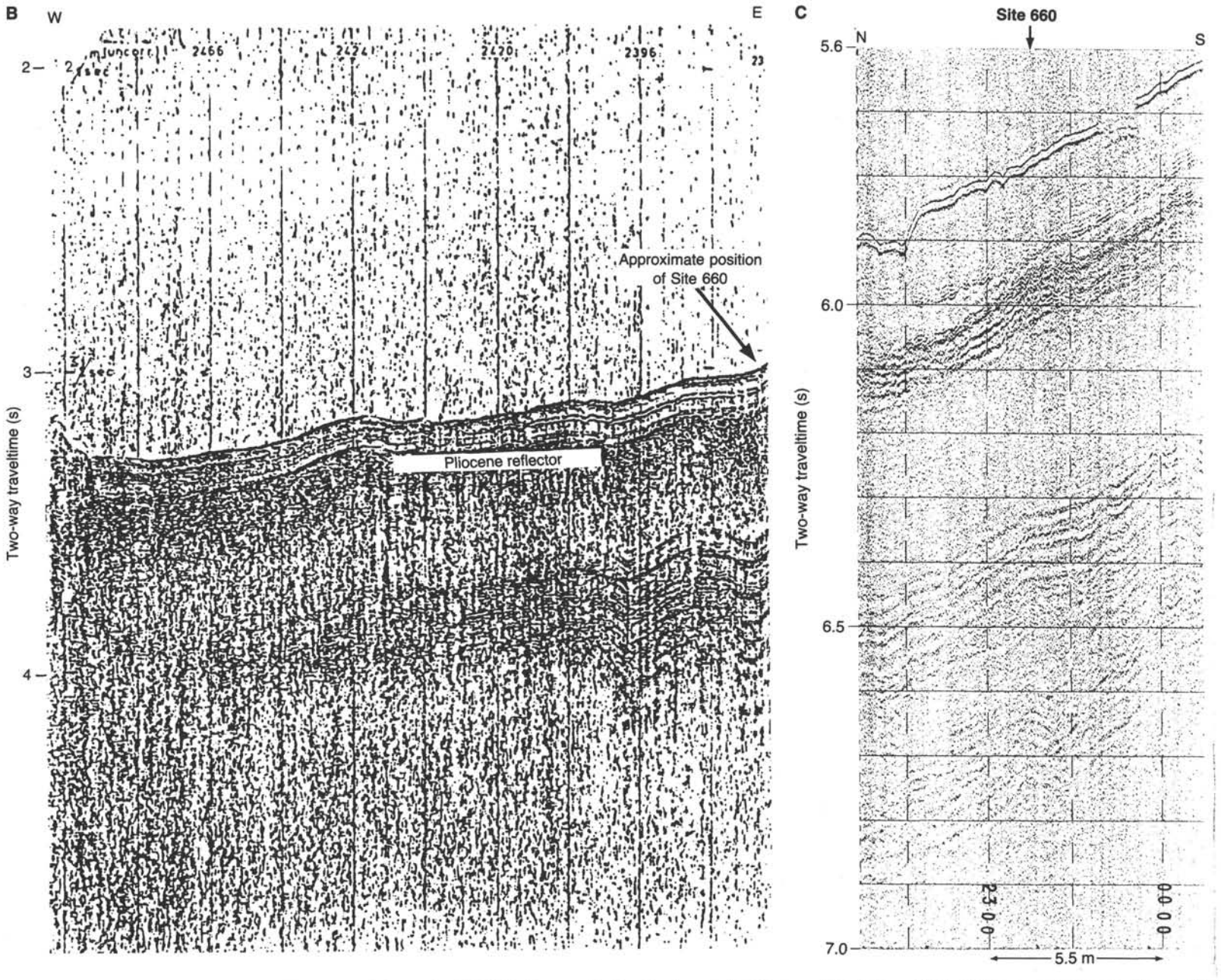

Figure 7. A) 3.5-kHz echogram *Meteor* 65-36a (Sarnthein et al., 1983). B) Air-gun seismic-reflection profile (Jones and Mgbatogu, 1982). C) Air-gun seismic-reflection profile GEOTROPEX'85, 15 October, E-F (Sarnthein et al., 1985). D) *JOIDES Resolution* water-gun seismic-reflection record near Site 660.

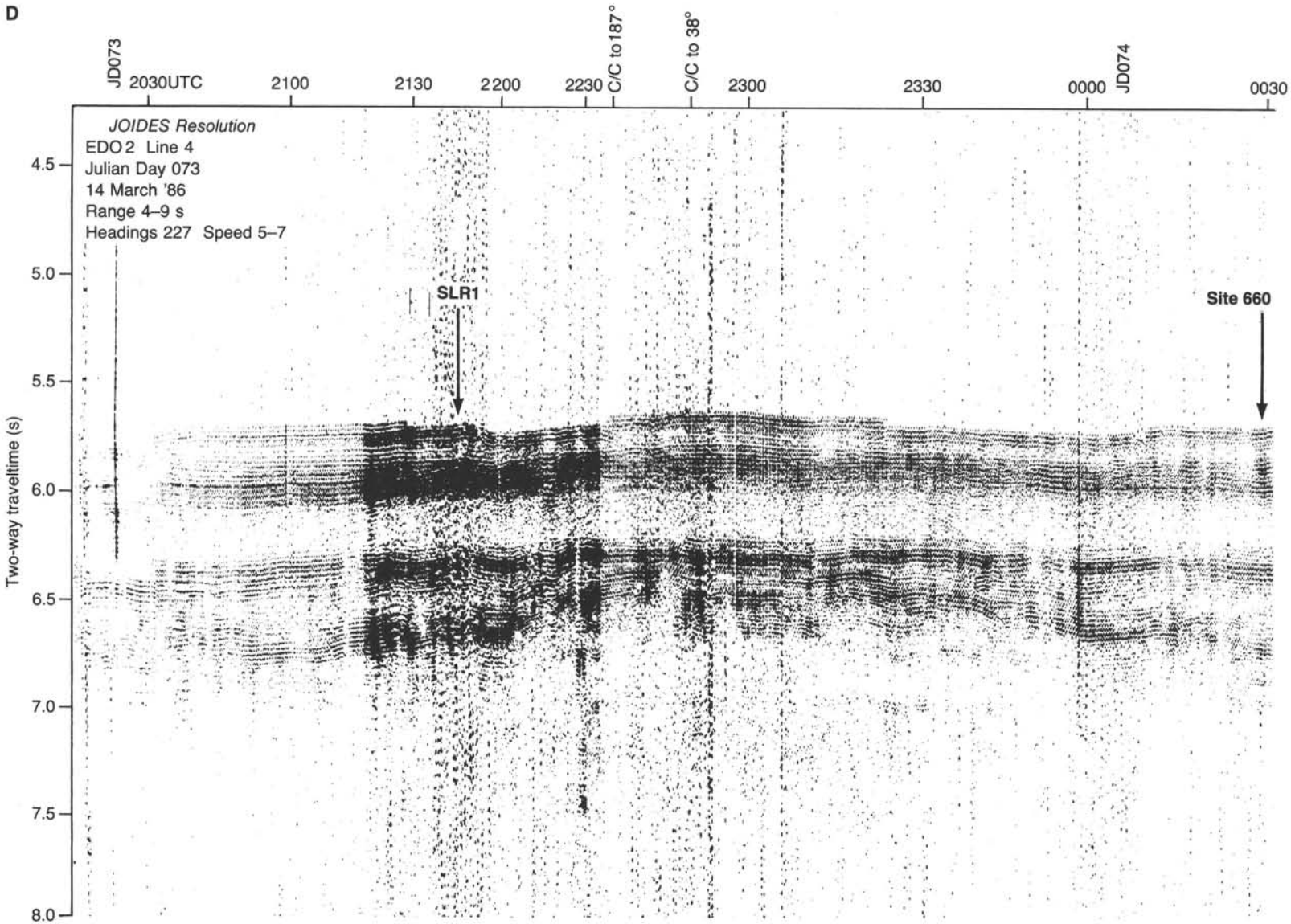

Figure 7 (continued).

Table 1. Positions of site-survey turning points.

Point no.	Location
1	10°04′N; 19°10.5′W
2	9°55.36′N; 19°18.84′W

ately bioturbated. The nannofossil ooze is white to light gray in color, contains minor amounts of mud, and is moderately bioturbated to massive.

Unit II

Cores 108-660A-9H-6, 120 cm, through -660A-13H; depth, 75.0–115.8 mbsf; thickness, 40.8 m; age, Miocene(?).
Cores 108-660B-8H-5, 90 cm, through -660B-13H-4; depth: 70.2–116.5 mbsf; thickness, 46.3 m; age, Miocene(?).

Unit II is composed of clay. This unit contains clay minerals (i.e., mainly kaolinite and montmorillonite; Fig. 10), silt-sized quartz (Fig. 10), and accessory minerals and is distinguished from the overlying Unit I by no measurable amounts of carbonate. This unit varies cyclically from brown to yellowish brown and is moderately bioturbated to massive.

Unit III

Cores 108-660A-14H through -660A-19X; depth, 115.8–164.9 mbsf; thickness, 49.1 m; age, middle Eocene.
Core 108-660B-13H-5; depth, 116.5–148.8 mbsf; thickness, 32.3 m; age, middle Eocene.

Unit III is composed of radiolarian ooze that contains trace amounts of sponge spicules and diatoms, less than 0.15% organic carbon, and variable amounts of pyrite. Sediments are relatively coarse-grained (clay-sized particles constitute less than 30% of these sediments), commonly massive or laminated, and, less commonly, slightly to moderately bioturbated. This unit varies cyclically from pale yellow to very pale brown or yellow when pyrite is absent; when pyrite is present (as it is in the upper part of the unit), sediments vary cyclically from very dark grayish brown to black.

Depositional History

The depositional history of the stratigraphic section encountered at Site 660 began during the middle Eocene, when a thick section of radiolarian ooze was deposited in an area characterized by high organic productivity (Unit III). This radiolarian ooze presumably was deposited in relatively deep waters below the carbonate compensation depth (CCD) and was reworked by strong bottom currents, for it is devoid of carbonate detritus and commonly is laminated. This phase was followed by deposition of brown clay (Unit II) at some time between the middle Eocene and latest Miocene to early Pliocene. This clay contains no siliceous or calcareous biogenic detritus, indicating that it was deposited below the CCD in an area characterized by low organic productivity. Finally, this latter phase was followed by deposition of interbedded silty clay and nannofossil ooze during the Pliocene and Pleistocene. Both sediment types are charac-

Table 2. ODP coring summary of Site 660.

Core no.	Date (March 1986)	Time (UTC)	Depths (mbsf)	Length cored (m)	Length recovered (m)	Recovery (%)
108-660A-1H	15	1005	0–1.8	1.8	1.9	103.0
108-660A-2H	15	1156	1.8–11.3	9.5	9.7	102.0
108-660A-3H	15	1258	11.3–20.8	9.5	9.6	101.0
108-660A-4H	15	1357	20.8–30.3	9.5	9.6	100.0
108-660A-5H	15	1511	30.3–39.8	9.5	9.7	102.0
108-660A-6H	15	1704	39.8–49.3	9.5	9.4	98.7
108-660A-7H	15	1858	49.3–58.8	9.5	9.7	102.0
108-660A-8H	15	2017	58.8–68.3	9.5	9.5	99.6
108-660A-9H	15	2115	68.3–77.8	9.5	9.7	102.0
108-660A-10H	15	2215	77.8–87.3	9.5	9.8	103.0
108-660A-11H	15	2310	87.3–96.8	9.5	9.5	100.0
108-660A-12H	16	0016	96.8–106.3	9.5	9.9	104.0
108-660A-13H	16	0120	106.3–115.8	9.5	9.8	103.0
108-660A-14H	16	0218	115.8–125.3	9.5	8.9	94.0
108-660A-15H	16	0328	125.3–134.8	9.5	9.4	98.5
108-660A-16H	16	0427	134.8–144.0	9.2	9.2	100.0
108-660A-17X	16	0620	144.0–153.5	9.5	8.8	92.4
108-660A-18X	16	0825	153.5–163.0	9.5	9.6	101.0
108-660A-19X	16	1140	163.0–164.9	1.9	0.2	11.0
108-660B-1H	16	1238	0–6.3	6.3	6.3	99.3
108-660B-2H	16	1335	6.3–15.8	9.5	9.1	95.9
108-660B-3H	16	1425	15.8–25.3	9.5	8.9	94.1
108-660B-4H	16	1528	25.3–34.8	9.5	9.2	96.9
108-660B-5H	16	1623	34.8–44.3	9.5	9.4	98.6
108-660B-6H	16	1720	44.3–53.8	9.5	8.9	93.3
108-660B-7H	16	1821	53.8–63.3	9.5	9.1	95.3
108-660B-8H	16	1922	63.3–72.8	9.5	8.7	91.9
108-660B-9H	16	2015	72.8–82.3	9.5	9.6	100.0
108-660B-10H	16	2114	82.3–91.8	9.5	9.3	97.8
108-660B-11H	16	2213	91.8–101.3	9.5	9.5	99.6
108-660B-12H	16	2311	101.3–110.8	9.5	7.8	82.2
108-660B-13H	17	0008	110.8–120.3	9.5	9.6	101.0
108-660B-14H	17	0112	120.3–129.8	9.5	9.6	101.0
108-660B-15X	17	0305	129.8–139.3	9.5	7.5	79.2
108-660B-16X	17	0445	139.3–148.8	9.5	9.6	101.0

Note: H = hydraulic piston. X = extended-core barrel. UTC = Universal Time Coordinated.

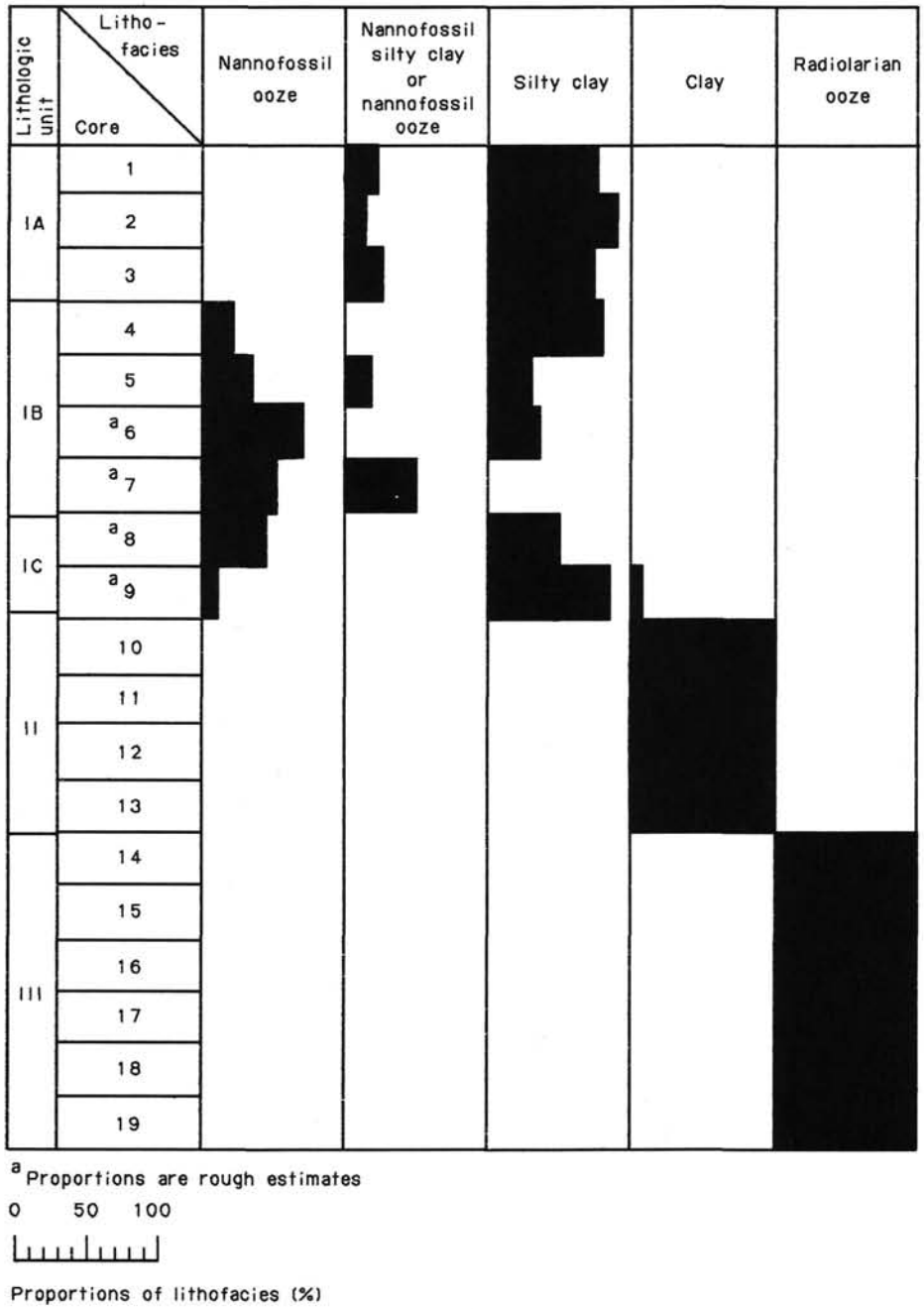

Figure 8. Summary of lithofacies for Site 660A. These same lithofacies were found at Site 660B; thus, are not shown.

terized by higher contents of organic carbon and biogenic silica in the uppermost 20.8 m (middle Pleistocene). The short-term fluctuations in carbonate, organic-carbon, biogenic-silica, and silty-clay contents may reflect glacial and interglacial controls upon paleoproductivity, carbonate dissolution, and/or the input of biogenic-silica and terrigenous sediments.

BIOSTRATIGRAPHY

Site 660, which constituted part of a depth transect on the eastern flank of the Kane Gap, was located in a water depth of 4332.2 m and consisted of two holes. Hole 660A reached a depth of 164.9 mbsf, and Hole 660B attained a depth of 148.8 mbsf. Sediments are middle Eocene and late Miocene through Holocene in age and are composed primarily of three sediment types: upper Miocene through Holocene nannofossil ooze, red clays of indeterminate age, and Eocene radiolarian ooze. Late Miocene through Holocene age and zonal assignments are shown in Figures 11 and 12.

Site 660 lies under waters of relatively high productivity with strong dissolution. Siliceous microfossils are rare in the post-Eocene section; planktonic foraminifers are present only in the Pliocene, and calcareous nannofossils are well preserved only in the upper Pleistocene. The red clays indicate deposition under bottom waters corrosive to carbonates. The change from red clay to nannofossil ooze in the uppermost Miocene suggests a change in ocean circulation. Unfortunately, the absence of biostratigraphic or magnetostratigraphic controls makes it impossible to determine the age of these red clays. The rich radiolar-

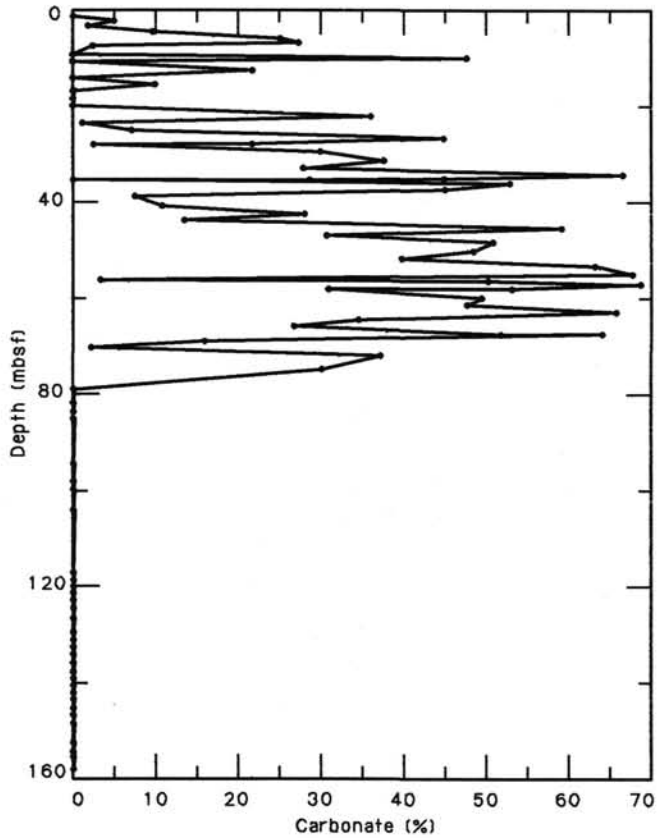

Figure 9. Carbonate content of sediments at Site 660A.

ian fauna of the Eocene section strongly suggests deposition under or near the equatorial high-productivity belt. The apparent size sorting of the radiolarian ooze probably indicates that winnowing has removed finer-grained sediments from that deposit.

Calcareous Nannofossils

Late Miocene through Holocene nannofossils occur in Cores 108-660A-1H through -660A-9H in both holes at Site 660. Nannofossil preservation is good in the upper Pleistocene, moderate in the middle Pleistocene, and poor in the Pliocene and upper Miocene. Severe etching of the coccolith assemblages is observed in the Pliocene and Miocene samples. Discoasters, especially *Discoaster brouweri* and *Discoaster pentaradiatus*, are common in the Pliocene and suggest a warm-water environment during deposition. Discoasters usually are well preserved, although scattered fragments occur. The nannofossil assemblages are similar to those observed at Site 659.

Pleistocene

Coccoliths are absent from Samples 108-660A-1H, CC and -660B-1H, CC but occur in other samples examined from Cores 108-660A-1H and -660B-1H. A scanning electron microscope was used to search for *Emiliania huxleyi* in samples from Cores 108-660A-1H and -660B-1H. The absence of this marker species allows us to assign Cores 108-660A-1H and -660B-1H to Zone NN20.

Samples examined from Cores 108-660A-2H and -660B-2H consist of abundant gephyrocapsids, few to common *Coccolithus pelagicus*, *Calcidiscus leptoporus*, *Helicosphaera carteri*, and few syracosphaerids. Without *Pseudoemiliania lacunosa*, this assemblage is characteristic of Zone NN20.

Rare specimens of *P. lacunosa* occur in samples examined from Sections 108-660A-3H-4 and -660B-3H-4, which allows us to assign these sections to Zone NN19. Core-catcher Samples 108-660A-3H, -660A-4H, -660A-5H, -660B-3H, and -660B-4H also are assigned to this zone. The last occurrence (LO) of *Calcidiscus macintyrei* occurs in Samples 108-660A-5H-2, 125 cm, and -660B-4H-6, 50 cm.

Pliocene

The coccolith assemblages are similar in composition throughout the Pliocene and are characterized by small reticulofenes-

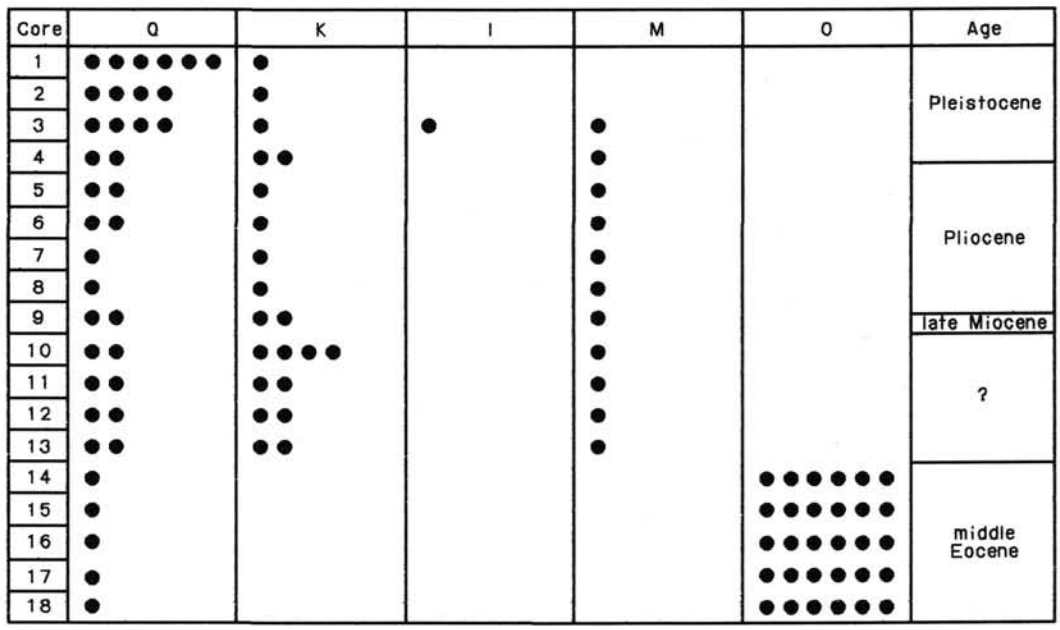

Figure 10. Summary of X-ray-diffraction data for bulk-sediment samples at Site 660A (qualitative estimates). Q = quartz, K = kaolinite, I = illite, M = montmorillonite, O = biogenic opal.

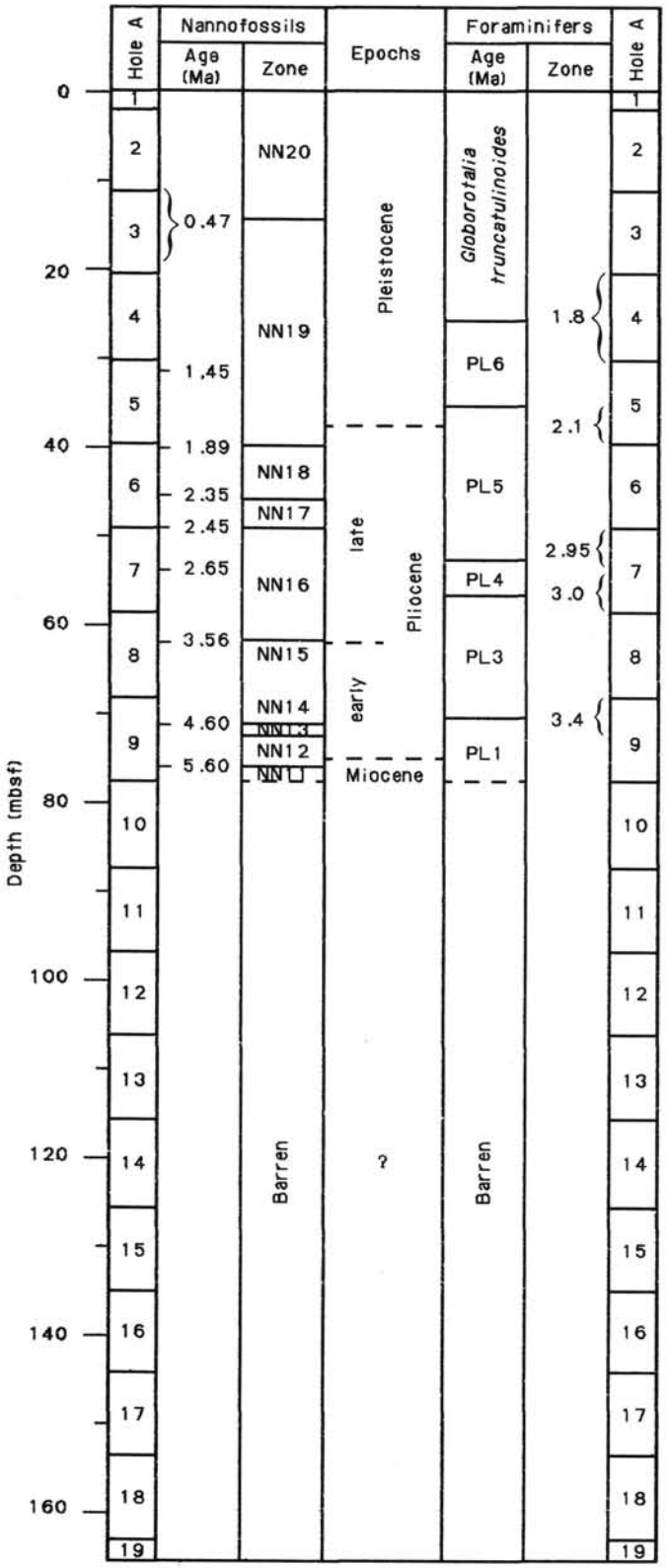

Figure 11. Zonal assignments for cores recovered from Hole 660A.

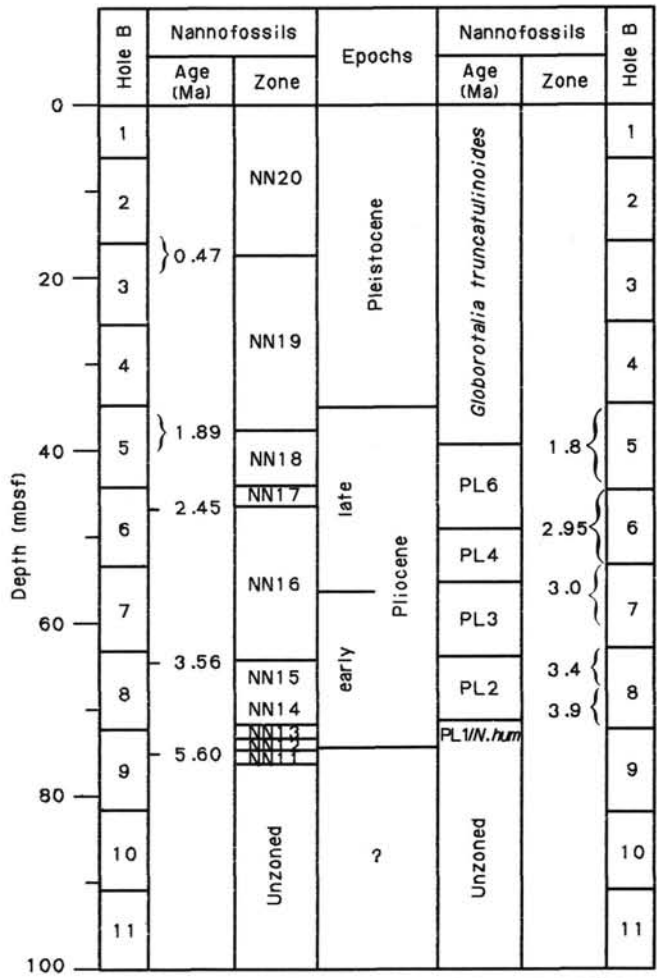

Figure 12. Zonal assignments for cores recovered from Hole 660B.

trids, *C. leptoporus*, *C. macintyrei*, *C. pelagicus*, *H. carteri*, *Helicosphaera sellii*, and numerous discoasters. The LO of *D. brouweri*, which marks the base of NN18, occurs between Samples 108-660A-6H-1, 85 cm, and -660A-5H-6, 33 cm, and between 108-660B-5H-3, 75 cm, and -660B-5H-3, 90 cm. The increased abundance of *Discoaster triradiatus* occurs between Samples 108-660A-6H-1, 134 cm, and -660A-6H-2, 140 cm.

The LO of *D. pentaradiatus*, which marks the top of NN17, occurs between Samples 108-660A-6H-5, 140 cm, and -660A-6H-4, 140 cm, and between 108-660B-6H-1, 100 cm, and -660B-6H-2, 20 cm. *Discoaster brouweri*, *D. pentaradiatus*, *Discoaster surculus*, *Discoaster variablis*, and *Discoaster intercalaris* occur in Samples 108-660A-6H-6, 140 cm, and -660B-6H-2, 120 cm. This assemblage is typical of Zone NN16 and suggests an age of about 2.41 Ma for these samples. The LO of *Discoaster tamalis* occurs between Samples 108-660A-7H-3, 70 cm, and -660A-7H-4, 70 cm, and between 108-660B-6H-4, 60 cm, and -660B-6H-5, 80 cm. The LO of *Discoaster asymmetricus* occurs in Hole 660B at a stratigraphic interval equivalent to the LO of *D. tamalis*.

Similar to their stratigraphic ranges at Site 659, *Sphenolithus abies* and *Sphenolithus neoabies* occur stratigraphically above the LO of *Reticulofenestra pseudoumbilica* at Site 660. These species occur in Sample 108-660A-8H-4, 10 cm, and in the interval between Samples 108-660B-7H-6, 120 cm, and -660B-8H-1, 30 cm.

The LO of *R. pseudoumbilica* is found in Samples 108-660A-8H-5, 10 cm, and -660B-8H-2, 30 cm, and marks the NN15/NN16 zonal boundary. Amaurolithids were observed up to Section 108-660A-9H-1, but preservational problems and low abundances made it difficult for us to say whether this level represents their extinction. The base of NN13 occurs between Samples 108-660A-9H-3, 55 cm, and -660A-9H-5, 20 cm.

Miocene

Upper Zone NN11 was recognized in Samples 108-660A-9H-6, 65 cm, and -660B-9H-2, 100 cm (at 76.8 m in Hole 660A and at 75.3 m in Hole 660B), owing to the co-occurrence of *Discoaster quinqueramus* and amaurolithids. Samples examined stratigraphically below Samples 108-660A-9H-6, 106 cm, and -660B-9H-3 have no coccoliths.

Planktonic Foraminifers

For the most part, planktonic foraminifers were absent at Site 660, occurring in abundance only in Pliocene sediments where preservation was moderate. Most of the Pleistocene sediment was black because of a relatively high organic-carbon content; these sediments contained no planktonic foraminifers. Zones PL2 through PL6 in the Pliocene contain abundant, but only moderately well-preserved, specimens (between 30% and 90% of the specimens were unbroken). In Zone PL1, preservation is poor with less than 30% of the specimens remaining intact. Below this level, the samples are barren. Thus, dissolution has biased all samples to some degree and made identification of less robust zonal markers, such as *Globorotalia margaritae*, difficult. The fauna reflects a tropical to subtropical environment removed from the influence of coastal upwelling and the Canary Current. The large numbers of *Globigerina bulloides* and *Neogloboquadrina pachyderma*, which characterized the more northerly sites (657, 658, and 659), are not seen.

The Quaternary fauna in both holes has been affected severely by dissolution. Samples 108-660A-1H, CC, -660A-2H, CC, and -660B-2H, CC were barren. Two samples with poor preservation, 108-660A-3H-7, 11 cm, and -660A-3H, CC, contained *Globorotalia truncatulinoides*, placing them in the *Globorotalia truncatulinoides* Zone. These samples also contained the tropical species *Neogloboquadrina dutertrei*, *Pulleniatina obliquiloculata*, *Sphaeroidinella dehiscens*, *Globorotalia menardii*, and *Globigerinoides trilobus*. Samples 660B-1H, CC, 660B-3H, CC, and 660A-4H, CC also contained these tropical species, as well as temperate to subpolar *N. pachyderma* (dextral) and *Globigerinita glutinata*. Although *G. truncatulinoides* is not found in Hole 660B, we assume these samples to be Pleistocene in age since they lie stratigraphically above Zone PL6.

Planktonic foraminifers increase substantially in abundance in Samples 108-660A-4H, CC and -660B-4H, CC. The top of Zone PL6, based on the LO of *Globigerinoides obliquus*, was identified in Samples 108-660A-4H, CC and -660B-5H, CC, indicating a late Pliocene age for these samples. While this LO may be an artifact of enhanced preservation, it does fall on the age-depth line generated using biostratigraphic datums farther downcore (see "Sediment-Accumulation Rates" section, this chapter). Zone PL6, also identified in Samples 108-660A-5H, CC and -660A-6H-3, 122 cm, is characterized by tropical species such as *N. dutertrei* and, to a lesser degree, by colder *N. pachyderma* (dextral).

Zone PL5, its base defined by the LO of *Dentoglobоquadrina altispira* and its top by the LO of *Globorotalia miocenica*, was identified in three samples in Hole 660A—108-660A-6H-5, 91 cm, -660A-6H, CC, and -660A-7H-4, 4 cm. Because of the low sedimentation rates (~15 m/m.y.) at this site, Zone PL5 was missed entirely in Hole 660B, falling between 108-660B-5H, CC (PL6) and -660B-6H, CC (PL4). *Globigerina bulloides* is more common within this zone, but whether this is because of cooler temperatures or enhanced preservation is difficult to determine. Other species that increase in abundance include *Globigerina decoraperta*, *Globorotalia puncticulata*, *Globorotalia crassula*, and *G. obliquus*. Isolated specimens of *Sphaeroidinellopsis seminulina* found within Zones PL5 and PL6 at Hole 660A indicate reworking.

Somewhat surprisingly, considering the low sedimentation rates, the short PL4 Zone, its base defined by the LO of *S. seminulina*, was identified at both holes. Few to rare *D. altispira* and no *S. seminulina* were found in 108-660A-7H-5, 133 cm, and -660B-6H, CC. The absence of *S. seminulina* in these samples cannot be attributed to preservation as this species seems quite resistant to dissolution. The same cannot be said for the PL2/PL3 zonal marker, *G. margaritae*. The rare and sporadic occurrence of this species makes the distinction between Zones PL3 and PL2 impossible. Samples 108-660A-7H, CC, -660A-8H, CC, and -660A-9H-1, 112 cm, from Hole 660A appear to lie within PL3, with the next sample, 108-660A-9H-3, 76 cm, belonging to Zone PL1 (with its top defined by the LO of *Globigerina nepenthes*). In Hole 660B, one sample (108-660B-8H-2, 19 cm) contained *G. margaritae*, while one sample above (108-660B-7H, CC) appeared to belong in Zone PL3, as do two samples below (108-660B-8H-3, 123 cm, and -660B-8H-5, 3 cm). Sample 108-660B-8H, CC contained *G. nepenthes*, indicating Zone PL1. Core-catcher samples from Cores 108-660A-9H and -660B-9H were barren, as were all samples examined from the red clays and radiolarian oozes. A few carbonate-rich layers within the red clay of Cores 108-660A-9H and -660B-9H contained *G. nepenthes*, but no other zonal markers, which indicates an age of 3.9 Ma or older.

Benthic Foraminifers

Benthic foraminifers occurred in core-catcher samples from 108-660A-4H through -660A-7H and 108-660B-6H through 108-660B-8H. The characteristic components of the assemblage are similar throughout the stratigraphic interval examined. Except for Sample 108-660A-7H, CC, benthic foraminifers are rare and have poor preservation. Common, well-preserved benthic foraminifers occur in Sample 108-660A-7H, CC. The assemblage is characterized by *Gyroidinoides soldanii* and *Epistominella exigua*. In addition, *Laticarinina pauperata*, *Pyrgo murrhyna*, *Oridorsalis tener*, and *Pleurostomella* spp. are scattered. This assemblage suggests middle bathyal to abyssal depths.

Diatoms

Diatoms occur in middle Eocene and Pleistocene sediments recovered at Site 660. The Pleistocene assemblage consists of a few specimens of species that have long stratigraphic ranges and that provide little chronological information. Preservation is generally poor. The assemblage contains warm to warm-temperate marine species with a minor freshwater, eolian component (*Melosira* spp.). The middle Eocene assemblage contains pelagic species somewhat similar to those described from DSDP Site 354 (Fenner, 1978) and from the Kellogg Shale (Barron et al., 1984). The Eocene assemblage has poor preservation and a low species diversity.

Sample 108-660A-1H, CC contains few specimens, and preservation is poor. The occurrence of *Pseudoeunotia doliolus* without *Nitzschia reinholdii* suggests placement of this sample in the *Pseudoeunotia doliolus* Zone of Burckle (1977). The assemblage is characterized by *Nitzschia interrupta*, *Nitzschia marina*, *Thalassionema nitzschioides* var. *parva*, *Thalassiosira eccentrica*, *Thalassiosira oestrupii*, and *Thalassiothrix longissima*. A few specimens of freshwater *Melosira* spp. also were observed.

With the exception of extremely rare specimens in Samples 108-660A-2H, CC, -660A-6H, CC, -660A-8H, CC, -660A-13H, CC, -660B-1H, CC, and -660B-2H, CC, samples examined from Cores 108-660A-3H through -660A-13H and 108-660B-3H through -660B-12H have no diatoms.

Core-catcher samples examined from Cores 108-660A-14H through -660A-17H and 108-660B-14H through -660B-16H contain rare to few, poorly to moderately well-preserved diatoms. *Triceratium barbadense* occurs in Samples 108-660A-16H, CC,

-660A-15H, CC, and Samples 108-660A-17H, CC, and -660B-14H, CC. This species is recorded from the middle Eocene of DSDP Site 354 (Fenner, 1978), the middle Eocene of the Kellogg Shale (Barron et al., 1984), and the late Eocene of the Norwegian Sea (Schrader and Fenner, 1976). The additional occurrence of *Triceratium brachiatum* in these samples suggests a middle Eocene age, similar to its occurrence at DSDP Sites 356 (Fenner, 1978) and 149 (Fenner, 1984).

Hemiaulus gondolaformis occurs in Samples 108-660A-16H, CC, -660A-17H, CC, -660B-15H, CC, and -660B-16H, and a rare fragment of *Pyxilla caput avis* occurs in Sample 108-660A-16H, CC. If the species observed at Site 660 have similar ranges to those at DSDP Site 354, the stratigraphic overlapping of these two species suggests placement of this sample into the *Hemiaulus gondolaformis* Zone of Fenner (1984). The first occurrence (FO) of this species in low latitudes marks the base of the middle Eocene *Hemiaulus gondolaformis* Zone and the LO of *P. caput avis* also occurs within this zone, according to Fenner (1984). Fenner (1984) correlated this zone with calcareous nannofossil Zones NP15 and NP16. Although such a correlation agrees with the results of the radiolarian stratigraphy at Site 660 (see following section), such a diatom-nannofossil correlation is extremely tentative until additional sections can be studied.

Radiolarians

Data in this section come from written communication with A. Palmer (1986). Three middle Eocene zones were recognized at Site 660: the closely spaced *Podocyrtis mitra*, *Podocyrtis chalara*, and *Podocyrtis goetheana* zones.

Samples 108-660B-16H-7, 9-11 cm, and 108-660B-16H-2, 42-44 cm, are assigned to the *Podocyrtis mitra* Zone. This zonal assignment is based on the occurrence of common *P. mitra* and only rare occurrences of its ancestor, *Podocyrtis sinuosa*. *Sethochytris triconiscus* appears in Sample 108-660B-16H-2, 42–44 cm, suggesting the middle-to-upper part of the zone; rare specimens of *Podocyrtis ampla* and *Podocyrtis trachodes* (which make their last appearances in the middle-to-upper part of the *Podocyrtis mitra* Zone) also were observed. Other species characteristic of, but not necessarily restricted to, this zone are *Lithocyclia ocellus*, *Thyrsocyrtis triacantha*, *Dictyoprora mongolfieri*, *Lithochytris vespertilio*, *Dictyophimus craticula*, *Eusyringium fistuligerum*, and *Calocyclas hispida*.

The *Podocyrtis chalara* Zone occurs in Sample 108-660B-15H-5, 42–44 cm, based on the predominance of this species over its ancestor, *P. mitra*. Associated species are the same as those in the underlying interval, with the addition of *Lithapium mitra* and the absence of *P. ampla* and *P. trachodes*. Samples 108-660B-15H-2, 42–44 cm, and -660B-14H-5, 42–44 cm, also are assigned to this zone. These samples appear to belong to the upper part of the zone, however, because common specimens of *P. chalara* intergraded with its descendant, *Podocyrtis goetheana*, are present. A noteworthy aspect of these samples is that they appear to have been winnowed; small radiolarians are completely absent, and large forms are concentrated.

The *Podocyrtis goetheana* Zone occurs in Sample 108-660B-14H-2, 42–44 cm, based on the predominance of this species over its ancestor, *P. chalara*, and over intergradational forms between them. A few specimens of *Lithocyclia aristotelis* are present; otherwise, associated species are similar to those in the underlying intervals. *Lithochytris vespertilio* and *S. triconiscus* also are present, suggesting that the lower part of the zone is represented in this sample (these species make their last appearances in the middle of the *Podocyrtis goetheana* Zone). Sample 108-660B-13H-2, 42–44 cm, was examined for radiolarians, but none were found.

PALEOMAGNETISM

Magnetostratigraphy

Continuous-core measurements were obtained from archive halves of core Sections 108-660A-1H through -660A-6H from Hole 660A. As usual, these cores were treated with alternating magnetic fields, peaking at 50 Oe. Despite a slight overprint not entirely removed by 50 Oe, results could be interpreted easily in terms of polarity. However, below about 50 mbsf, the natural-remanent-magnetization (NRM) data were overprinted heavily and continuous measurements provided little magnetostratigraphic information. Accordingly, subsamples borrowed from shipboard scientists helped us make the final interpretation.

At least one sample per core was subjected to increased demagnetization. About 300 samples from Cores 108-660A-1H through -660A-16H were treated several times with alternating magnetic fields. The overprint was subdued mostly by fields of 100 to 150 Oe, after which the NRM decayed monotonically to below the noise level. The high stability and general tractability of remanence from this site came as a surprise, owing to the substantial organic content of the sediments. In Figure 13, we plot declination and inclination data obtained from the upper 70 mbsf of Hole 660A. A single declination correction was applied to each core, adjusting the mean-normal data to 90° and the mean-reversed data to 270°. Both the declination and inclination data provided a record of exceptional quality that was correlated readily to the time scale.

The record below about 60 mbsf is shown in Figure 14. Specimens are strongly magnetized, but lose 90% of their remanent intensity by 150 Oe, indicating low stability. Moreover, most inclinations are positive, and we suspect total overprinting of the primary remanence. Such results commonly are observed in highly dissolved red clays. It is possible that careful thermal demagnetization of closely spaced samples may reveal more reliable magnetostratigraphy. Such analyses will be attempted during our post-cruise studies.

Magnetic Susceptibility

We again measured the whole-core-volume susceptibility of all suitable cores at 3-cm intervals. The susceptibility stratigraphy can be divided into four intervals:

1. ca. 0–25 mbsf. This corresponds approximately to lithologic Subunit IA (Pleistocene). Susceptibility values average around 200×10^{-6} SI units, and the fluctuations are of relatively low amplitude.
2. ca. 25–50 mbsf (Pliocene-Pleistocene). This corresponds approximately to lithologic Subunit IB. Susceptibility values average around 300×10^{-6} SI units, and the record exhibits a pattern of high-frequency Milankovitch-type fluctuations.
3. ca. 50–113 mbsf (latest Miocene-Pliocene). This corresponds approximately to lithologic Subunit IC and to Unit II. This interval has susceptibility values up to around 600×10^{-6} SI units. The higher values probably reflect the absence of carbonate over this interval and, consequently, the relative concentration of magnetic material.
4. ca. 113–156 mbsf (the base of Hole 660A, middle Eocene). This corresponds approximately to lithologic Unit III. Susceptibility values are relatively low (around 100×10^{-6} SI units) throughout.

It is possible to establish detailed susceptibility correlations throughout the recovered intervals in Holes 660A and 660B. Figure 15 shows a typical example. Comparison of the complete susceptibility records for both holes shows that the between-

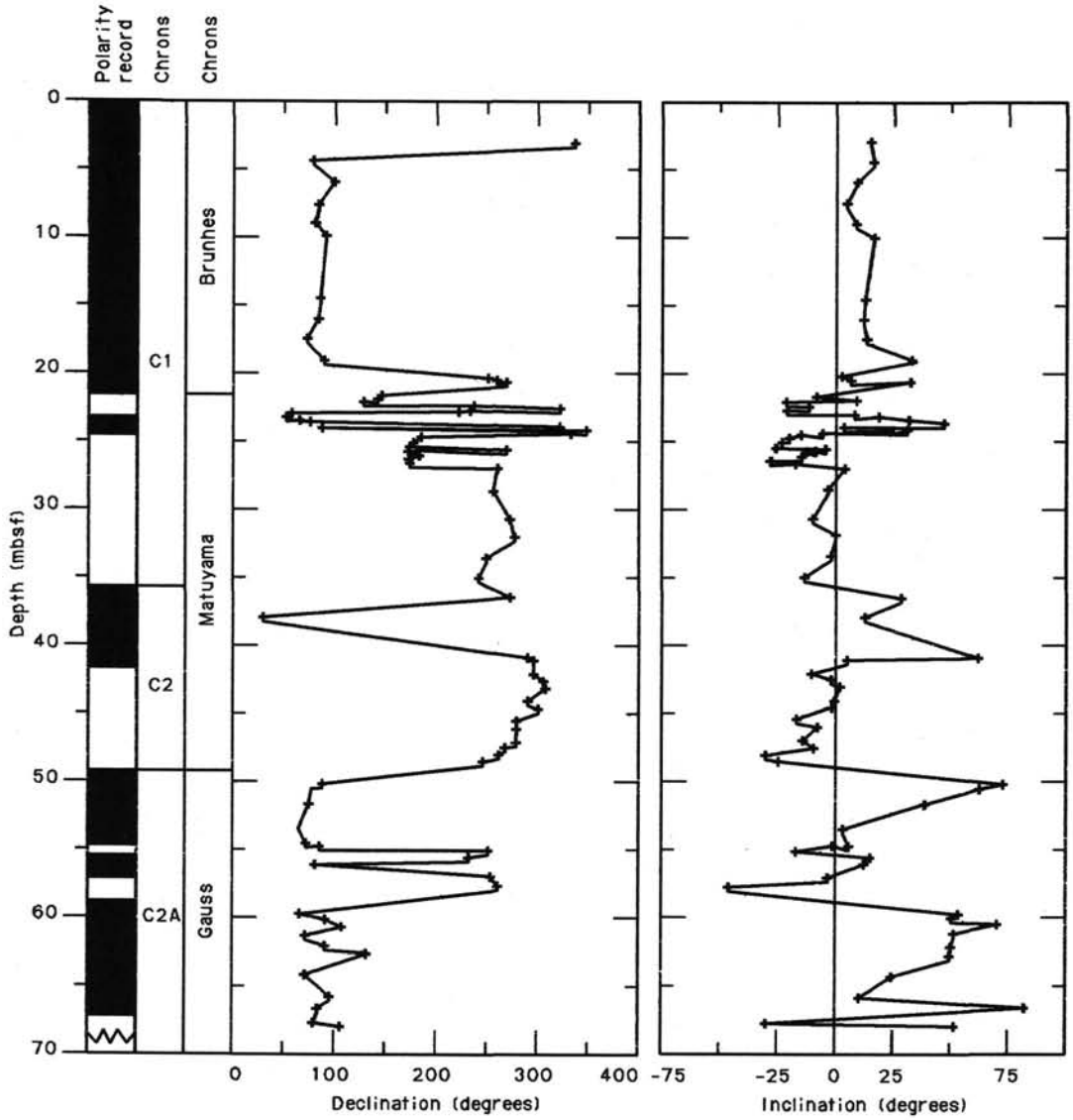

Figure 13. Declination and inclination data from Cores 108-660A-2H through -660A-8H. Declinations have been adjusted by a single declination correction applied to each core so that normal directions average 90° and reversed directions average 270°. Correlation of polarity zones to the time scale is shown at the right of the figure.

hole core breaks are offset by approximately one-half core length throughout, demonstrating that a complete, perfectly recovered sequence was obtained at this site.

SEDIMENT-ACCUMULATION RATES

Holes 660A and 660B were cored to 164.9 and 148.8 mbsf, respectively. We have good magnetostratigraphic and biostratigraphic controls in the upper 70 m of the cored sequence (approximately 0 to 3.9 Ma; Table 3; Fig. 16). The lithology gradually changes downhole from calcareous oozes to red clays, beginning at about 70 mbsf, in association with increased dissolution of calcareous microfossils. The deepest nannofossil-bearing sediment (76.8 mbsf, Hole 660A) contains a nannofossil assemblage of late Miocene age (Zone NN11). The available data between approximately 70 and 77 mbsf indicate that drastic changes in sediment-deposition rates occurred in conjunction with changes in the lithofacies.

Middle Eocene, radiolarian-rich ooze was cored from 130 mbsf to the chert layer, at which time coring was terminated. Unfortunately, no time control is available between approximately 77 and 130 mbsf (approximately 6 to 41 Ma) because the sediment contained no microfossils. During the Brunhes Chron (0.73 Ma to the present), sediments at Site 660 accumulated at a rate of 25 m/m.y., decreased to 16 m/m.y. during the interval 0.73 to 3.9 Ma (at the base of Zone PL2), and further decreased to an average accumulation rate of 3 m/m.y. between 3.9 and approximately 6.05 Ma.

Vane-shear-strength data (see "Physical Properties" section, this chapter) suggest hiatuses at 67 and 75 mbsf in Hole 660A. If these gaps exist, they would lead us to underestimate sediment-accumulation rates in the Pliocene. Presently, we cannot constrain the time intervals spanned by hiatuses; consequently, our calculated accumulation rates reflect the average rates of accumulation throughout the last 6 m.y.

The LO of *Discoaster tamalis* (at an estimated 2.65 Ma), deviates from the suggested age-depth model. The cause of this discrepancy is not clear at present, but it may indicate either a problem of calibration to the geomagnetic polarity scale or that the true LO of *D. tamalis* occurs higher in the sequence than indicated in Figure 16.

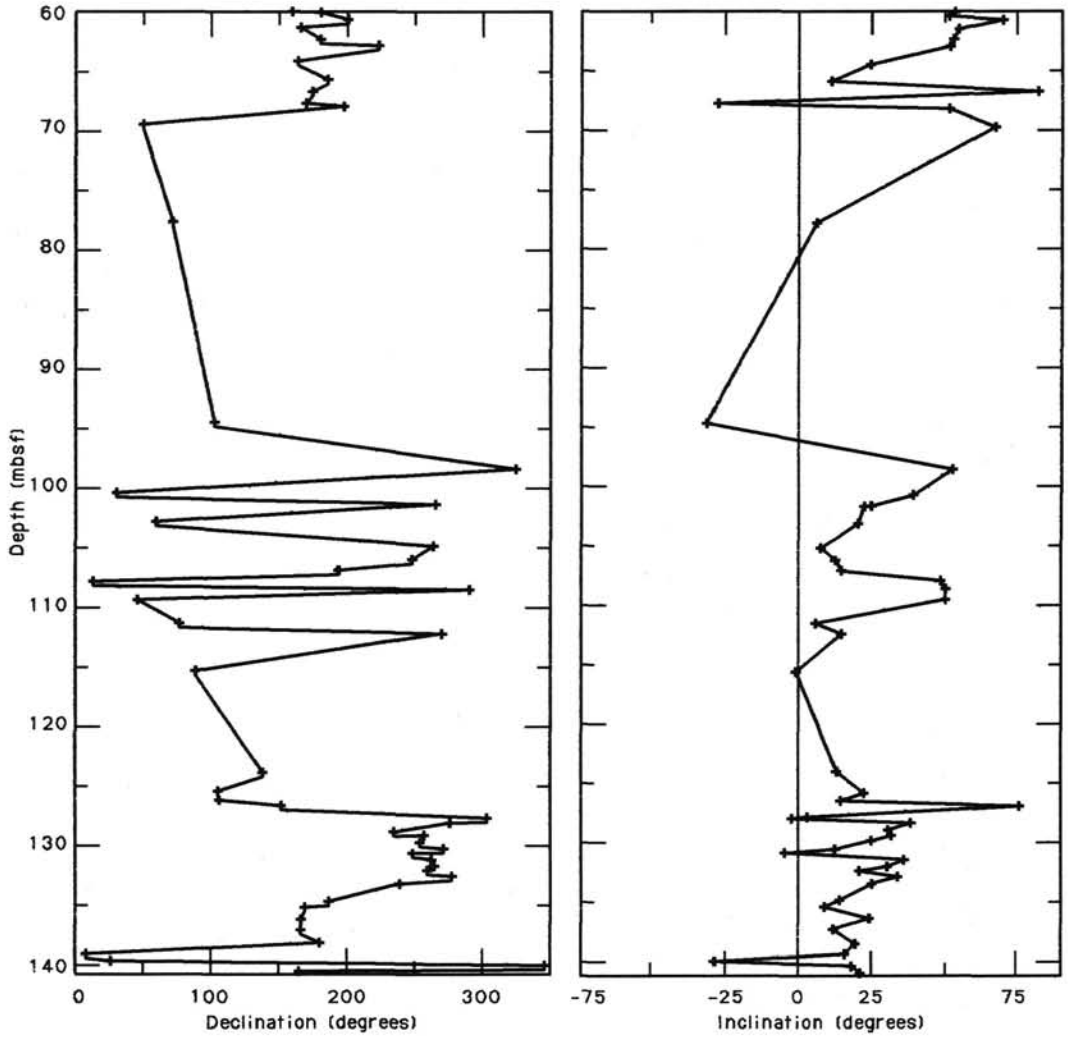

Figure 14. Paleomagnetic data from Cores 108-660A-9H through -660A-16H. Declinations are uncorrected, and data are considered to be substantially overprinted.

INORGANIC GEOCHEMISTRY

Interstitial-water samples were squeezed from four sediment samples taken routinely from approximately every 50 m in Hole 660A (Core 108-660A-17X) and Hole 660B (Cores 108-660B-2H, -660B-7H, and -660B-12H). Values of pH and alkalinity were measured in conjunction using a Metrohm 605 pH-meter, followed by titration with 0.1N HCl. Salinities were measured using an optical refractometer, and chlorinities were determined by titration with silver nitrate to a potassium chromate end point. Calcium, magnesium, and sulfate analyses were conducted by ion chromatography using a Dionex 2120i instrument.

An additional sample was obtained by syringe from a vug in Core 108-660A-3H. After filtration, only enough of the sample remained for ion chromatography dilution. Results of these analyses are presented in Table 4.

ORGANIC GEOCHEMISTRY

At Site 660, Hole 660A, 83 samples were investigated for total-organic-carbon (TOC) and carbonate contents. Some samples also were analyzed by Rock-Eval pyrolysis.

Organic and Inorganic Carbon

Inorganic carbon (IC) was determined using the Coulometrics Carbon Dioxide Coulometer. Total carbon (TC) was measured on the Perkin Elmer 240C Elemental Analyzer, and TOC values were calculated by the difference. Analytical methods are discussed and data presented in the Appendix (this volume).

The TOC values determined at Site 660A vary from 0% to 1.6% (Fig. 17). Highest values occur in the upper three cores (i.e., in the upper 20.8 mbsf) and range from about 0.33% to 1.6% (with a mean value of about 0.7%). This interval corresponds to lithologic Subunit IA (see "Lithostratigraphy and Sedimentology" section, this chapter). Lithologic Subunit IB is characterized by lower TOC values, ranging from 0% to 0.8% (with a mean value of about 0.35%; Fig. 17). Below about 56 mbsf (i.e., Core 108-660A-8H downward) and corresponding to Subunit IC, Unit II, and Unit III, TOC contents are extremely low (0% to 0.15%, Fig. 17).

According to the carbonate content, the sediment sequence at Site 660 can be divided into two parts that correspond to both lithologic Unit I and to lithologic Units II and III. Unit I is characterized by high-amplitude variations ranging from 0% to 75%. Lower carbonate values of generally less than 30% are concentrated in the upper part of this unit (corresponding to Subunit IA), whereas a general increase in carbonate content (to a maximum value of 75%) was observed in Subunit IB. In Subunit IC, the carbonate decreases (Fig. 17). Unit II (i.e., the red clay) and Unit III (i.e., the radiolarian ooze) differ from the overlying Unit I by a carbonate content of 0% (Fig. 17).

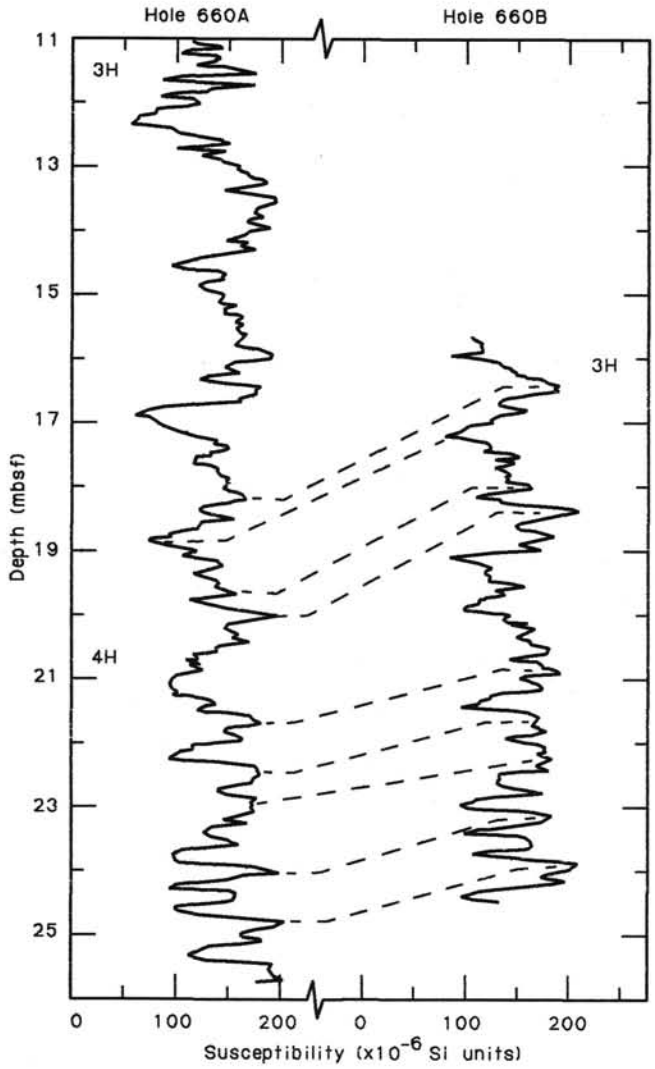

Figure 15. Between-hole susceptibility correlations.

Rock-Eval Pyrolysis

The Rock-Eval pyrolysis (Espitalié et al., 1977) was used to characterize type and maturity of the organic matter in some of the relatively organic-carbon-rich samples. Results are shown in Figure 18 in the form of a van Krevelen diagram (Tissot and Welte, 1984). Two groups of data points can be distinguished. Group A is characterized by low-hydrogen-index (HI) values of less than 150 and high-oxygen-index (OI) values of more than 2500 (Fig. 18 and Table 5). T_{max} values are less than 435°C (Table 5), which is typical for immature sediments. The organic matter probably is mostly terrigenous in origin (type III) and/or strongly oxidized. Group B is characterized by high to very high HI values (about 350 to almost 800) and OI values between 70 and 250 (Fig. 18, Table 5), suggesting the dominance of marine organic matter. However, the T_{max} values are unusually high in all of the group B samples, ranging between 450 and almost 470°C (these values were checked by double and triple measurements with similar results). These high-temperature values could imply the input of more mature recycled organic matter, although the position of the data points in the van Krevelen diagram (Fig. 18) argues for immaturity of the organic matter. Further analyses are required to explain this disagreement.

Table 3. Depths and age estimates of biostratigraphic and magnetostratigraphic indicators used to establish accumulation rates for Hole 660A.

	Datum	Depth (mbsf)	Age (Ma)
LO	*Pseudoemiliania lacunosa*	11.3–16.5	0.47
	Brunhes/Matuyama	19.1–19.1	0.73
	Matuyama/Jaramillo	22.9–22.9	0.91
	Jaramillo/Matuyama	24.6–24.6	0.98
LO	*Calcidiscus macintyrei*	32.3–33.1	1.45
	Matuyama/Olduvai	36.3–36.3	1.66
	Olduvai/Matuyama	38.4–38.4	1.88
LO	*Discoaster brouweri*	39.8–40.9	1.89
FO	*D. triradiatus* acme	41.6–42.7	2.07
LO	*Globorotalia miocenica*	44.0–45.2	2.20
LO	*Discoaster pentaradiatus*	45.7–47.2	2.35
LO	*D. surculus*	47.2–48.7	2.45
	Matuyama/Gauss	48.5–50.2	2.47
LO	*D. tamalis*	53.0–54.5	2.65
	Gauss/Kaena	54.7–55.0	2.92
LO	*Dentogloboquadrina altispira*	53.8–56.6	2.90
	Kaena/Gauss	55.0–55.5	2.99
LO	*Sphaeroidinellopsis seminulina*	56.6–58.8	3.00
	Gauss/Mammoth	56.2–57.0	3.08
	Mammoth/Gauss	57.7–59.8	3.18
LO	*Sphenolithus* spp.	61.9–63.4	3.45
LO	*Reticulofenestra pseudoumbilica*	63.4–64.9	3.56
LO	*Globigerina nepenthes*	69.4–72.1	3.90
FO	*Ceratolithus rugosus* present	72.3–74.5	4.60
	Within upper NN11	76.8–76.8	5.60
	Within upper NN11	76.8–76.8	6.50

LO = last occurrence. FO = first occurrence.

Discussion

In the upper 58 m (i.e., during the last 3 Ma), mean TOC values are between 0.3 and 0.7. These values are distinctly higher than those during the preceding time interval, where the TOC content is negligible (Fig. 17). The high values of organic matter in the uppermost 20 m (i.e., in the last 0.7 Ma) are similar to those recorded in this area in Holocene sediments (Tiedemann, 1985). Up to 90% of this organic matter is probably of marine origin (estimated using HI values; according to Stein et al., 1986b). Because sedimentation rates distinctly increased in the upper 20 m (see "Sediment-Accumulation Rates" section, this chapter), the accumulation rates of marine organic matter are also markedly higher in this time interval. This increased flux of marine organic matter during the last 0.7 Ma may be related to increased productivity caused by intensified upwelling in the North Equatorial Divergence Zone and/or to increased preservation of organic carbon from oxygen-poor bottom water below 4300 m. Short-term fluctuations in the amount and composition of organic matter and in carbonate content (Fig. 17) may reflect glacial/interglacial changes in paleoproductivity, carbonate dissolution, and/or input of both biogenic silica and terrigenous (eolian) matter.

The radiolarian ooze (Unit III) may indicate an interval of high oceanic productivity, probably caused by a paleoposition of Site 660 below the equatorial upwelling zone during Eocene time. However, this ooze is characterized by negligible TOC contents. This means that the organic-carbon content cannot be used to indicate paleoproductivity in this case. The absence of organic matter may have resulted from relatively intense circulation of oxygen-rich deep water, preventing the deposition of clay minerals and the deposition or preservation of organic carbon (i.e., winnowing of fine fraction). The position of Site 660 below the CCD during that time (indicated by 0% of $CaCO_3$) and the influence of (bottom) currents may explain the occurrence of organic-carbon-deficient, relatively coarse-grained radiolar-

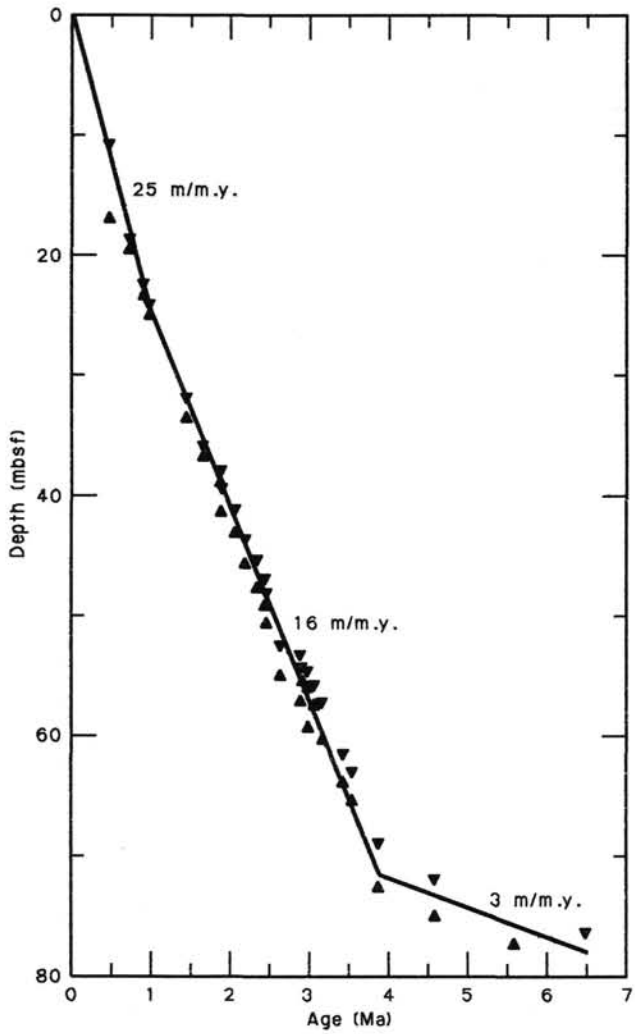

Figure 16. Graphic representation of the sediment-accumulation rates.

ian ooze ("lag sediment"). It is also possible that the radiolarian oozes are displaced sediments. Further detailed sedimentological studies and a more precise stratigraphy are required to verify these preliminary interpretations.

PHYSICAL PROPERTIES AND MAGNETIC SUSCEPTIBILITY

The techniques used for shipboard physical-properties and magnetic-susceptibility measurements at Site 660 are outlined in the "Introduction and Explanatory Notes" (this volume). Tables 6 and 7 show the index-properties and vane-shear-strength data for Holes 660A and 660B. The compressional-wave-velocity (*P*-wave-logger) data for Hole 660A are shown in Table 8. Most data for Holes 660A and 660B are presented graphically in Figures 19 through 25 (the calcium carbonate profile is shown in Figure 23 for comparison with the other properties). No data presented in this section were screened for bad data points. Sample volumes (and, hence, some of the index properties) for Hole 660B were calculated using wet and dry weights and an assumed average grain density of 2.66 g/cm^3. This assumption causes a surprisingly small error in the calculated index properties for the siliceous lithologies, where the grain density is significantly lower. For example, in a siliceous ooze with a porosity of 77% and a grain density of 1.8 g/cm^3, the porosity calculated by assuming a grain density of 2.65 g/cm^3 is 83%.

The wet-bulk density (Fig. 19) increases steadily through lithologic Unit I (see "Lithostratigraphy and Sedimentology" section, this chapter) from values of about 1.2 g/cm^3 at the mud line to about 1.6 at 75 mbsf, as the average percentage calcium carbonate increases. Wet-bulk-density values decline slightly through Unit II, then decrease rapidly to about 1.2 g/cm^3 at a depth of 115 m, and remain at this low level throughout the siliceous Unit III. This behavior also is reflected by other, closely related, index properties (Figs. 20 through 22).

The grain-density profile for Hole 660A (Fig. 23) clearly shows the change between lithologic Units II and III, with the grain densities of the siliceous Unit III being much lower than those in Units I and II. The high-grain-density peak of 3.21 g/cm^3 in Unit III may be explained by the occurrence of manganite (Fig. 24).

Figure 25 shows similar shear-strength profiles for both Holes 660A and 660B. The highest values, around 110 kPa, lie within the clay-rich lithology of Unit II. Very low values (around 30 kPa) were recorded in Unit III. An exception is a shear-strength peak of 79 kPa (at 126 mbsf), which is coincidental with a high-grain-density peak.

The *P*-wave-velocity profile for Hole 660A, shown in Figure 26, is a synthesis of all *P*-wave-logger data. Surprisingly, the large decrease in wet-bulk density occurring between Units II and III at a depth of 115 mbsf (Fig. 19) is not accompanied by an associated decrease in the average velocity. The only explanation for this apparent discrepancy is to assume that the shear modulus (and, hence, the shear-wave velocity) of the siliceous Unit III is relatively high. This high rigidity could be accounted for by the angular nature of the biogenic-siliceous grains. No suitable shear-wave transducers were on board to verify this hypothesis.

Detailed whole-core logs of magnetic susceptibility and *P*-wave velocity have proved valuable for interhole correlations without the need to understand fundamental sedimentological reasons for the signatures in these logs. In Figures 27 and 28, the signatures of two cores (108-660B-8H and -660B-11H, respectively) are used to illustrate the potential detailed sedimentological information that may be available from a comparative study of these logs. In Figure 27 (Core 108-660B-8H), generally a strong positive correlation exists between the two logs, with oscillations at wavelengths of tens of centimeters. The peaks in both logs may be caused by a relatively high input of terrigenous material, causing both a higher susceptibility and a higher velocity, through an increase in bulk density. Interestingly, in the

Table 4. Results of inorganic-geochemical analyses conducted for Site 660.

Core/ section	pH	Alkalinity (mmol/L)	Salinity (‰)	Chlorinity (mmol/L)	SO_4^{2-} (mmol/L)	Mg^{2+} (mmol/L)	Ca^{2+} (mmol/L)
108-660B-2H-5	7.73	5.07	34.2	555	23.34	43.62	[a]low
108-660B-7H-3	7.61	3.81	34.2	559	22.40	45.61	14.17
108-660B-12H-3	7.43	3.80	33.8	541	20.78	46.40	17.78
108-660A-17X-2	7.48	4.73	34.3	557	21.03	44.56	17.78
108-660A-3H-4					23.03	49.91	13.30

[a] Ca^{2+} cannot be detected in standards containing 7.24 mmol/L.

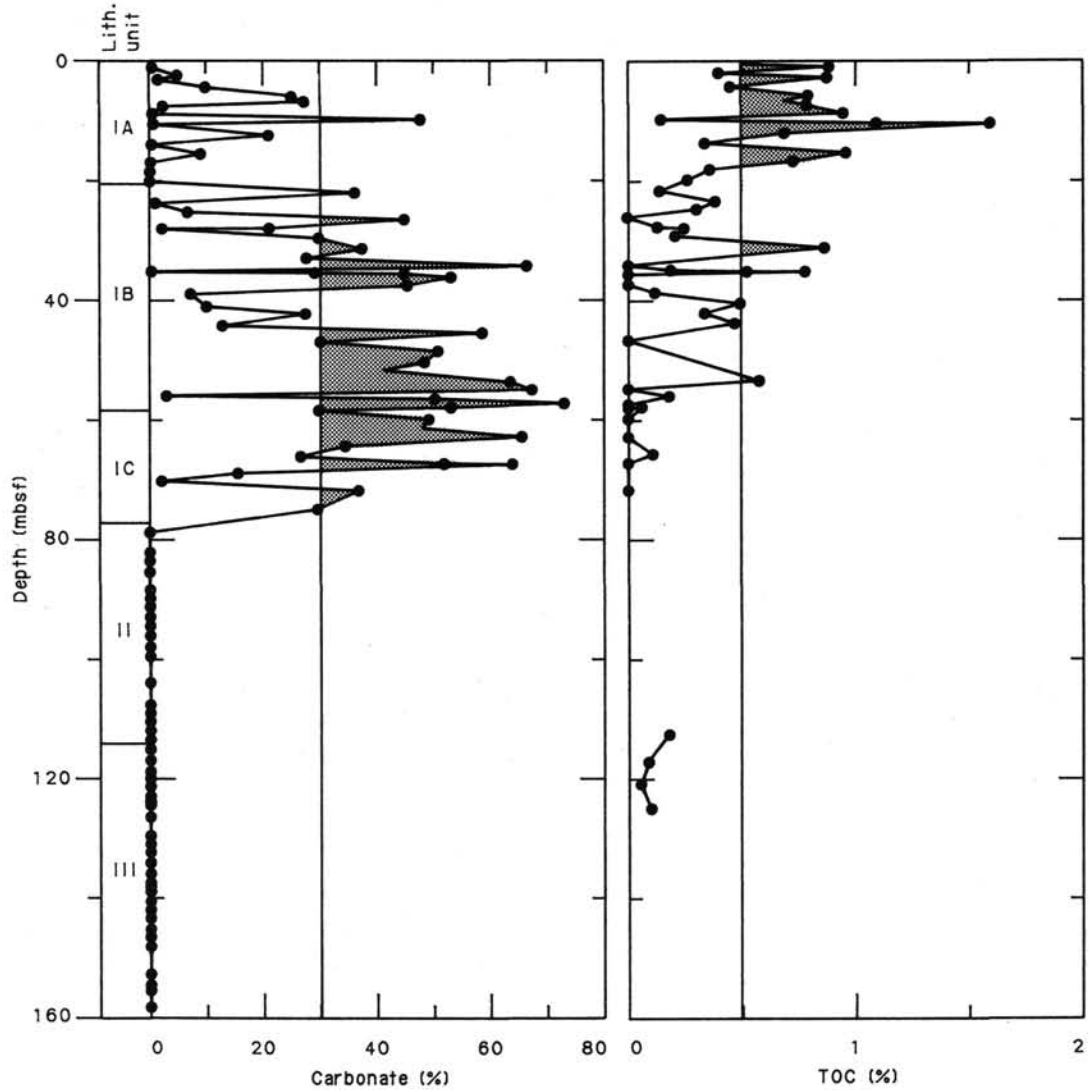

Figure 17. Organic-carbon and carbonate records for Site 660.

lower 2 m of this core, the strong susceptibility signal is not matched by the velocity signal. This could possibly indicate a different set of sedimentological conditions. In Figure 28 (Core 108-660B-11H), generally a strong negative correlation exists between the two logs. We can postulate in this case that the troughs in the susceptibility record could indicate that magnetically susceptible, fine-grained, terrigenous components were winnowed away, leaving a relatively coarse-grained lithology with a correspondingly high velocity. However, even in this record, substantial variations occur; for example, the high peak velocity at about 0.7 m is not matched by a similar susceptibility feature. This possibly indicates yet another variation of the sedimentological parameters. All whole-core sections were logged continuously using the GRAPE.

SEISMIC STRATIGRAPHY

Several high-resolution, seismic-reflection profiles (3.5-kHz) and 20- to 500-kHz-reflection profiles were recorded near and at Site 660 (see "Background and Scientific Objectives" section, this chapter). The GEOTROPEX'85 seismic profile E-F (Figs. 6, 7C, and 29) best records the local seismic structures drilled at Site 660; the nearby (processed) seismic line obtained by Jones and Mbgatogu (1982) provided a better view of the fine seismic layering characteristic of the northern Kane Gap region (Figs. 7B and 30).

The record of both profiles is characterized by a three-part upper section (Table 9). Seismic unit 1 extends 0.148 s below the seafloor (bsf) in Figure 30 and 0.153 sbsf in Figure 29. Except for an artifact reflector near the surface and a few faint laminations, this unit is almost transparent in Figure 29. In Figure 30, two sub-bottom reflectors can be seen down to 0.03 sbsf, with two distinct double reflectors farther below, between 0.616 and 0.123 sbsf (Table 9). Seismic unit 2 is uniformly and heavily reverberant in the profile of Figure 30. However, Figure 29 shows more details. From 0.153 to 0.173 sbsf, the figure reveals a faint double reflector with a transparent layer below that varies from 0.01 to 0.05 s thick over a short distance downslope. From 0.173 to 0.209 sbsf, dark, closely spaced reflectors form a mound-like structure, the nucleus of which is built in part by three to four massive, widely spaced reflectors from 0.209 to 0.255 sbsf. Farther below, the profile is transparent for almost 0.3 s (Seismic unit 3), shown in Figure 30; however, Seismic units 2 and 3 cannot be distinguished. The *JOIDES Resolution* seismic record (Fig. 7D) shows basically these same seismic units, although they appear less distinct.

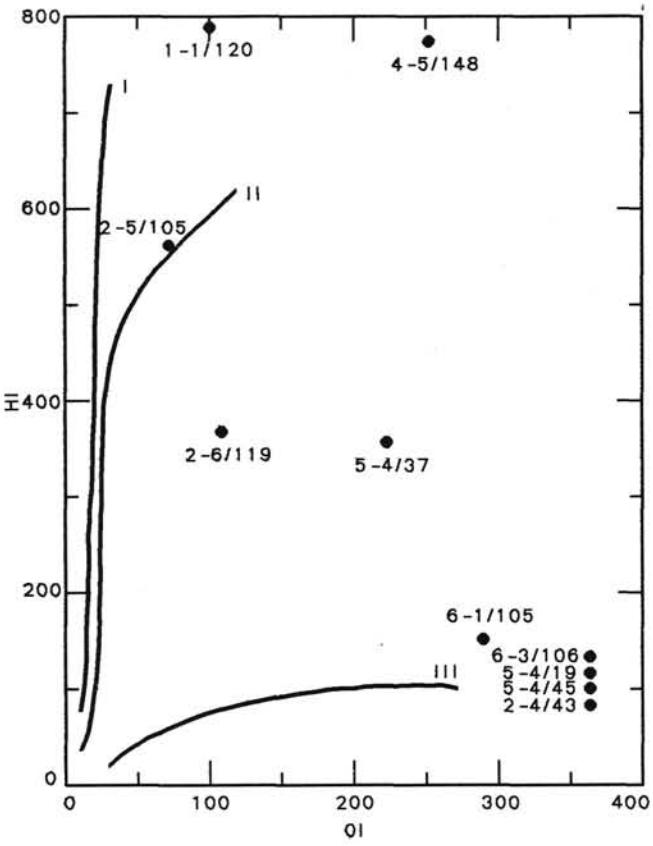

Figure 18. Hydrogen Index vs. Oxygen Index (van Krevelen diagram). Groups A and B are discussed in the text.

Table 5. Results of Rock-Eval pyrolysis.

Sample interval (cm)	TOC[a] (%)	HI[b]	OI[c]	T_{max} (°C)
1-1, 120	0.89	792	104	457
2-4, 043	0.65	82	1165	426
2-4, 043	0.65	88	1123	374
2-5, 105	0.96	556	68	468
2-6, 119	1.60	426	101	450
2-6, 119	1.60	304	120	459
4-5, 148	0.67	690	293	460
4-5, 148	0.67	776	252	447
4-5, 148	0.67	910	155	452
5-4, 019	0.21	119	2867	367
5-4, 037	0.80	230	301	467
5-4, 037	0.80	355	221	433
5-4, 045	0.54	144	439	—
5-4, 045	0.54	100	1294	435
6-1, 105	0.60	153	288	426
6-3, 105	0.49	141	367	476

[a] TOC = total organic carbon.
[b] HI = hydrogen index.
[c] OI = oxygen index.

The source of these reflectors was inferred from (1) known sound velocities of the sediment profiles (see "Physical Properties" section, this chapter) and (2) a number of sedimentological events that resulted in increased or strongly reduced shear strength and anomalously high impedance contrasts at well-defined sub-bottom depths. Details of our preliminary seismic correlations are summarized in Table 9.

Seismic unit 1 correlates with lithologic Units I and II. Reflectors 1 and 2 parallel major changes of the $CaCO_3$ content at 22 and 46 mbsf within lithologic Unit I. Reflector 3 may correspond to the onset of interbedded silty clay beds marking the top of lithologic Subunit IC at about 59 mbsf. Reflector 5 can be ascribed to a marked change observed in the shear-strength profile at about 95 mbsf (Fig. 24).

Seismic unit 2 correlates with lithologic Unit III. At its top, Reflector 6 clearly matches the top of middle Eocene radiolarian ooze at about 116 mbsf. Reflectors 5 and 6 can be traced to the west up to the Kane Gap, where Reflector 5 pinches out and the underlying sediment is covered by manganese nodules (see "Background and Scientific Objectives" section, this chapter). Reflector 7 mantles a mound of reverberations down to Reflector 8 and may match the salient peak of shear strength associated with a manganese-rich sediment bed at 126 mbsf within the radiolarian ooze facies (Fig. 24). This mound has a height of 0.13 s (10 m) in relation to its surroundings and appears to consist of radiolarian ooze. The mound may be explained as a depositional structure resembling sediment dunes. The strong, broad reflectors between Reflectors 8 and 9 may be interpreted as layers of chert, the top layer of which was recovered just in Core 108-660A-18X at about 165 mbsf. This prevented any further penetration of the drill string at Site 660 down to the level of Reflector 9, the base of this zone. Seismic unit 3 was not cored.

COMPOSITE-DEPTH SECTION

The lithologic units recovered from Holes 660A and 660B, which lie about 15 m apart, are essentially identical (see "Lithostratigraphy and Sedimentology" section, this chapter). We succeeded in correlating the interbedded clay-nannofossil ooze and brown-clay profiles of both holes in perfect detail by comparing continuous magnetic susceptibility curves, which show short-term, cyclic fluctuations down through Cores 108-660A-13H and -660B-13H. Similar results also were achieved by comparing continuous *P*-wave-logging curves for the same cores (see "Physical Properties and Magnetic Susceptibility" section, this chapter). However, neither log provided a reproducible record between the holes below a depth of about 116 mbsf in the radiolarian ooze facies. In this facies, a narrow shear-strength peak at a nominal depth of about 126 mbsf was the only marker useful for correlating the two holes.

As a result of our correlations, the nominal depth below seafloor (based on the drilling record) of several susceptibility, lithostratigraphic, and biostratigraphic features was offset by 1 m or more between Holes 660A and 660B (Fig. 31). The offset direction is not constant from core to core, but reverses several times downhole. This irregular displacement of pelagic-sediment cycles (see "Lithostratigraphy and Sedimentology" section, this chapter) is unlikely to be related to irregular small-scale seafloor topography, based on the regular sediment drape observed in the sub-bottom seismic profile (e.g., Fig. 7A). Because gains or losses of core length generally are tied to breaks between succeeding cores (Fig. 31), we regard them as artifacts of coring and of ODP conventions for recording depths.

We have, therefore, adjusted core depths in the two holes to arrive at a composite-depth section of complete and uncontorted core sections (Table 10). The following criteria and rationales explain our procedures:

1. The top of Core 108-660A-2H was moved from 1.85 to 1.95 mbsf with respect to Hole 660B, based on a more complete recovery of the uppermost Pleistocene (and Holocene) sediments in Core 108-660B-1H. Accordingly, the whole composite-depth section used sediments in Hole 660B as its major reference unit.
2. Points in the undisturbed portion of the sediment record, which approximate the upper and lower boundary of each core

Table 6. Index-properties and vane-shear-strength data for Hole 660A.

Section	Interval (cm)	Depth (m)	Grain density (g/cm^3)	Wet-water content (%)	Dry-water content (%)	Wet-bulk density (g/cm^3)	Dry-bulk density (g/cm^3)	Porosity (%)	Vane shear strength (kPa)
1-1	121	1.21	2.46	68.11	213.54	1.25	0.44	84.02	10.20
2-1	107	2.87	2.67	69.80	231.08	1.25	0.42	86.04	10.20
2-2	107	4.34	2.43	61.49	159.69	1.31	0.56	79.42	11.60
2-3	107	5.94	2.53	67.85	211.08	1.26	0.46	84.23	8.60
2-4	107	7.34	2.53	66.16	195.53	1.28	0.47	83.14	9.00
2-5	107	8.84	23.5	69.97	232.96	1.23	0.41	84.57	11.80
2-6	107	10.34	2.36	73.07	271.36	1.20	0.37	86.57	10.40
3-1	107	12.37	2.33	66.27	196.49	1.26	0.47	82.06	10.20
3-2	107	13.82	2.43	61.15	157.40	1.32	0.55	79.24	13.00
3-3	107	15.32	2.34	68.95	222.07	1.24	0.42	83.86	12.40
3-4	107	16.82	2.63	68.04	212.90	1.27	0.44	84.83	14.00
3-5	107	18.32	2.35	63.71	175.57	1.28	0.51	80.49	13.20
3-6	107	19.82	2.62	59.43	146.48	1.36	0.59	79.23	12.20
4-1	107	21.87	2.17	59.15	144.80	1.30	0.60	75.79	16.00
4-2	107	23.35	2.34	57.65	130.14	1.34	0.60	76.00	21.00
4-3	107	24.85	2.49	62.05	163.47	1.31	0.53	80.25	33.00
4-4	107	26.35	2.46	50.53	102.16	1.44	0.75	71.39	27.00
4-5	107	27.85	2.46	59.70	148.14	1.33	0.57	78.36	27.00
4-6	107	29.35	2.44	52.29	109.62	1.41	0.71	72.66	25.00
5-1	107	31.37	2.52	55.67	125.57	1.39	0.65	75.87	32.00
5-2	107	32.87	2.49	52.40	110.07	1.42	0.72	73.10	30.00
5-3	107	34.37	2.45	57.05	132.81	1.36	0.63	76.41	37.00
5-4	107	35.87	2.53	53.62	115.63	1.41	0.70	74.38	40.00
5-5	107	37.37	2.34	52.34	109.80	1.40	0.73	71.86	35.00
5-6	107	38.87	2.53	50.61	102.46	1.45	0.77	71.95	21.00
6-1	107	40.82	2.72	53.63	115.66	1.44	0.72	75.73	42.00
6-2	107	42.32	2.54	49.84	99.37	1.46	0.79	71.45	36.00
6-3	107	43.82	2.58	49.29	97.21	1.47	0.80	71.32	33.00
6-4	107	45.32	2.39	53.09	113.19	1.40	0.70	72.91	39.00
6-5	107	46.82	2.30	47.96	92.15	1.44	0.81	67.77	33.00
6-6	107	48.32	2.44	51.70	107.05	1.42	0.73	72.17	48.00
7-1	107	50.37	2.63	51.40	105.78	1.45	0.75	73.38	26.00
7-2	107	51.87	2.49	45.55	83.65	1.50	0.86	67.33	33.00
7-3	107	53.37	2.59	51.34	105.52	1.45	0.75	73.07	31.00
7-4	107	54.87	2.51	45.85	84.67	1.50	0.86	67.80	25.00
7-5	107	56.37	2.53	43.72	77.68	1.54	0.92	66.00	25.00
7-6	107	57.87	2.55	42.87	75.03	1.55	0.93	65.45	25.00
8-1	107	59.87	2.53	43.60	77.31	1.54	0.91	65.97	15.00
8-2	106	61.29	2.79	41.37	70.56	1.62	0.98	66.04	12.00
8-3	106	62.79	2.63	43.13	75.84	1.56	0.93	66.34	10.00
8-4	106	64.29	2.66	39.68	65.78	1.62	1.03	63.31	20.00
8-5	107	65.80	2.65	40.36	67.66	1.61	1.01	63.89	21.00
8-6	107	67.30	2.61	43.74	77.75	1.55	0.92	66.71	15.00
9-1	106	67.36	2.62	42.91	75.17	1.57	0.93	66.11	22.50
9-2	106	68.84	2.68	41.60	71.23	1.60	0.96	65.33	44.00
9-3	106	70.34	2.61	40.80	68.92	1.60	0.99	63.99	52.50
9-4	106	71.84	2.62	40.82	68.99	1.60	0.99	64.10	53.00
9-5	106	73.34	2.58	38.93	63.74	1.62	1.03	61.86	57.00
9-6	106	74.84	2.67	39.97	66.58	1.62	1.01	63.70	50.00
10-1	106	78.36	2.59	42.83	74.91	1.56	0.95	65.72	60.00
10-2	106	79.86	2.56	42.23	73.11	1.56	0.95	64.94	51.00
10-3	106	81.36	2.55	41.23	70.15	1.58	0.98	63.91	49.00
10-4	106	82.86	2.67	42.41	73.63	1.58	0.97	66.01	51.00
10-5	106	83.36	2.55	41.19	70.04	1.58	0.98	63.81	55.00
10-6	106	85.86	2.62	41.66	71.40	1.58	0.97	64.90	64.00
11-1	106	88.36	2.52	42.24	73.13	1.55	0.95	64.55	45.00
11-2	106	89.86	2.66	42.29	73.27	1.58	0.96	65.85	64.00
11-3	106	91.36	2.59	41.86	71.99	1.58	0.97	64.86	62.00
11-4	106	92.86	2.62	39.43	65.09	1.62	1.03	62.77	54.00
11-5	106	94.36	2.65	39.66	65.73	1.62	1.03	63.21	76.00
11-6	106	95.86	2.50	43.67	77.54	1.53	0.92	65.73	87.00
12-1	106	97.86	2.56	40.72	68.68	1.59	0.99	63.51	82.00
12-2	106	99.36	2.47	42.29	73.29	1.54	0.95	64.15	64.00
12-3	106	100.86	2.52	39.00	63.95	1.60	1.04	61.42	95.00
12-4	106	102.36	2.55	45.32	82.87	1.52	0.88	67.68	115.00
12-5	106	103.86	2.43	42.10	72.72	1.54	0.96	63.60	100.00
12-6	106	105.36	2.54	43.69	77.58	1.54	0.91	66.08	115.00
13-1	106	107.36	2.61	44.96	81.69	1.53	0.89	67.81	87.50
13-2	106	108.86	2.58	44.19	79.17	1.54	0.90	66.90	87.50
13-3	106	110.36	2.59	43.17	75.95	1.56	0.93	66.04	90.00
13-4	106	111.86	2.58	46.08	85.46	1.51	0.86	68.61	115.00
13-5	106	113.36	2.60	45.62	83.88	1.52	0.87	68.36	107.50
13-6	106	114.86	2.55	46.70	87.62	1.50	0.84	68.89	107.50
14-1	106	116.86	2.20	62.24	164.83	1.28	0.53	78.37	43.00
14-2	106	118.36	2.11	64.44	181.22	1.25	0.48	79.28	42.00

Table 6 (continued).

Section	Interval (cm)	Depth (m)	Grain density (g/cm^3)	Wet-water content (%)	Dry-water content (%)	Wet-bulk density (g/cm^3)	Dry-bulk density (g/cm^3)	Porosity (%)	Vane shear strength (kPa)
14-3	106	119.86	2.00	64.18	179.20	1.24	0.48	78.19	34.00
14-4	106	121.36	1.93	63.86	176.69	1.23	0.49	77.35	35.00
14-5	106	122.76	2.07	64.40	180.90	1.24	0.48	78.95	34.00
14-6	106	124.09	2.18	61.28	158.27	1.28	0.54	77.48	55.00
15-1	106	126.36	3.21	63.80	176.25	1.35	0.51	84.89	79.00
15-2	106	127.83	2.23	62.76	168.53	1.28	0.52	78.96	31.00
15-3	106	129.33	2.03	63.76	175.97	1.24	0.49	78.14	28.00
15-4	106	131.83	1.42	75.75	312.40	1.10	0.30	82.29	13.00
15-5	106	132.29	1.98	65.41	189.08	1.23	0.47	79.00	29.00
15-6	106	133.79	1.99	63.74	175.78	1.24	0.49	77.83	38.00
16-1	106	135.86	1.94	69.17	224.36	1.19	0.41	81.40	38.00
16-2	106	137.33	1.85	75.75	312.39	1.14	0.34	85.47	31.00
16-3	106	138.81	2.22	67.23	205.17	1.24	0.45	82.02	34.00
16-4	106	140.31	2.09	66.10	194.96	1.23	0.45	80.32	33.00
16-5	106	141.81	2.06	67.60	208.63	1.22	0.43	81.22	43.00
16-6	106	143.31	2.08	67.92	211.68	1.22	0.44	81.56	28.00
17-1	106	145.06	1.95	66.37	197.34	1.21	0.45	79.45	41.00
17-2	106	146.56	2.00	66.80	201.21	1.22	0.44	80.18	31.00
17-3	106	147.94	1.60	65.98	193.94	1.16	0.46	75.91	28.00
17-6	106	150.64	2.06	65.98	193.97	1.23	0.45	80.01	26.00
18-1	106	154.56	2.19	69.19	224.60	1.22	0.41	83.14	27.00
18-2	61	155.61	2.08	65.19	187.29	1.24	0.47	79.63	27.00
18-4	4	156.46	2.18	65.11	186.59	1.25	0.47	80.26	25.00

Table 7. Index-properties and vane-shear-strength data for Hole 660B.

Section	Interval (cm)	Depth (m)	Wet-water content (%)	Dry-water content (%)	Porosity (%)	Wet-bulk density (g/cm^3)	Dry-bulk density (g/cm^3)	Vane shear strength (kPa)
1-1	106	1.06	68.63	218.80	84.02	1.28	0.42	6.20
1-2	106	2.53	60.74	154.73	79.15	1.36	0.55	6.20
1-3	106	4.03	69.77	230.75	84.67	1.27	0.41	11.00
1-4	106	5.23	61.45	159.42	79.62	1.36	0.54	9.00
2-1	106	7.36	71.87	255.52	85.85	1.25	0.37	5.60
2-2	106	8.83	71.40	249.61	85.59	1.26	0.38	5.60
2-3	106	10.33	64.80	184.07	81.73	1.32	0.48	14.00
2-4	106	11.83	60.09	150.59	78.72	1.37	0.56	15.00
2-5	106	13.33	65.01	185.78	81.86	1.32	0.48	15.00
2-6	106	14.83	67.39	206.63	83.29	1.30	0.44	27.00
3-1	106	16.86	64.61	182.53	81.61	1.32	0.49	14.00
3-2	106	18.36	61.03	156.63	79.34	1.36	0.55	24.00
3-3	106	19.86	65.99	194.07	82.46	1.31	0.46	27.00
3-4	106	21.36	62.31	165.35	80.17	1.35	0.53	20.00
3-5	106	22.86	62.31	165.35	80.17	1.35	0.53	20.00
3-6	106	24.36	56.38	129.23	76.18	1.41	0.63	31.00
4-1	106	26.36	58.32	139.94	77.53	1.39	0.60	35.00
4-2	106	27.86	53.59	115.46	74.16	1.44	0.68	19.00
4-3	106	29.36	49.24	97.00	70.82	1.50	0.77	20.00
4-4	106	30.86	52.44	110.28	73.31	1.46	0.71	20.00
4-5	106	32.36	52.26	109.46	73.17	1.46	0.71	26.00
5-1	106	36.86	55.58	125.11	75.61	1.42	0.65	35.00
5-2	106	38.36	55.02	122.32	75.21	1.43	0.66	32.00
5-3	106	39.86	54.62	120.37	74.92	1.43	0.66	31.00
5-4	106	41.36	58.57	141.36	77.70	1.39	0.59	34.00
5-5	106	42.86	56.40	129.38	76.20	1.41	0.63	38.00
5-6	106	44.36	51.51	106.23	72.60	1.47	0.73	37.00
6-1	106	45.36	51.55	106.40	72.63	1.47	0.73	36.00
6-2	106	46.82	56.45	129.65	76.24	1.41	0.63	44.00
6-3	106	48.32	51.64	106.79	72.70	1.47	0.72	43.00
6-4	106	49.82	50.94	103.85	72.16	1.48	0.74	37.00
6-5	106	51.32	50.33	101.33	71.68	1.49	0.75	57.00
6-6	106	52.82	47.93	92.04	69.76	1.52	0.80	25.00
7-1	106	54.86	46.40	86.57	68.49	1.54	0.84	20.00
7-2	106	56.36	46.78	87.90	68.81	1.53	0.83	22.00
7-3	106	57.86	49.54	98.19	71.06	1.50	0.77	21.00
7-4	106	59.36	42.22	73.08	64.83	1.60	0.93	27.00
7-5	106	60.86	40.50	68.07	63.23	1.62	0.97	26.00
7-6	106	62.36	42.33	73.41	64.93	1.59	0.93	20.00
8-1	106	64.36	43.31	76.40	65.81	1.58	0.91	28.00
8-2	106	65.86	44.37	79.75	66.74	1.57	0.88	20.00
8-3	106	67.36	42.88	75.08	65.43	1.59	0.92	21.00
8-4	106	68.86	44.85	81.31	67.16	1.56	0.87	18.00

Table 7 (continued).

Section	Interval (cm)	Depth (m)	Wet-water content (%)	Dry-water content (%)	Porosity (%)	Wet-bulk density (g/cm^3)	Dry-bulk density (g/cm^3)	Vane shear strength (kPa)
8-5	106	70.36	40.77	68.82	63.48	1.62	0.97	34.00
8-6	100	71.80	41.29	70.32	63.97	1.61	0.95	35.00
9-1	106	73.86	39.31	64.77	62.10	1.64	1.00	65.00
9-2	106	75.36	39.46	65.19	62.24	1.64	1.00	47.00
9-3	106	76.86	41.13	69.87	63.82	1.61	0.96	48.00
9-4	106	78.36	41.87	72.02	64.50	1.60	0.94	53.00
9-5	106	79.86	39.97	66.58	62.73	1.63	0.99	56.00
9-6	100	80.36	34.20	51.99	56.91	1.73	1.14	52.00
10-1	106	83.36	42.65	74.38	65.22	1.59	0.92	51.00
10-2	106	84.86	41.71	71.54	64.35	1.60	0.94	49.00
10-3	106	85.36	40.77	68.84	63.49	1.62	0.97	57.00
10-4	106	87.86	39.04	64.03	61.83	1.65	1.01	59.00
10-5	106	89.36	42.79	74.78	65.34	1.59	0.92	59.00
10-6	106	90.86	37.94	61.14	60.76	1.66	1.04	61.00
11-1	106	92.86	36.36	57.12	59.16	1.69	1.08	76.00
11-2	106	94.36	40.86	69.09	63.57	1.62	0.97	84.00
11-3	106	95.86	39.17	64.40	61.96	1.64	1.01	83.00
11-4	106	97.36	35.37	54.72	58.14	1.71	1.11	95.00
11-5	106	98.86	40.47	67.98	63.20	1.62	0.98	115.00
11-6	106	100.36	37.79	60.73	60.60	1.67	1.04	112.50
12-1	106	102.36	39.64	65.68	62.42	1.64	1.00	100.00
12-2	106	103.86	41.13	69.86	63.82	1.61	0.96	97.50
12-3	106	105.36	39.95	66.52	62.71	1.63	0.99	100.00
12-4	106	106.86	42.06	72.60	64.68	1.60	0.94	115.00
12-5	106	108.36	40.53	68.17	63.26	1.62	0.97	112.50
13-1	106	111.80	49.47	97.89	71.00	1.50	0.77	45.00
13-2	106	113.30	47.16	89.24	69.12	1.53	0.82	75.00
13-3	106	114.80	46.69	87.57	68.73	1.53	0.83	65.00
13-4	106	116.30	48.01	92.34	69.82	1.52	0.80	67.50
13-5	106	117.51	64.32	180.27	81.43	1.33	0.49	15.00
13-6	106	119.01	64.05	178.18	81.27	1.33	0.50	27.50
14-1	106	121.36	65.98	193.94	82.45	1.31	0.47	20.00
14-2	106	122.63	64.35	180.50	81.45	1.33	0.49	27.00
14-3	106	124.13	63.74	175.81	81.07	1.33	0.50	55.00
14-4	106	125.63	61.38	158.95	79.57	1.36	0.54	65.00
14-5	106	127.13	65.22	187.50	81.99	1.32	0.48	63.00
14-6	106	128.63	63.01	170.32	80.61	1.34	0.51	32.00
15-1	106	130.86	65.57	190.43	82.20	1.31	0.47	12.00
15-2	106	132.36	65.12	186.66	81.92	1.32	0.48	22.00
15-3	106	133.86	66.47	198.26	82.75	1.31	0.46	14.00
15-4	106	135.36	66.44	198.01	82.73	1.31	0.46	28.00
15-5	106	136.86	67.10	203.91	83.12	1.30	0.45	9.00
16-1	106	140.36	65.60	190.70	82.22	1.31	0.47	31.00
16-2	106	141.86	65.82	192.61	82.36	1.31	0.47	26.00
16-3	106	143.06	67.87	211.21	83.57	1.29	0.44	18.00
16-4	106	144.56	67.14	204.28	83.14	1.30	0.45	18.00

in both holes, were used as switch points to generate a continuous "pathway" of between-hole correlation.

3. This continuous correlation of cores with staggered penetration depths resulted in composite depth numbers that persistently increase in relation to the nominal depth below seafloor of both holes down to about 85 mbsf, where the cumulative gain in penetration depth amounted to more than 5 m (and thus, accumulation rates increased by up to 8%). Farther below, adjustment of core boundaries in many cases did not affect the nominal penetration depth. In other cases, this adjustment led to losses of nominal penetration depth, probably because of flow-in processes at the core's end.

4. Our correlations and adjustments led to complete overlapping of sections of "good core" down to a composite depth of 130 mbsf. Probably, this well-preserved, complete section reaches farther down to an extrapolated composite depth of about 150 mbsf, but no evidence exists for between-hole correlation at this depth range.

5. In a few cases, we observed a slight, unexplained telescoping of good-core sections, e.g., when comparing Cores 108-660A-3H with lower -660B-2H, upper 108-660A-6H with lower -660B-5H, and lower 108-660A-7H with upper -660B-7H (Fig. 31).

The composite-depth section (Table 10) presents the closest approximation to *in-situ* stratigraphy and should reveal our best estimates of sedimentation rates (Fig. 32) as well as the best match with seismic stratigraphy. In addition, the section shows how voids and contorted sections in cores with poor recovery can be bypassed successfully by sampling a companion hole.

REFERENCES

Barron, J. A., Bukry, D., and Poore, R. Z., 1984. Correlation of the middle Eocene Kellogg Shale of northern California. *Micropaleontol.*, 30:138–170.

Burckle, L. H., 1977. Pliocene and Pleistocene diatom datum levels from the equatorial Pacific. *Quat. Geol.*, 7:330–340.

Curry, W. B., and Lohmann, G. P., 1983. Reduced advection into Atlantic Ocean deep eastern basins during the last glacial maximum. *Nature* 306:577–580.

_____, 1984. Carbon deposition rates and deep water residence time in the equatorial Atlantic Ocean throughout the last 160,000 years. *Proc., Am. Geol. Union Chapman Conf. on Natural Variations in Carbon Dioxide and the Carbon Cycle*, 285–301.

Espitalié, J., Madec, M., and Tissot, B. P., 1977. Source rock characterization method for petroleum exploration. *Proc., 9th Annu. Offshore Technol. Conf.*, Houston, May 2–5: 439–448.

Fenner, J., 1978. Cenozoic diatom biostratigraphy of the equatorial and southern Atlantic Ocean. *In* Supko, P. R., Perch-Nielsen, K., et al., *Init. Repts. DSDP*, Suppl. to Vols. 38–40: Washington (U.S. Govt. Printing Office), 491–624.

———, 1984. Eocene-Oligocene planktic diatom stratigraphy in the low latitudes and the high southern latitudes. *Micropaleontol.*, 30: 319–342.

Hobart, M. A., Bunce, E. T., and Sclater, J. G., 1975. Bottom-water flow through the Kane Gap, Sierra Leone Rise, Atlantic Ocean. *J. Geophys. Res.*, 80:5083–5088.

Hooghiemstra, H., and Agwu, C.O.C., in press. Distribution of palynomorphs in marine sediments: a record for seasonal wind patterns over northwest Africa and adjacent Atlantic. *Geol. Rdsch.*, 75.

Jones, E.J.W., and Mgbatogu, C.C.S., 1982. The structure and evolution of the West African continental margin off Guine Bissau, Guinee, and Sierra Leone. *In* Scrutton, R. A., and Talwani, M. (Eds.), *The Ocean Floor*: New York (Wiley), 165–202.

Lonsdale, P., 1978. Bedforms and the benthic boundary layer in the North Atlantic: a cruise report of *Indomed* Leg 11. SIO Reference, 78–30.

Mantyla, A. W., and Reid, J. L., 1983. Abyssal characteristics of the world ocean waters. *Deep-Sea Res.*, 30:805–833.

McIntyre, A., Karlin, K., and Molfino, B., 1982. Orbital forcing and the response of the ice-age tropical Atlantic Ocean. *Geol. Soc. Am. Abstracts*, 561.

Mienert, J., 1985. Akustostratigraphie im aequatorialen Ostatlantik: Zur Entwicklung der Tiefenwasserzirkulation der letzten 3.5 Millionen Jahre [Unpubl. Ph.D. dissert.]. Univ. of Kiel, Federal Republic of Germany.

Pokras, E. M., and Mix, A. C., 1985. Late Pleistocene climatic changes in tropical Africa recorded in Atlantic deep-sea sediments. *Quat. Res.*, 24:137–149.

Sarnthein, M., Tetzlaff, G., Koopmann, B., Wolter, K., and Pflaumann, U., 1981. Glacial and interglacial wind regimes over the eastern subtropical Atlantic and northwest Africa. *Nature*, 293:193–196.

Sarnthein, M., Thiede, J., Pflaumann, U., Erlenkeuser, H., Fuetterer, D., Koopmann, B., Lange, H., and Seibold, E., 1982. Atmospheric and oceanic circulation patterns off northwest Africa during the past 25 million years. *In* von Rad, U., et al. (Eds.), *Geology of the Northwest African Continental Margin*: Berlin-Heidelberg (Springer-Verlag), 545–604.

Sarnthein, M., Koegler, F. C., and Werner, F., 1983. Forschungsschiff "Meteor," Reise No. 65. Berichte der wissenschaftlichen Leiter. Geology-Palaeontology Inst., Univ. of Kiel, Berichte-Reports, 2:1–90.

Sarnthein, M., Haake, F., Mayer, L., Pflaumann, U., Springer, M., Werner, F., and Wiederhold, H., 1985. Bericht über die "Polarstern" Fahrt ANT IV/Ic in den Äquatorialen Atlantik GEOTROPEX '85, Dakar–Rio de Janeiro, 14.10–3.11.1985. Geology-Palaeontology Inst., Univ. of Kiel, Berichte-Reports, 11.

Schrader, H. J., and Fenner, J., 1976. Norwegian Sea Cenozic diatom biostratigraphy. *In* Talwani, M., Udinstev, G., et al., *Init. Repts. DSDP*, 38: Washington (U.S. Govt. Printing Office), 921–1100.

Stein, R., 1985. The post-Eocene sediment record of DSDP Site 366: Implications for African climate and plate tectonic drift. *In* Kennett, J. P. (Ed.), *The Miocene Ocean: Paleoceanography and Biogeography*, Geol. Soc. Am. Mem., 163:305–315.

Stein, R., Sarnthein, M., and Suendermann, J., 1986a. Neogene events of bottom-water erosion along the northeast Atlantic continental margin. *In* Summerhays, C., and Shackleton, N. (Eds.), *North Atlantic Paleoceanography*, Geol. Soc. London Spec. Publ., 21:103–118.

Stein, R., Rullkötter, J., and Welte, D. H., 1986b. Accumulation of organic-carbon-rich sediments in the Late Jurassic and Cretaceous Atlantic Ocean—a synthesis. *Chem. Geol.*, 56:1–32.

Tetzlaff, G., and Wolter, W., 1980. Meteorological patterns and the transport of mineral dust from the North African continent. *Paleoecology of Africa*, 12:31–42.

Tiedemann, R., 1985. Verteilung von organischem Kohlenstoff in Oberfächensedimenten und die örtliche Primärproduktion im äquatorialen Ostatlantik, 0–20°N, 15–25°W [Unpubl. M.S. thesis]. Univ. of Kiel, Federal Republic of Germany.

Tissot, B. P., and Welte, D. H., 1984. *Petroleum Formation and Occurrence*: Berlin-Heidelberg (Springer-Verlag).

Table 8. *P*-wave-logger-velocity data for Hole 660A.

Depth (m)	*P*-wave Velocity (km/s)	Depth (m)	*P*-wave Velocity (km/s)	Depth (m)	*P*-wave Velocity (km/s)
1.00	1.51	51.40	1.50	99.00	1.58
2.80	1.51	52.50	1.51	99.40	1.54
3.80	1.52	52.80	1.50	99.80	1.59
4.60	1.52	53.90	1.52	99.90	1.55
5.30	1.51	54.50	1.51	100.30	1.60
6.30	1.52	55.10	1.53	100.60	1.52
6.80	1.52	55.60	1.51	100.80	1.57
7.30	1.51	56.80	1.51	101.10	1.54
7.90	1.53	57.50	1.51	101.80	1.57
8.30	1.52	58.00	1.52	102.00	1.54
8.80	1.52	59.20	1.51	102.20	1.57
9.60	1.51	59.40	1.53	102.60	1.54
10.00	1.52	60.40	1.55	103.10	1.55
10.30	1.52	61.00	1.51	103.90	1.54
11.00	1.52	61.90	1.54	104.30	1.53
12.00	1.51	63.10	1.51	104.70	1.57
12.80	1.52	63.30	1.53	105.20	1.54
13.30	1.51	63.60	1.52	107.30	1.54
14.30	1.52	63.70	1.53	108.30	1.54
15.30	1.52	63.90	1.51	108.80	1.57
15.90	1.53	64.90	1.55	109.00	1.53
16.30	1.52	65.30	1.52	109.60	1.55
16.90	1.52	65.80	1.53	110.30	1.54
17.50	1.52	66.80	1.52	111.30	1.54
18.30	1.51	67.00	1.53	112.30	1.54
18.90	1.53	67.20	1.51	112.90	1.53
19.80	1.51	67.90	1.54	113.10	1.54
20.60	1.53	68.80	1.52	113.30	1.53
21.80	1.51	70.30	1.53	114.10	1.56
22.80	1.51	71.30	1.55	114.60	1.57
24.30	1.51	71.80	1.53	115.00	1.54
24.80	1.51	72.40	1.54	115.30	1.58
25.40	1.53	73.50	1.55	115.50	1.54
25.60	1.50	73.70	1.53	116.80	1.55
26.80	1.52	75.00	1.55	117.80	1.55
27.30	1.51	76.30	1.54	118.80	1.56
28.80	1.52	76.50	1.51	119.80	1.55
30.30	1.52	77.00	1.54	120.80	1.55
31.00	1.54	77.20	1.56	121.80	1.57
31.40	1.51	78.10	1.56	122.80	1.56
32.00	1.54	81.00	1.54	126.30	1.55
32.80	1.52	81.40	1.56	127.30	1.54
33.00	1.55	81.80	1.54	128.30	1.56
33.50	1.52	82.80	1.53	129.30	1.56
34.80	1.53	83.70	1.55	129.90	1.58
35.50	1.51	84.80	1.53	130.30	1.56
36.10	1.53	85.60	1.58	131.30	1.57
36.80	1.51	87.30	1.54	132.30	1.55
38.00	1.53	88.00	1.56	133.30	1.56
39.30	1.51	88.70	1.53	134.30	1.56
40.30	1.50	89.00	1.57	136.80	1.55
41.30	1.52	90.20	1.53	137.80	1.57
41.80	1.50	90.70	1.57	138.00	1.58
42.90	1.52	90.90	1.53	138.80	1.56
43.80	1.50	92.60	1.53	139.80	1.56
44.60	1.51	93.10	1.56	140.80	1.56
45.20	1.50	93.20	1.54	141.80	1.55
45.90	1.51	93.90	1.57	145.00	1.56
46.00	1.50	94.20	1.54	146.00	1.57
46.60	1.53	94.80	1.55	148.00	1.57
47.60	1.51	95.50	1.60	152.50	1.57
48.30	1.51	96.00	1.54	154.50	1.55
49.50	1.50	97.70	1.56	155.50	1.55
50.60	1.50	98.80	1.55		

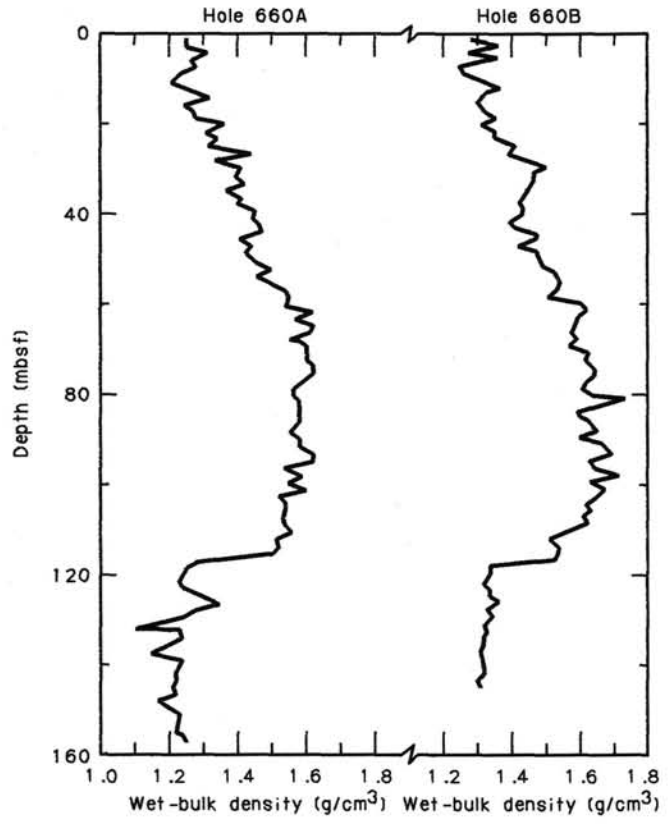

Figure 19. Wet-bulk-density profiles.

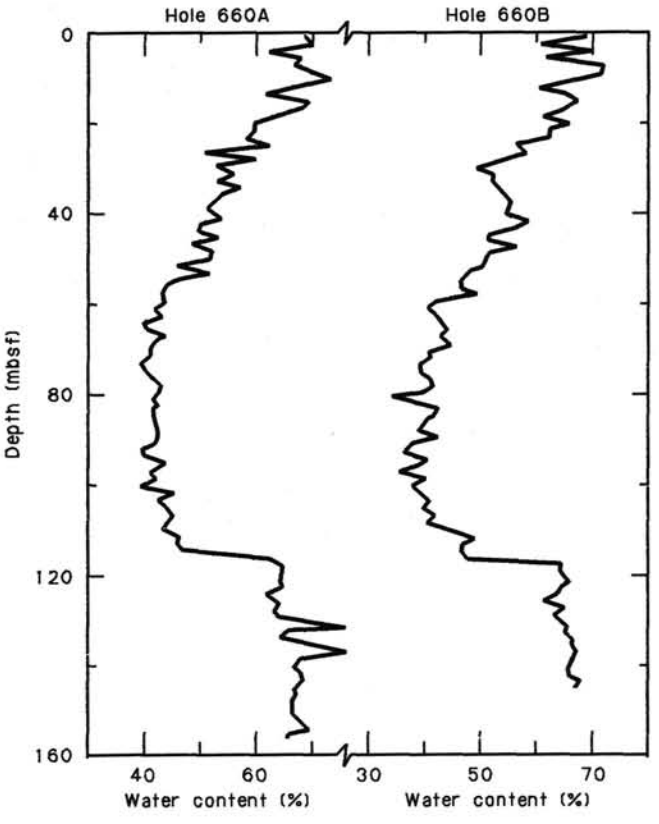

Figure 21. Water-content profiles.

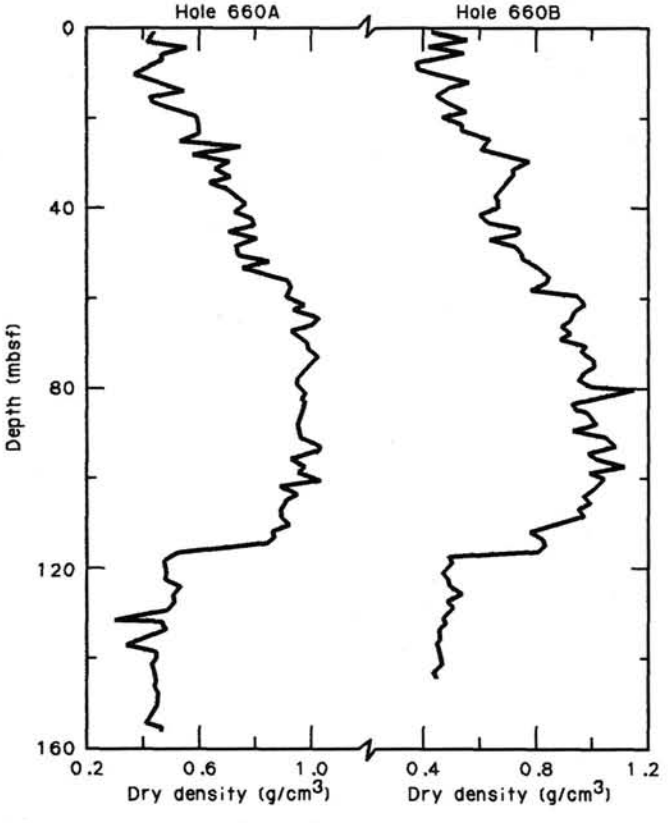

Figure 20. Dry-bulk-density profiles.

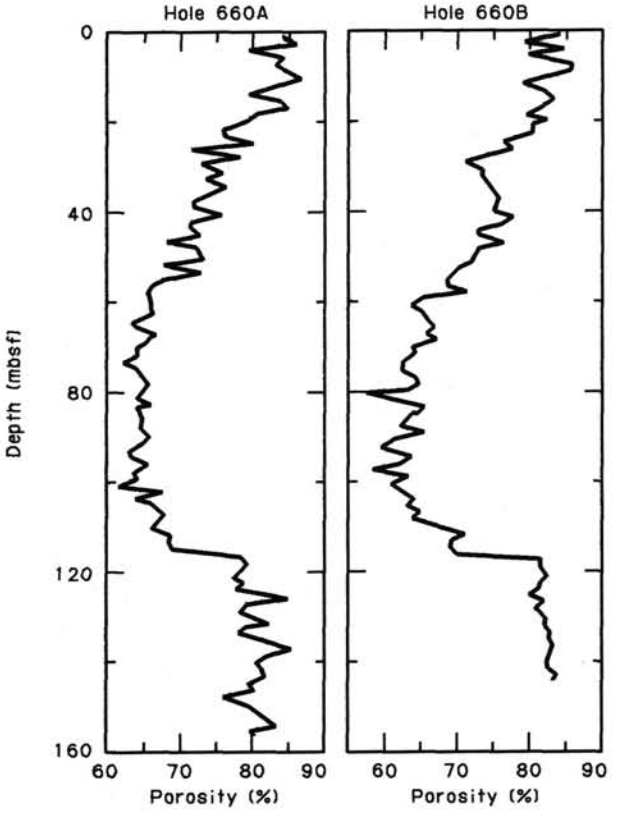

Figure 22. Porosity profiles.

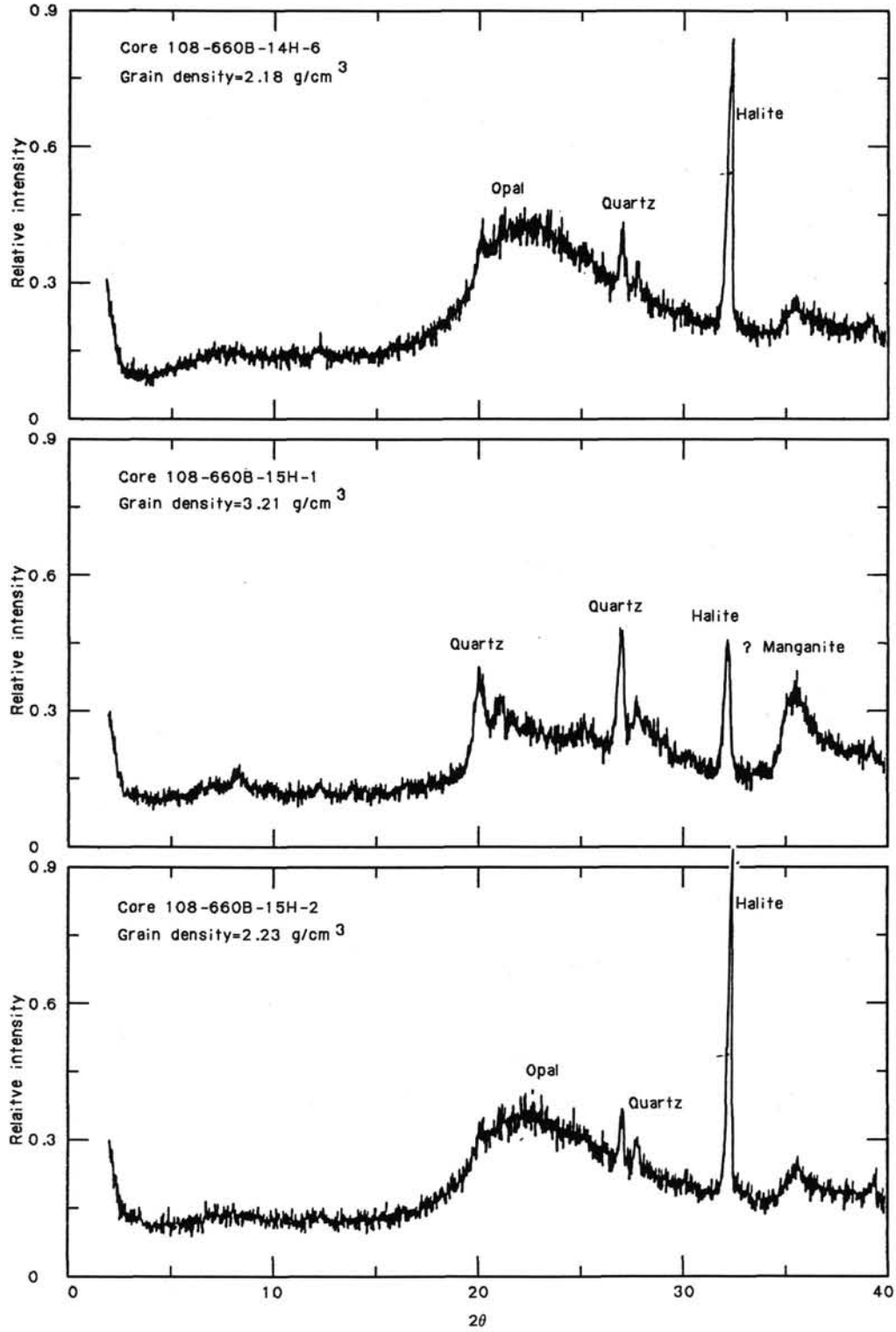

Figure 24. X-ray-diffractograms (Cores 108-660B-14H-6, -660B-15H-1, and -660B-15H-2).

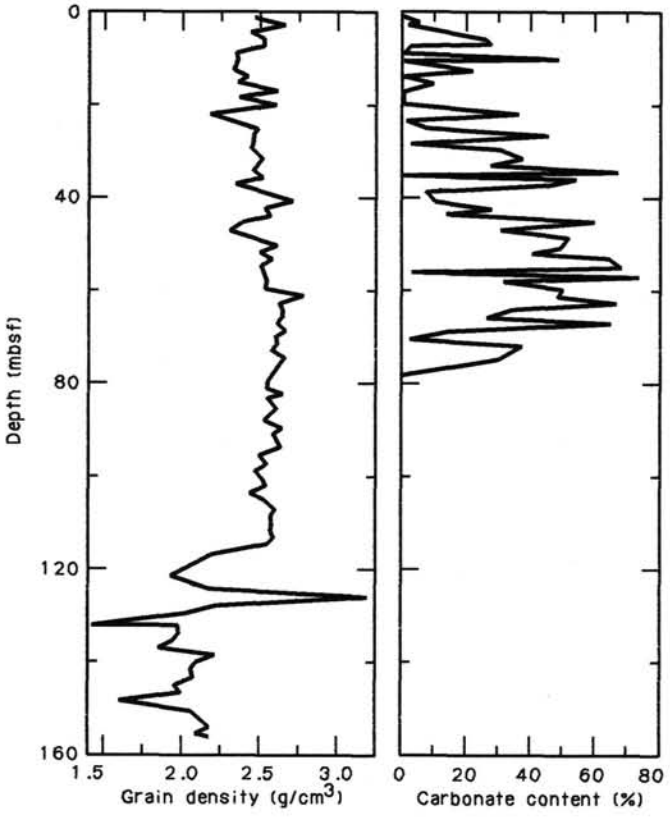

Figure 23. Grain-density and carbonate-content profiles for Hole 660A.

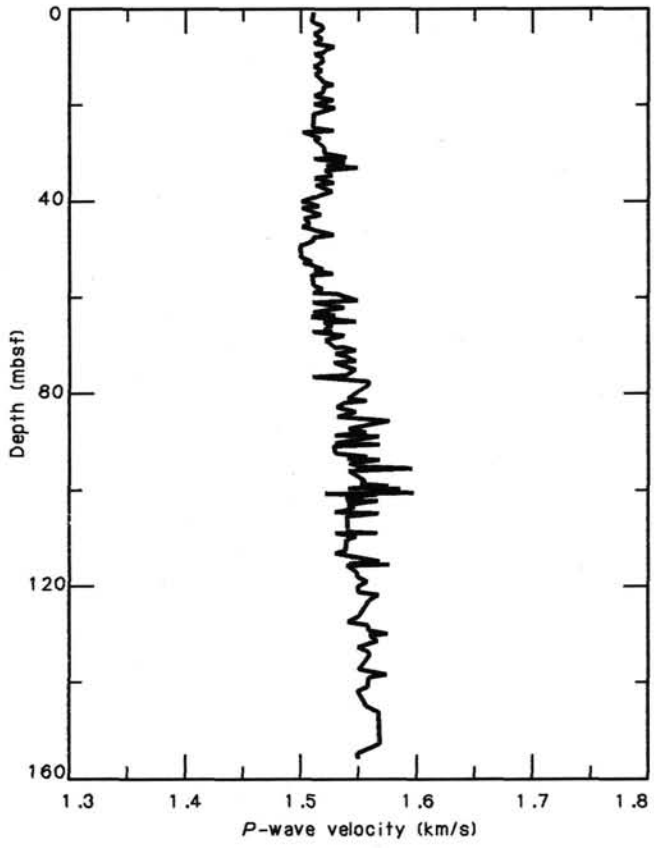

Figure 26. *P*-wave-logger-velocity profile for Hole 660A.

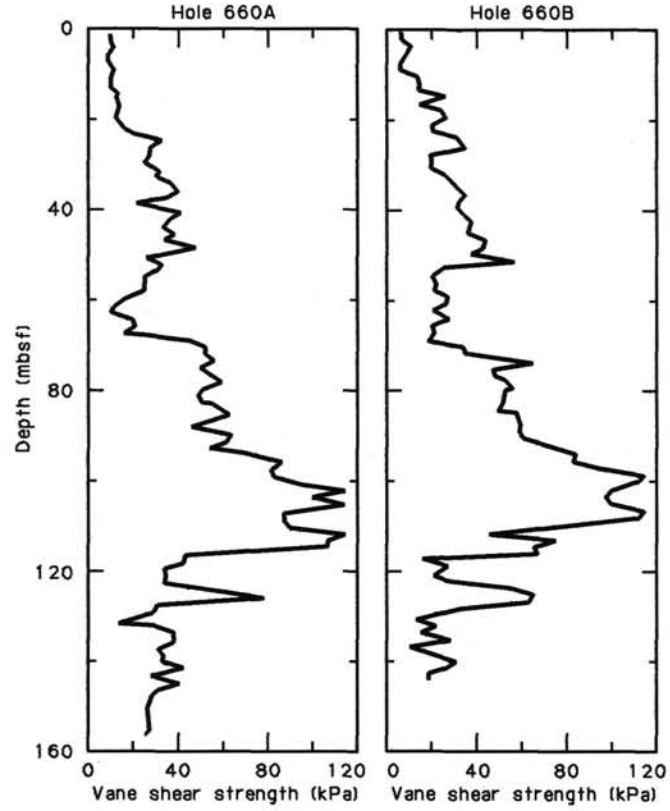

Figure 25. Vane-shear-strength profiles.

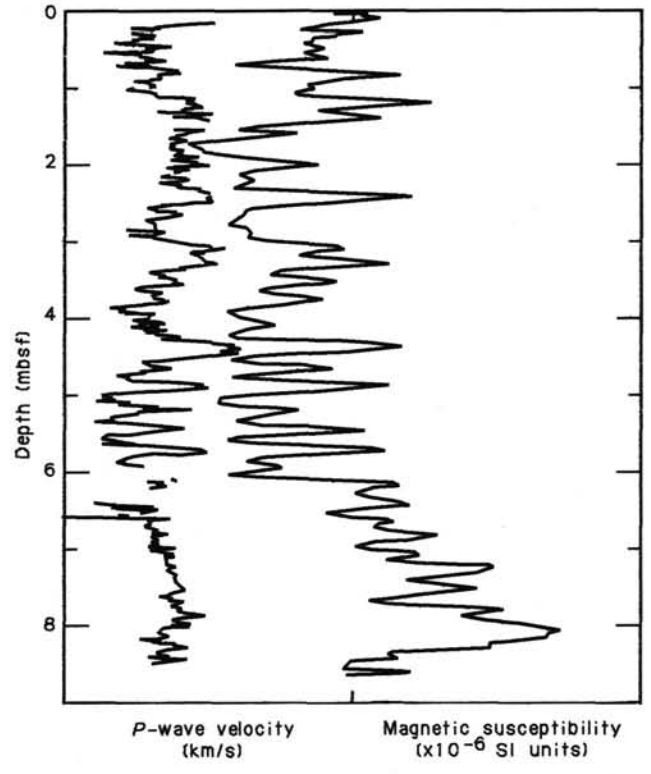

Figure 27. Profiles of *P*-wave-logger velocity and magnetic susceptibility for Core 108-660B-8H.

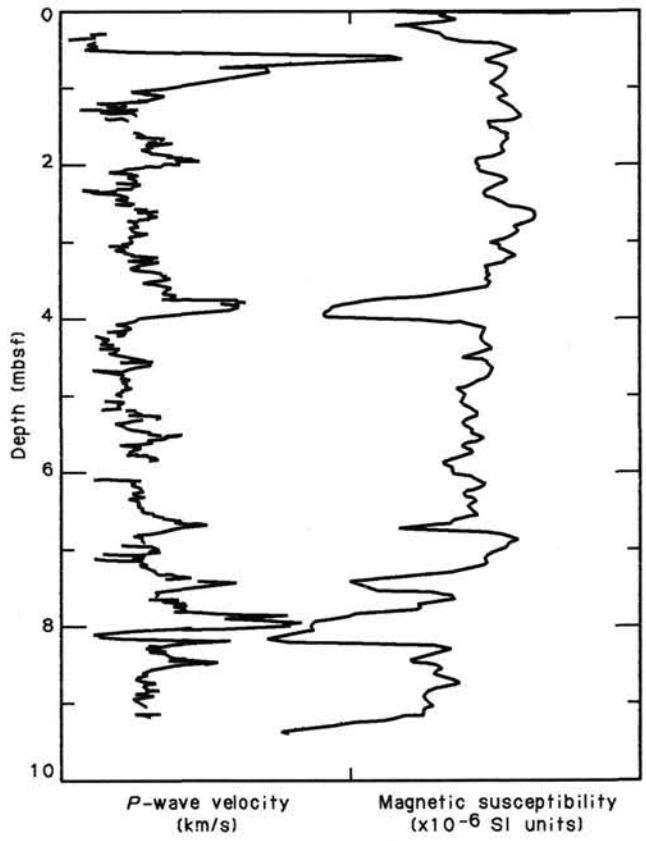

Figure 28. Profiles of *P*-wave-logger velocity and magnetic susceptibility for Core 108-660B-11H.

Table 9. Water- and air-gun seismic correlations, Site 660.

Seismic unit no.	Reflectors (no.)	Reflectors (sbsf)	Reflector depth 1510 m/s (mbsf)	Reflector depth 1530 m/s (mbsf)	Source	Age	Lithologic unit
Seismic air-gun profile of Jones and Mbgatogu (1982)							
							IA
	1	0.03	22.5		Top of $CaCO_3$ increase	ca. 0.85 Ma	————
	2	0.62	46.5		Top of $CaCO_3$ increase	ca. 2.4 Ma	IB
	3	0.079	59.65		Top of interbedded silty clay beds	ca. 3.2 Ma	————
(1)							
	4	0.113	86.45		(?)	(?)	IC, II
	5	0.123		94.10	Increase in shear strength	Miocene(?)	
———	6	0.148		113.2	Top of radiolarian ooze	middle Eocene	————
							III
GEOTROPEX '85 seismic water-gun profile							
———	6	0.153		117	Top of radiolarian ooze	middle Eocene	————
(2)	7	0.173		132	(?)Mn-rich layer		III
	8	0.209		160	Top of chert	middle Eocene	
———	9	0.255		195	(?) Base of chert		

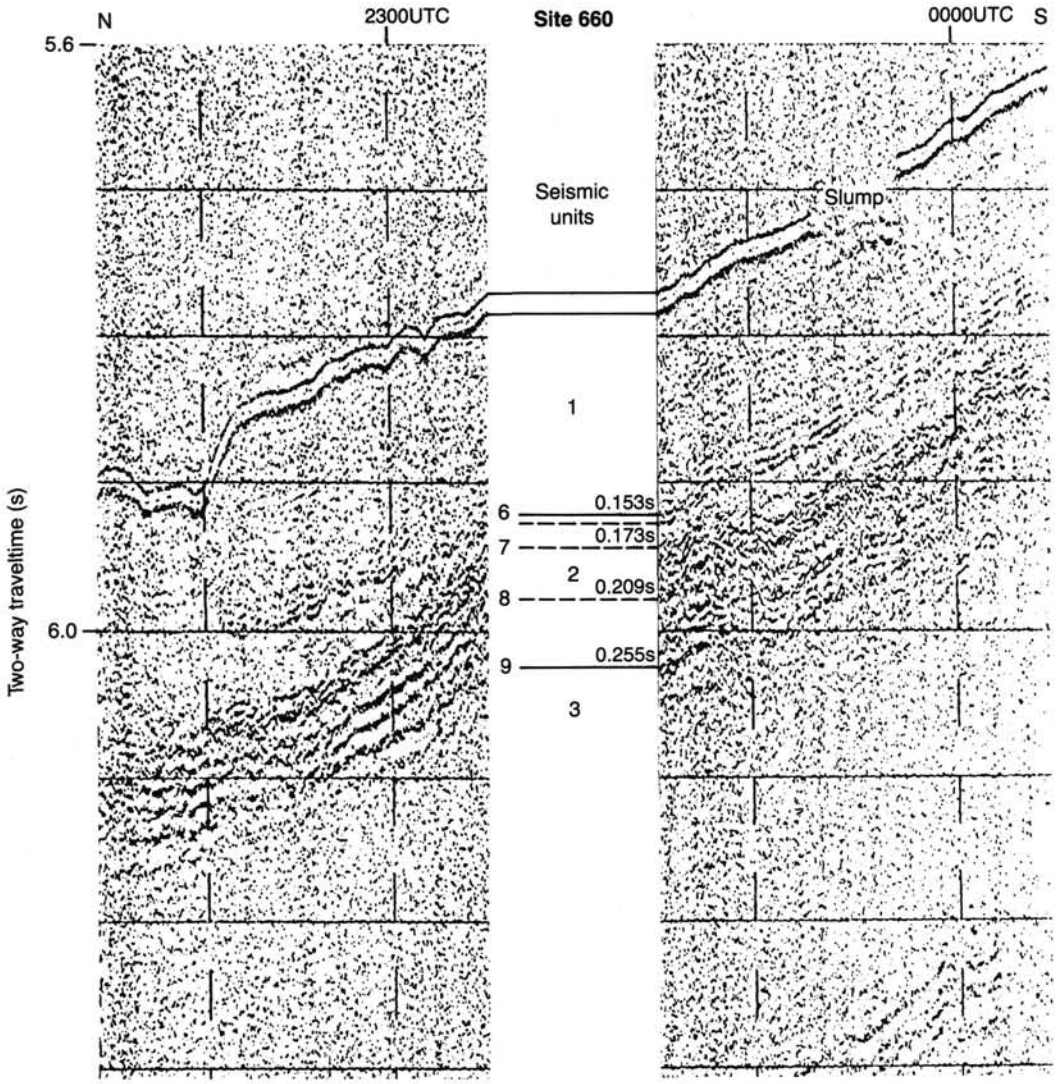

Figure 29. GEOTROPEX '85 seismic water-gun profile over Site 660 showing the seismic sequence described in the text.

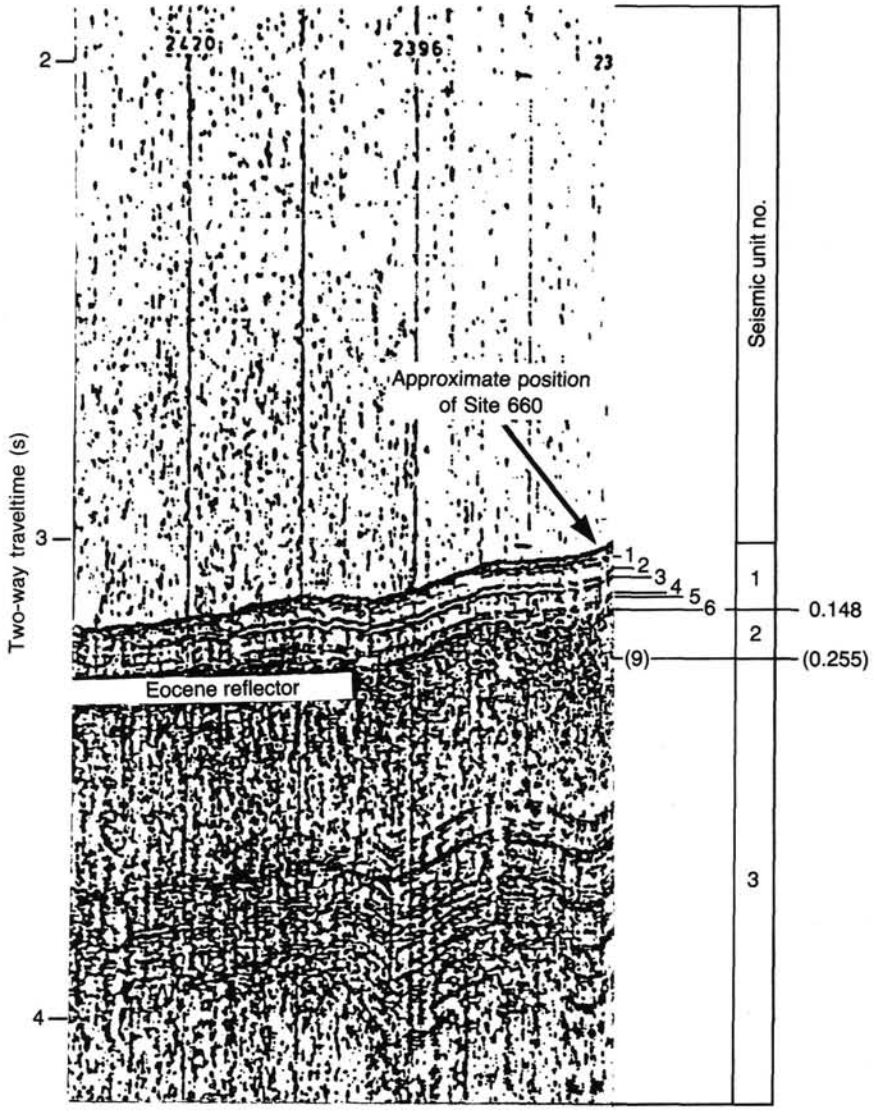

Figure 30. Seismic air-gun profile of Jones and Mbgatogu (1982) near Site 660 showing the seismic sequence described in the text.

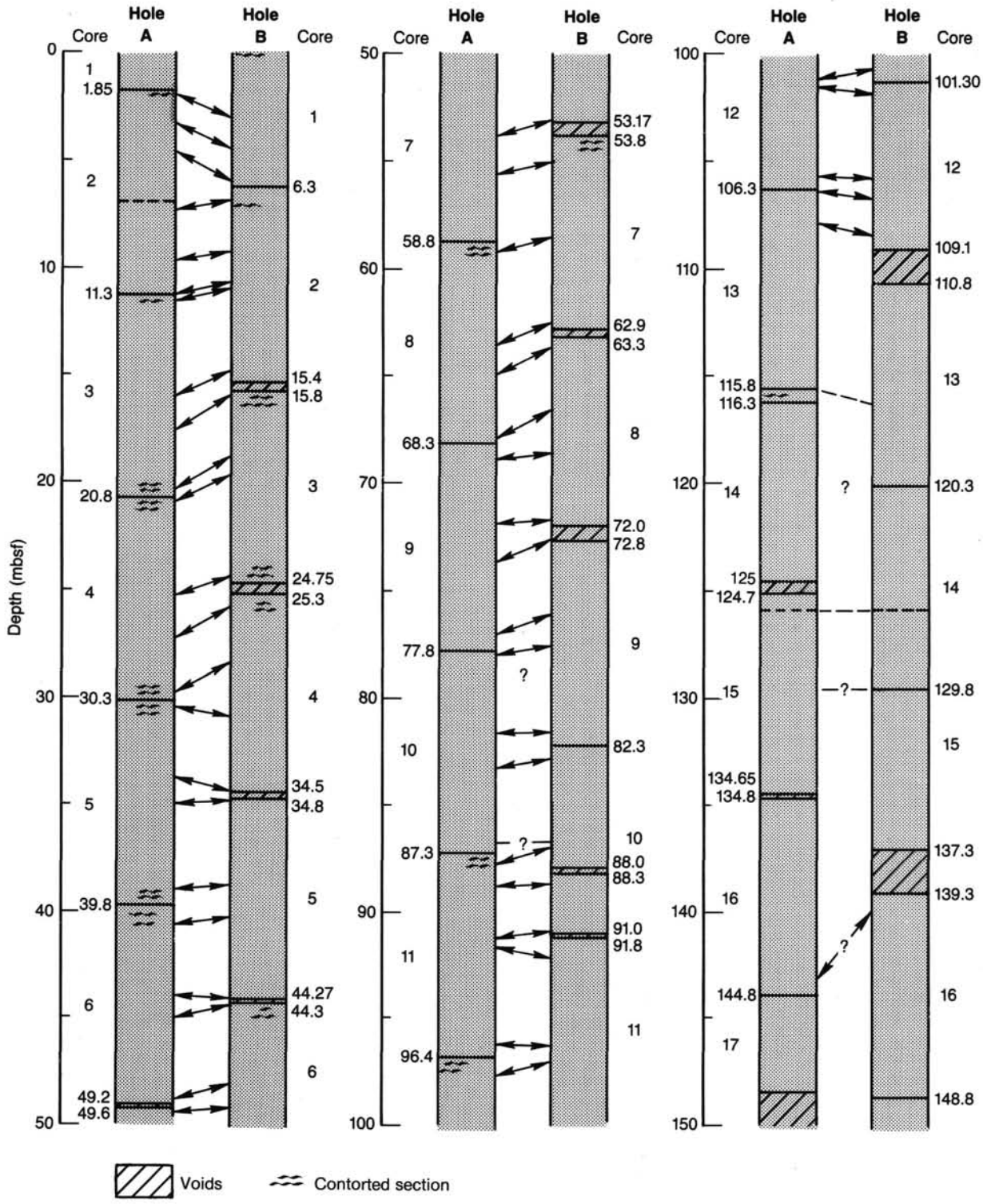

Figure 31. Depth correlation between Holes 660A and 660B. Nominal depth in meters below seafloor of penetration and core numbers appear along the graphs of the single holes.

Table 10. Composite depth levels used to correlate cores from Holes 660A and 660B.

Composite depth (mbsf)	Gain/loss[a] (m)	Cumulative gain (m)	Nominal depth (mbsf)	
			Hole 660A	Hole 660B
3.1			2.0	3.1
6.1			4.75	6.1
8.85	+1.75	1.75	7.5	7.1
16.7			16.2	14.95
18.1	+0.35	2.1	17.6	16.0
26.6			25.4	24.5
28.6	+0.7	2.8	27.4	25.8
37.3			33.8	34.5
38.6	+0.8	3.6	35.1	35.0
47.7			44.0	44.1
48.8	+0.8	4.4	45.1	44.4
57.5			54.0	53.1
58.0	−0.6	3.8	54.5	54.2
66.5			63.7	62.7
67.75			65.05	63.95
75.7			72.0	71.9
77.45	+0.85	4.65	73.75	72.8
86.4			81.75	81.75
88.05	+0.4	5.05	83.4	83.0
92.05			87.8	87.0
93.25	−0.6	4.45	89.0	88.8
100.75			96.2	96.3
105.25			101.35	100.8
105.7	−0.75	3.7	101.8	102.0
112.2			108.1	108.5
115.1	+0.1	3.8 (about 4.5%)	111.0	111.3

[a] Gains and losses of sediment at core breaks are presented in relation to Hole 660B and are derived by subtracting the differences of depths below seafloor for two succeeding switch points in the two holes, respectively.

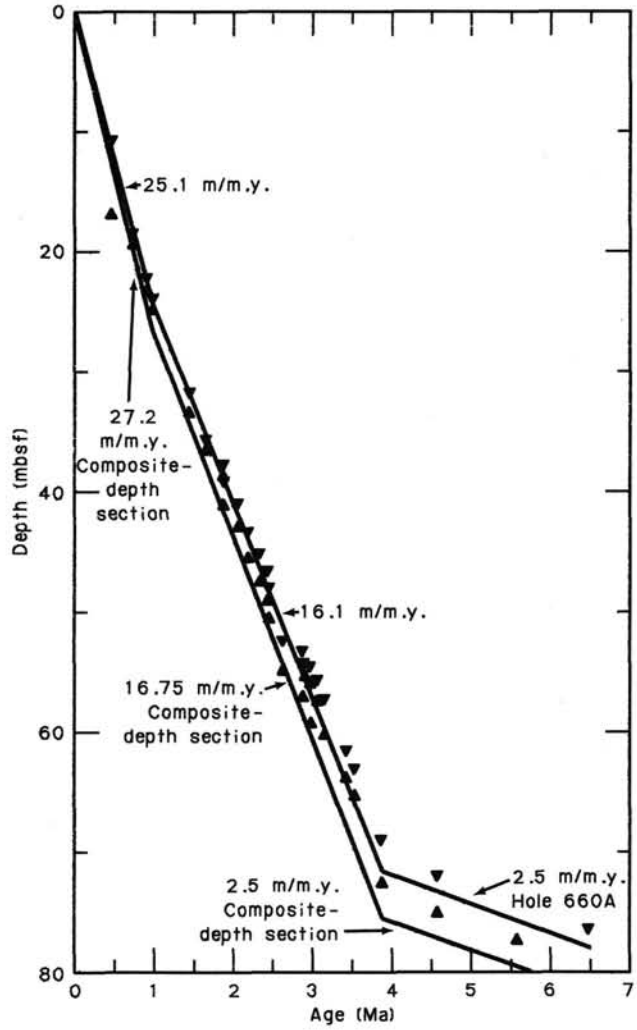

Figure 32. Age-depth section of Site 660 (using biostratigraphic data from "Biostratigraphy" section, this chapter) that compares the age-depth curve based on nominal depths in Hole 660A with that based on new composite-depth estimates.

SITE 660 HOLE A CORE 1 H CORED INTERVAL 4332.2–4334.0 mbsl; 0 –1.80 mbsf

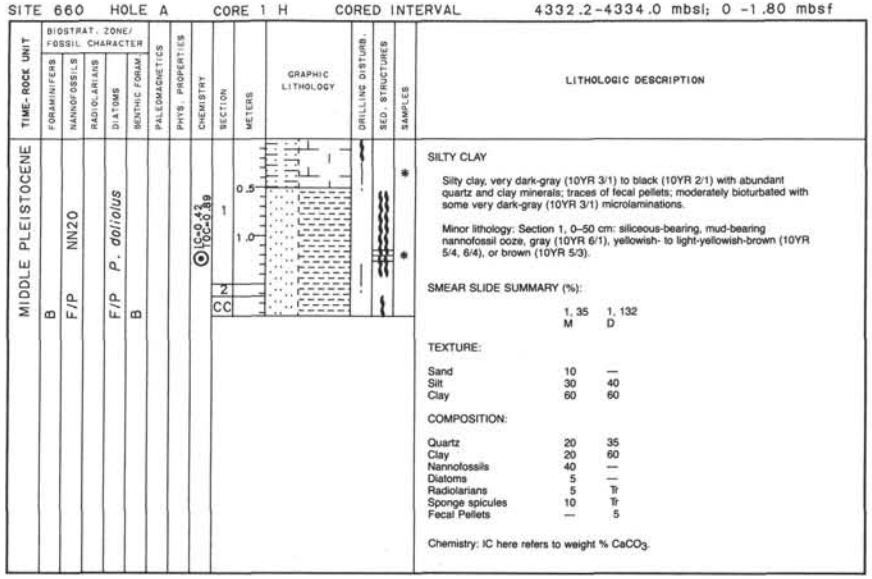

LITHOLOGIC DESCRIPTION

SILTY CLAY

Silty clay, very dark-gray (10YR 3/1) to black (10YR 2/1) with abundant quartz and clay minerals; traces of fecal pellets; moderately bioturbated with some very dark-gray (10YR 3/1) microlaminations.

Minor lithology: Section 1, 0–50 cm: siliceous-bearing, mud-bearing nannofossil ooze, gray (10YR 6/1), yellowish- to light-yellowish-brown (10YR 5/4, 6/4), or brown (10YR 5/3).

SMEAR SLIDE SUMMARY (%):

	1, 35 M	1, 132 D
TEXTURE:		
Sand	10	—
Silt	30	40
Clay	60	60
COMPOSITION:		
Quartz	20	35
Clay	20	60
Nannofossils	40	—
Diatoms	5	—
Radiolarians	5	Tr
Sponge spicules	10	Tr
Fecal Pellets	—	5

Chemistry: IC here refers to weight % $CaCO_3$.

SITE 660 HOLE A CORE 2 H CORED INTERVAL 4334.0–4343.5 mbsl; 1.80–11.3 mbsf

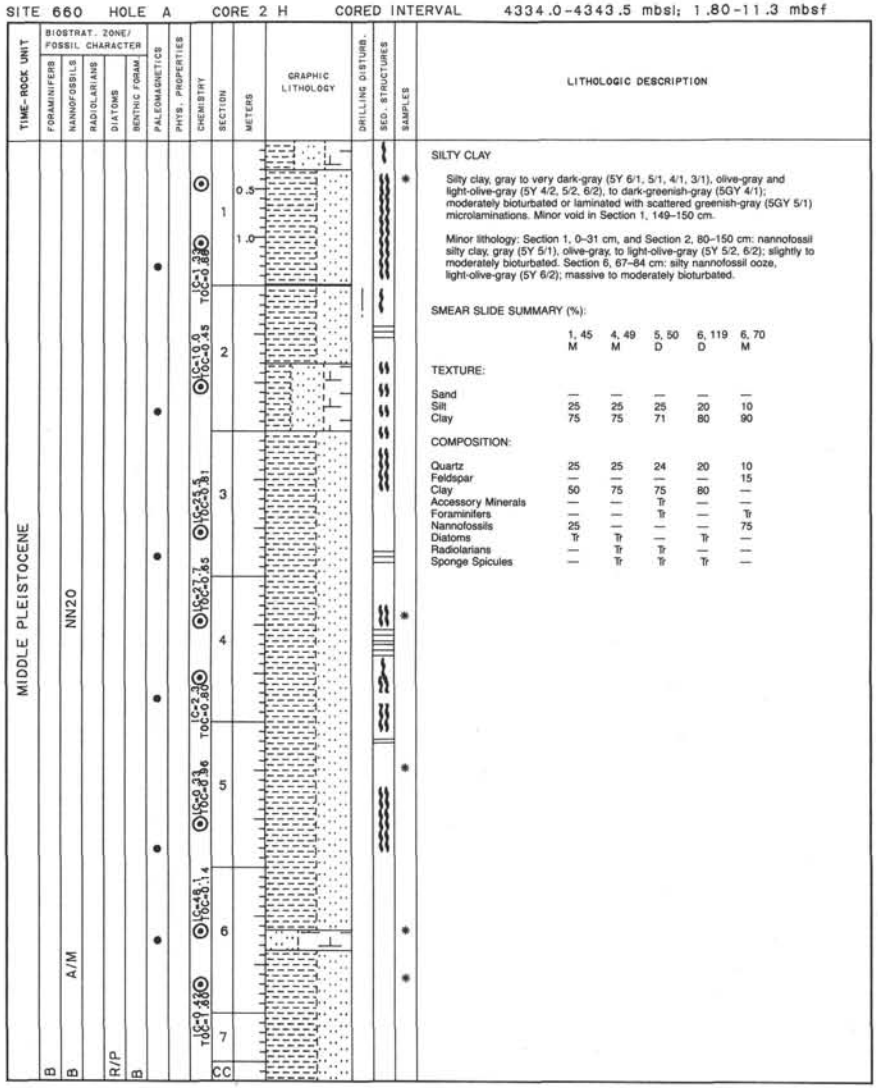

LITHOLOGIC DESCRIPTION

SILTY CLAY

Silty clay, gray to very dark-gray (5Y 6/1, 5/1, 4/1, 3/1), olive-gray and light-olive-gray (5Y 4/2, 5/2, 6/2), to dark-greenish-gray (5GY 4/1); moderately bioturbated or laminated with scattered greenish-gray (5GY 5/1) microlaminations. Minor void in Section 1, 149–150 cm.

Minor lithology: Section 1, 0–31 cm, and Section 2, 80–150 cm: nannofossil silty clay, gray (5Y 5/1), olive-gray, to light-olive-gray (5Y 5/2, 6/2); slightly to moderately bioturbated. Section 6, 67–84 cm: silty nannofossil ooze, light-olive-gray (5Y 6/2); massive to moderately bioturbated.

SMEAR SLIDE SUMMARY (%):

	1, 45 M	4, 49 M	5, 50 D	6, 119 D	6, 70 M
TEXTURE:					
Sand	—	—	—	—	—
Silt	25	25	25	20	10
Clay	75	75	71	80	90
COMPOSITION:					
Quartz	25	25	24	20	10
Feldspar	—	—	—	—	15
Clay	50	75	75	80	—
Accessory Minerals	—	—	Tr	—	—
Foraminifers	—	—	Tr	—	Tr
Nannofossils	25	—	—	—	75
Diatoms	Tr	Tr	—	Tr	—
Radiolarians	—	Tr	Tr	—	—
Sponge Spicules	—	Tr	Tr	Tr	—

SITE 660 HOLE A CORE 3 H CORED INTERVAL 4343.5-4353.0 mbsl; 11.30-20.80 mbsf

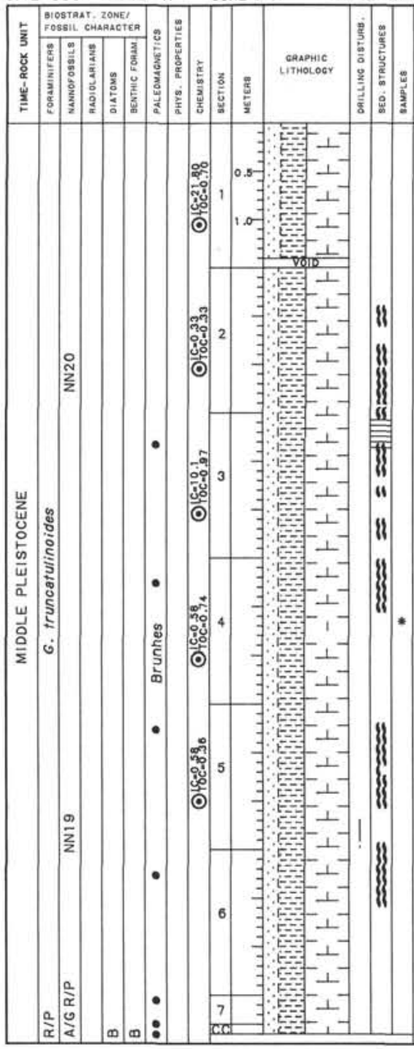

LITHOLOGIC DESCRIPTION

SILTY CLAY and NANNOFOSSIL OOZE

Silty clay, gray to very dark-gray (5Y 5/1, 4/1, 3/1) or grayish-brown (5Y 5/2); massive to moderately bioturbated; less commonly laminated with scattered microlaminations, very dark-gray (5Y 3/1) sediment, alternating with and grading up into nannofossil ooze, gray, light-olive-gray, or pale-olive (5Y 6/1, 6/2, 6/3); massive to moderately bioturbated.

SMEAR SLIDE SUMMARY (%):

	4, 66 M
TEXTURE:	
Sand	—
Silt	10
Clay	90
COMPOSITION:	
Quartz	5
Clay	45
Foraminifers	5
Nannofossils	45
Diatoms	Tr
Radiolarians	Tr
Sponge spicules	Tr

SITE 660 HOLE A CORE 4 H CORED INTERVAL 4353.0-4362.5 mbsl; 20.8-30.3 mbsf

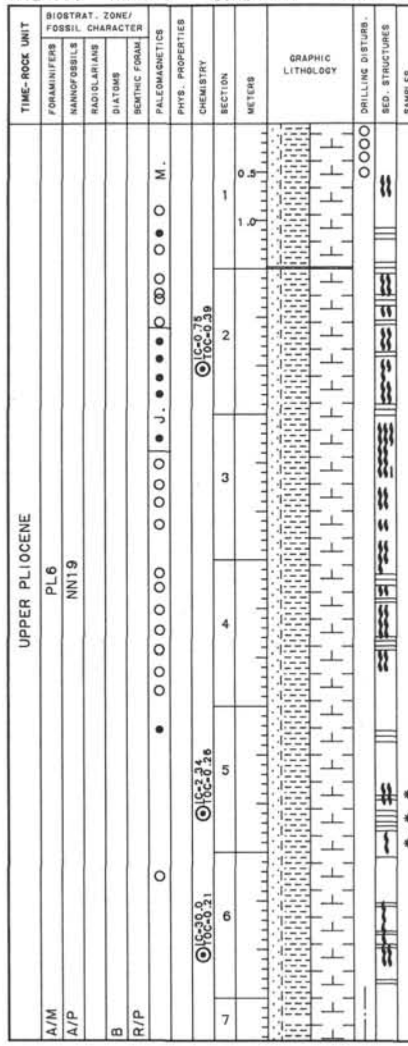

LITHOLOGIC DESCRIPTION

SILTY CLAY and CLAY-BEARING, FORAMINIFER-BEARING NANNOFOSSIL OOZE

Silty clay, gray to very dark-gray (5Y 5/1, 4/1, 3/1) or grayish-brown (5Y 5/2); moderately to extensively bioturbated; less commonly massive or laminated; scattered microlaminations, very dark-gray (5Y 3/1) to greenish (5G 6/2) sediment, alternating with and grading up into clay-bearing, foraminifer-bearing nannofossil ooze, light-gray (5Y 6/1, 7/1) or light-olive-gray (5Y 6/2); slightly to moderately bioturbated. Minor void in Section 1, 147–150 cm.

SMEAR SLIDE SUMMARY (%):

	5, 90 D	5, 120 D	5, 144 D
TEXTURE:			
Sand	15	—	—
Silt	25	35	20
Clay	60	65	80
COMPOSITION:			
Quartz	5	25	15
Clay	15	65	80
Accessory Minerals	Tr	5	2
Foraminifers	20	—	—
Nannofossils	60	Tr	—
Fish Remains	—	Tr	—
Plant Debris	—	—	2
Pellets	—	<5	—

SITE 660 HOLE A CORE 5 H CORED INTERVAL 4362.5-4372.0 mbsl; 30.3-39.8 mbsf

LITHOLOGIC DESCRIPTION

SILTY CLAY and MUD-BEARING, FORAMINIFER-BEARING NANNOFOSSIL OOZE

Silty clay, gray to very dark-gray (5Y 5/1, 4/1, 3/1) or grayish-brown (5Y 5/2); moderately bioturbated with microlaminations, very dark-gray (5Y 3/1) to greenish (5G 6/2, 5/2) sediment, alternating with and grading up into mud-bearing, foraminifer-bearing nannofossil ooze, light-gray (5Y 6/1, 7/1, 7/2) or light-olive-gray (5Y 6/2); massive to moderately bioturbated; less commonly laminated.

SMEAR SLIDE SUMMARY (%):

	4, 17 D	4, 30 D	4, 38 D
TEXTURE:			
Sand	10	—	—
Silt	25	30	35
Clay	65	70	65
COMPOSITION:			
Quartz	10	30	30
Clay	10	70	60
Accessory Minerals	tr	tr	—
Foraminifers	20	—	—
Nannofossils	60	tr	—
Diatoms	tr	—	—
Radiolarians	tr	tr	—
Fish Remains	—	—	—

SITE 660 HOLE A CORE 6 H CORED INTERVAL 4372.0-4381.5 mbsl; 39.8-49.3 mbsf

LITHOLOGIC DESCRIPTION

SILTY CLAY and MUD-BEARING, FORAMINIFER-BEARING NANNOFOSSIL OOZE

Silty clay, gray to very dark-gray (5Y 5/1, 4/1, 3/1); laminated to moderately bioturbated with scattered microlaminations, dark-gray (5Y 4/1) to greenish (5G 6/2, 5/2) sediment, alternating with and grading up into mud-bearing, foraminifer-bearing nannofossil ooze, light-gray (5Y 6/1, 7/1, 7/2) or light-olive-gray (5Y 6/2); massive to moderately bioturbated.

SMEAR SLIDE SUMMARY (%):

	2, 146 D	3, 7 D	3, 25 D
TEXTURE:			
Sand	—	—	—
Silt	10	20	30
Clay	90	80	70
COMPOSITION:			
Quartz	5	20	30
Clay	10	80	70
Foraminifers	5	—	—
Nannofossils	80	—	—

SITE 660 HOLE A CORE 7 H CORED INTERVAL 4381.5-4371.0 mbsl; 49.3-58.8 mbsf

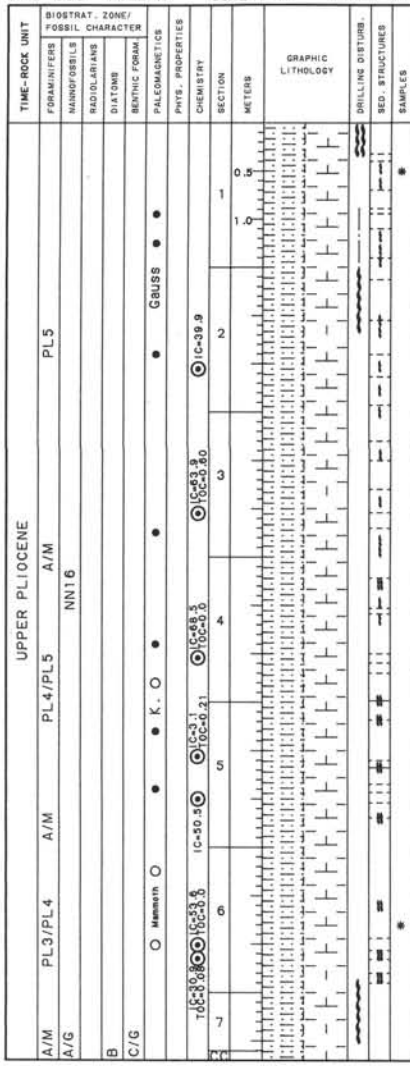

LITHOLOGIC DESCRIPTION

MUDDY NANNOFOSSIL OOZE and FORAMINIFER-BEARING, MUDDY NANNOFOSSIL OOZE

Muddy nannofossil ooze, gray (5Y 6/1), grayish-brown or light-grayish-brown (2.5Y 5/2, 6/2); massive to slightly bioturbated, alternating with and grading up into foraminifer-bearing, muddy nannofossil ooze, light-gray (2.5Y 7/2, 5Y 7/1) to white (5Y 8/1); massive to slightly bioturbated.

SMEAR SLIDE SUMMARY (%):

	1, 60 D	6, 80 D
TEXTURE:		
Sand	5	10
Silt	35	30
Clay	60	60
COMPOSITION:		
Quartz	25	15
Rock Fragments	5	5
Clay	15	10
Accessory Minerals	—	5
Foraminifers	—	10
Nannofossils	55	55

SITE 660 HOLE A CORE 8 H CORED INTERVAL 4391.0-4400.5 mbsl; 58.8-68.3 mbsf

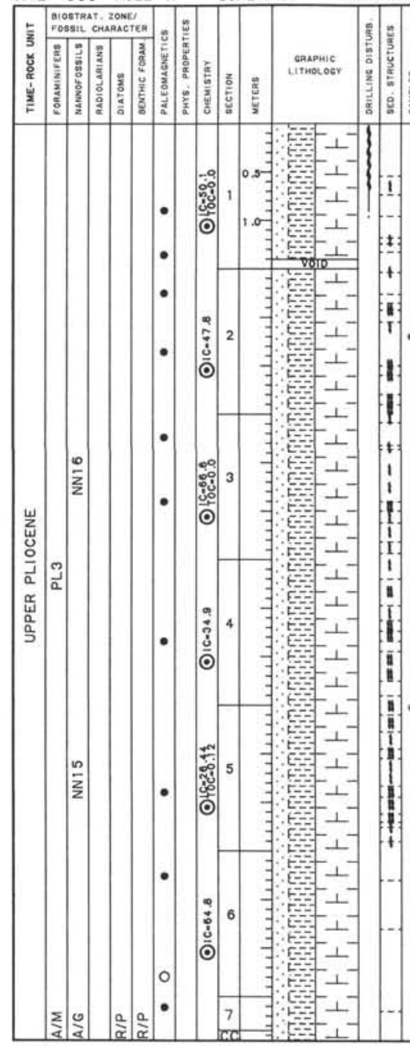

LITHOLOGIC DESCRIPTION

NANNOFOSSIL-BEARING, SILTY CLAY and MUD-BEARING NANNOFOSSIL OOZE

Nannofossil-bearing, silty clay, light-olive-gray (5Y 6/2), pale-olive (5Y 6/3), to olive (5Y 5/3, 5/4); slightly to moderately bioturbated, alternating with and grading up into mud-bearing nannofossil ooze, light-gray to white (5Y 7/1, 8/1); massive to slightly bioturbated. Minor void in Section 1, 143–150 cm.

SMEAR SLIDE SUMMARY (%):

	2, 70 X	5, 5 X
TEXTURE:		
Sand	5	5
Silt	20	45
Clay	75	50
COMPOSITION:		
Quartz	5	40
Clay	10	45
Accessory Minerals	5	—
Foraminifers	10	Tr
Nannofossils	70	15

SITE 660 HOLE A CORE 9 H CORED INTERVAL 4400.5-4410.0 mbsl; 68.30-77.30 mbsf

LITHOLOGIC DESCRIPTION

NANNOFOSSIL-BEARING, SILTY CLAY and MUD-BEARING NANNOFOSSIL OOZE

Nannofossil-bearing, silty clay, light-olive-gray (5Y 6/2), pale-olive (5Y 6/3), or olive (5Y 5/3, 5/4); slightly to moderately bioturbated, alternating with and grading up into mud-bearing nannofossil ooze, light-gray to white (5Y 7/1, 8/1); massive to slightly bioturbated. Minor void in Section 1, 148–150 cm.

Minor lithology: Section 6, 120 cm to CC: silty clay, brown (10YR 5/3); slightly bioturbated.

SMEAR SLIDE SUMMARY (%):

	4, 85 D	7, 30 D
TEXTURE:		
Sand	—	—
Silt	15	15
Clay	85	85
COMPOSITION:		
Quartz	5	15
Rock Fragments	5	—
Clay	5	85
Nannofossils	85	—

SITE 660 HOLE A CORE 10 H CORED INTERVAL 4410.0-4419.5 mbsl; 77.8-87.3 mbsf

LITHOLOGIC DESCRIPTION

CLAY

Clay, brown (10YR 5/3), pale-brown (10YR 6/3), yellowish-brown (10YR 5/4), or light-yellowish-brown (10YR 6/4); massive to moderately bioturbated.

SMEAR SLIDE SUMMARY (%):

	3, 70 D
TEXTURE:	
Sand	—
Silt	5
Clay	95
COMPOSITION:	
Quartz	5
Clay	90
Accessory Minerals	5

SITE 660 HOLE A CORE 11 H CORED INTERVAL 4419.5-4429.0 mbsl; 87.3-96.8 mbsf

LITHOLOGIC DESCRIPTION

CLAY

Clay, light-yellowish-brown (10YR 6/4) or brown (7.5YR 5/4); massive to moderately bioturbated with minor amounts of silt in Section 6, 64–88 cm.

SMEAR SLIDE SUMMARY (%):

	2, 80 D	6, 80 M
TEXTURE:		
Sand	—	—
Silt	5	25
Clay	95	75
COMPOSITION:		
Quartz	5	20
Rock Fragments	Tr	75
Clay	95	—
Accessory Minerals	Tr	5

SITE 660 HOLE A CORE 12 H CORED INTERVAL 4429.0-4438.5 mbsl; 96.8-106.3 mbsf

LITHOLOGIC DESCRIPTION

CLAY

Clay, alternating units of light-yellowish-brown (10YR 6/4) with strong brown (7.5YR 5/6); massive to moderately bioturbated with minor amounts of silt in Section 3, 75 cm.

SMEAR SLIDE SUMMARY (%):

	1, 75 D	1, 90 D	3, 75 M	7, 36 X
TEXTURE:				
Sand	—	—	—	—
Silt	5	10	25	5
Clay	95	90	75	95
COMPOSITION:				
Quartz	5	8	20	25
Rock Fragments	Tr	—	—	—
Clay	95	90	75	95
Accessory Minerals	Tr	2	5	—

SITE 660 HOLE A CORE 13 H CORED INTERVAL 4438.5-4448.0 mbsl; 106.3-115.8 mbsf

TIME-ROCK UNIT	BIOSTRAT. ZONE/ FOSSIL CHARACTER: FORAMINIFERS	NANNOFOSSILS	RADIOLARIANS	DIATOMS	BENTHIC FORAM.	PALEOMAGNETICS	PHYS. PROPERTIES	CHEMISTRY	SECTION	METERS	GRAPHIC LITHOLOGY	DRILLING DISTURB.	SED. STRUCTURES	SAMPLES	LITHOLOGIC DESCRIPTION
	B	B		R/P	B			IC-0.01	1	0.5					CLAY
										1.0					Clay, alternating units of light-brown (7.5YR 6/4) with very pale-brown (10YR 7/3); massive to moderately bioturbated.
								IC-0.0	2						
								IC-0.0	3						
								IC-0.0	4						
								IC-0.0	5						
								IC-0.0	6						
									7						
									CC						

SITE 660 HOLE A CORE 14 H CORED INTERVAL 4448.0-4457.5 mbsl; 115.8-125.3 mbsf

TIME-ROCK UNIT	BIOSTRAT. ZONE/ FOSSIL CHARACTER: FORAMINIFERS	NANNOFOSSILS	RADIOLARIANS	DIATOMS	BENTHIC FORAM.	PALEOMAGNETICS	PHYS. PROPERTIES	CHEMISTRY	SECTION	METERS	GRAPHIC LITHOLOGY	DRILLING DISTURB.	SED. STRUCTURES	SAMPLES	LITHOLOGIC DESCRIPTION
MIDDLE EOCENE	B	B	C/G	F/P	B			IC-0.08	1	0.5				•	RADIOLARIAN OOZE
			P. mitra							1.0					Radiolarian ooze, alternating units of pale-yellow (2.5Y 7/4), very pale-brown (10YR 7/4) or yellow (10YR 7/6) and very dark-grayish-brown (10YR 3/2) or black (10YR 2/1) ooze; laminated to slightly bioturbated. Minor void in Section 4, 140–150 cm.
								IC-0.42	2					•	
									3					•	SMEAR SLIDE SUMMARY (%):
									4		VOID				
									5		VOID				TEXTURE:
								IC-0.25			VOID				Sand 20 20 5
								IC-0.42	6						Silt 60 60 90
									CC						Clay 20 20 5

	2, 110 D	2, 70 D	1, 65 D
TEXTURE:			
Sand	20	20	5
Silt	60	60	90
Clay	20	20	5
COMPOSITION:			
Radiolarians	100	96	95
Sponge spicules	—	—	5
Organic Matter	—	4	—

SITE 660 HOLE A CORE 15 H CORED INTERVAL 4457.5-4467.0 mbsl; 125.3-136.8 mbsf

TIME-ROCK UNIT: MIDDLE EOCENE

BIOSTRAT. ZONE/FOSSIL CHARACTER: FORAMINIFERS: B; NANNOFOSSILS: B; RADIOLARIANS: C/G *P. mitra*; DIATOMS: F/P *Hemiaulus gondolaformis*; BENTHIC FORAM.: B

PALEOMAGNETICS

PHYS. PROPERTIES

CHEMISTRY: ⊙IC-0.17; ⊙IC-0.42; ⊙IC-0.17

SECTION: 1, 2, 3, 4, 5, 6, 7, CC

METERS: 0.5, 1.0

GRAPHIC LITHOLOGY

DRILLING DISTURB.

SED. STRUCTURES

SAMPLES: *

LITHOLOGIC DESCRIPTION

RADIOLARIAN OOZE

Radiolarian ooze, alternating units of yellow or very pale-brown (10YR 8/6, 8/4, 7/4) with dark or very dark-grayish-brown (10YR 4/2, 3/2) to very dark-gray (5Y 3/1); slighty laminated in some sections, massively in others; rarely bioturbated; darker laminations contain abundant pyrite. Minor void in Section 4, 146–150 cm.

SMEAR SLIDE SUMMARY (%):

	4, 55 D
TEXTURE:	
Sand	25
Silt	75
Clay	–
COMPOSITION:	
Pyrite?	5
Radiolarians	90
Sponge spicules	5

SITE 660 HOLE A CORE 16 H CORED INTERVAL 4467.0-4476.5 mbsl; 134.8-144.0 mbsf

TIME-ROCK UNIT: MIDDLE EOCENE

BIOSTRAT. ZONE/FOSSIL CHARACTER: FORAMINIFERS: B; NANNOFOSSILS: B; RADIOLARIANS: C/G *P. mitra*; DIATOMS: R/P *Hemiaulus gondolaformis*; BENTHIC FORAM.: B

PALEOMAGNETICS

PHYS. PROPERTIES

CHEMISTRY: ⊙IC-0.08; ⊙IC-0.42; ⊙IC-0.17; ⊙IC-0.50

SECTION: 1, 2, 3, 4, 5, 6, CC

METERS: 0.5, 1.0

GRAPHIC LITHOLOGY: Void

DRILLING DISTURB.

SED. STRUCTURES

SAMPLES: *

LITHOLOGIC DESCRIPTION

RADIOLARIAN OOZE

Radiolarian ooze, very pale-brown (10YR 8/4, 8/3, 7/3) ooze, generally massive, with frequent dark (pyritic) layers. Color changes in Section 6, 91 cm, light-gray (5Y 7/2). Minor void in Section 1, 143–150 cm.

SMEAR SLIDE SUMMARY (%):

	6, 130 D
TEXTURE:	
Sand	–
Silt	–
Clay	–
COMPOSITION:	
Radiolarians	100

SITE 660 HOLE A CORE 17 X CORED INTERVAL 4476.5-4486.0 mbsl; 144.0-153.50 mbsf

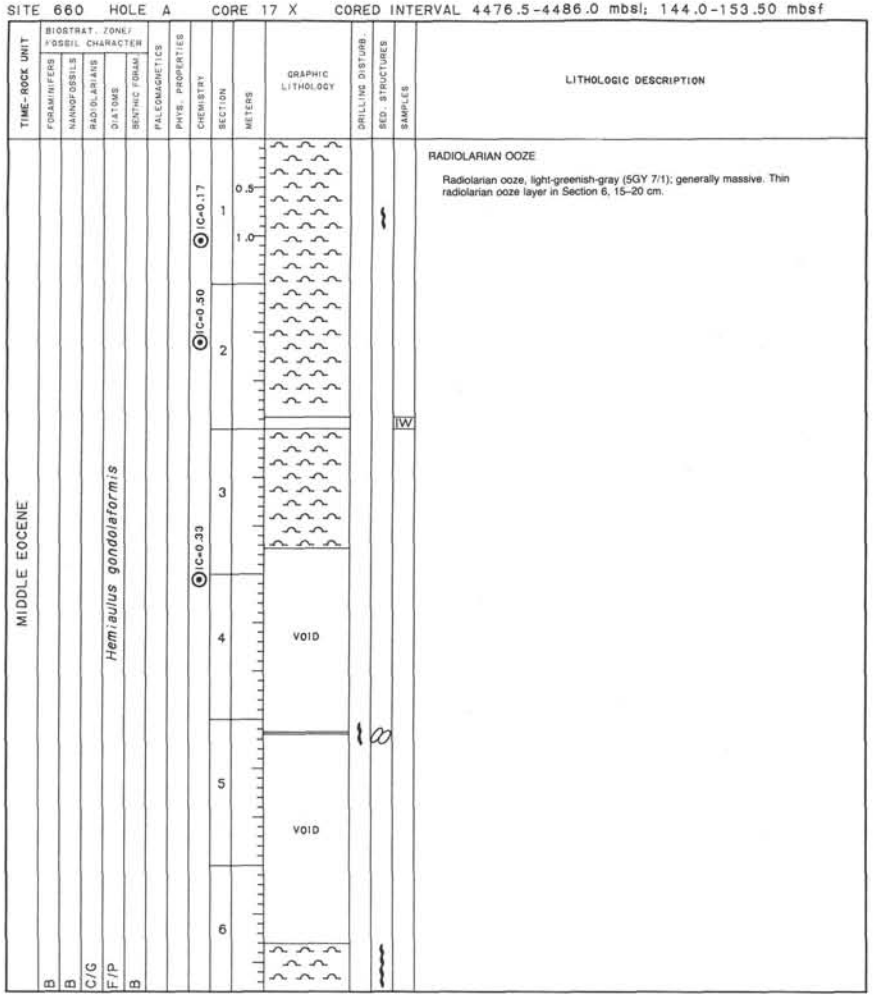

RADIOLARIAN OOZE

Radiolarian ooze, light-greenish-gray (5GY 7/1); generally massive. Thin radiolarian ooze layer in Section 6, 15–20 cm.

SITE 660 HOLE A CORE 18 X CORED INTERVAL 4486.0-4495. mbsl; 153.5-163.0 mbsf

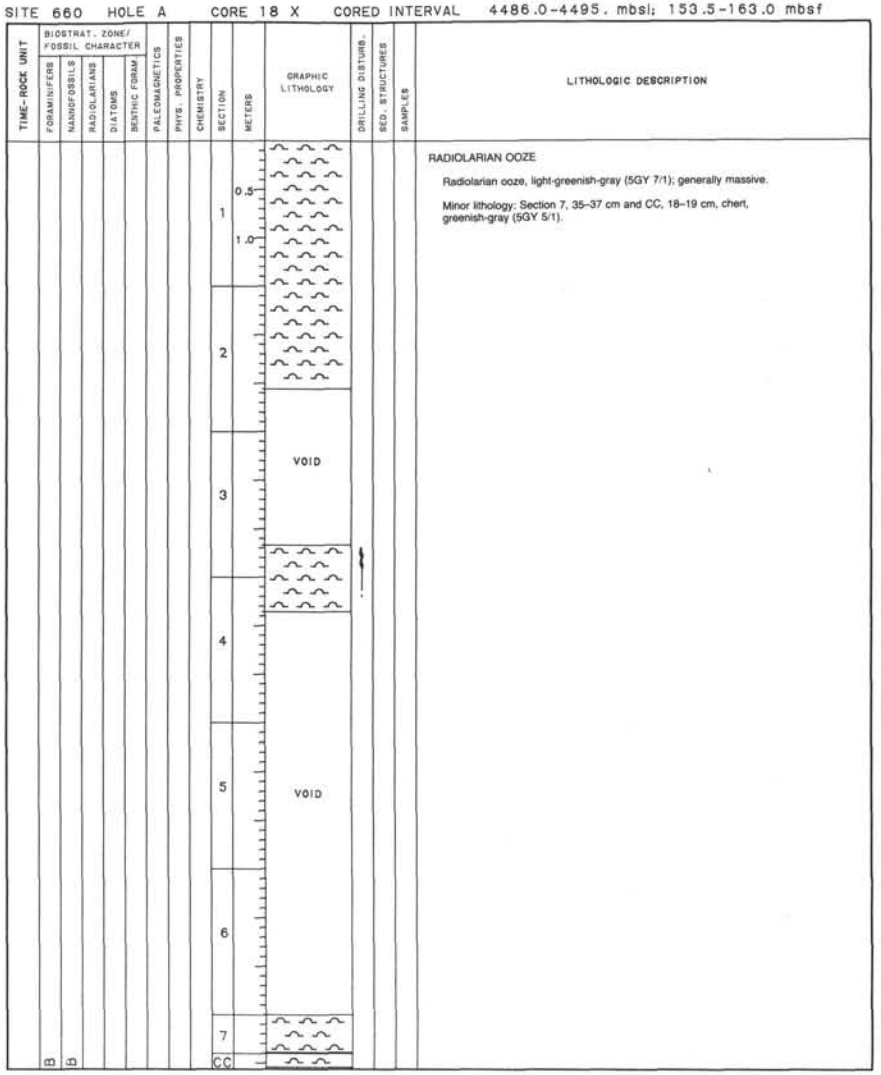

RADIOLARIAN OOZE

Radiolarian ooze, light-greenish-gray (5GY 7/1); generally massive.

Minor lithology: Section 7, 35–37 cm and CC, 18–19 cm, chert, greenish-gray (5GY 5/1).

SITE 660 HOLE A CORE 19 X CORED INTERVAL 4495.5-4505.0 mbsl; 163.0-164.90 mbsf

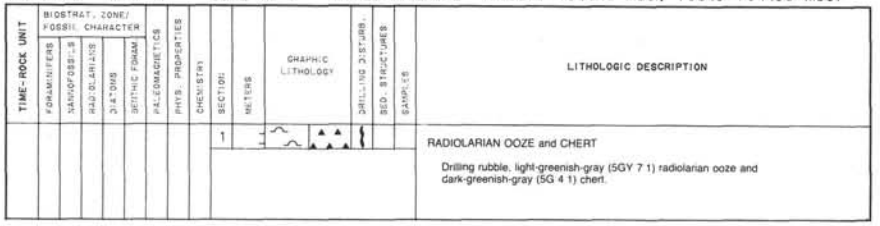

RADIOLARIAN OOZE and CHERT

Drilling rubble, light-greenish-gray (5GY 7 1) radiolarian ooze and dark-greenish-gray (5G 4 1) chert.

SITE 660 HOLE B CORE 1 H CORED INTERVAL 4332.3–4338.6 mbsl; 0–6.3 mbsf

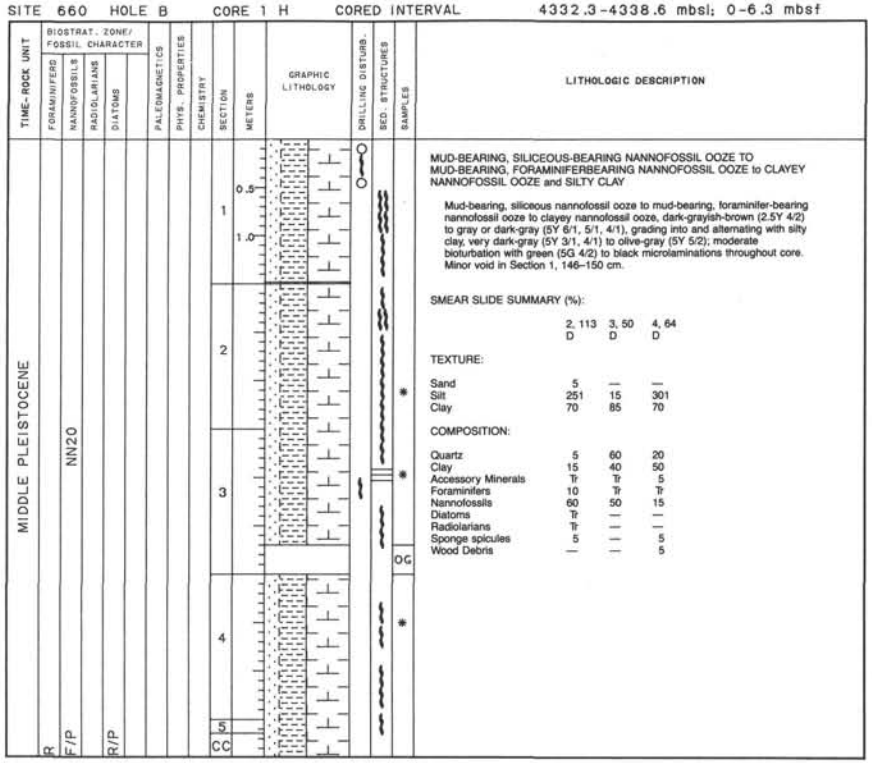

LITHOLOGIC DESCRIPTION

MUD-BEARING, SILICEOUS-BEARING NANNOFOSSIL OOZE TO MUD-BEARING, FORAMINIFERBEARING NANNOFOSSIL OOZE to CLAYEY NANNOFOSSIL OOZE and SILTY CLAY

Mud-bearing, siliceous nannofossil ooze to mud-bearing, foraminifer-bearing nannofossil ooze to clayey nannofossil ooze, dark-grayish-brown (2.5Y 4/2) to gray or dark-gray (5Y 6/1, 5/1, 4/1), grading into and alternating with silty clay, very dark-gray (5Y 3/1, 4/1) to olive-gray (5Y 5/2); moderate bioturbation with green (5G 4/2) to black microlaminations throughout core. Minor void in Section 1, 146–150 cm.

SMEAR SLIDE SUMMARY (%):

	2, 113 D	3, 50 D	4, 64 D
TEXTURE:			
Sand	5	—	—
Silt	251	15	301
Clay	70	85	70
COMPOSITION:			
Quartz	5	60	20
Clay	15	40	50
Accessory Minerals	Tr	Tr	5
Foraminifers	10	Tr	Tr
Nannofossils	60	50	15
Diatoms	Tr	—	—
Radiolarians	Tr	—	—
Sponge spicules	5	—	5
Wood Debris	—	—	5

SITE 660 HOLE B CORE 2 H CORED INTERVAL 4338.6–4348.1 mbsl; 6.3–15.8 mbsf

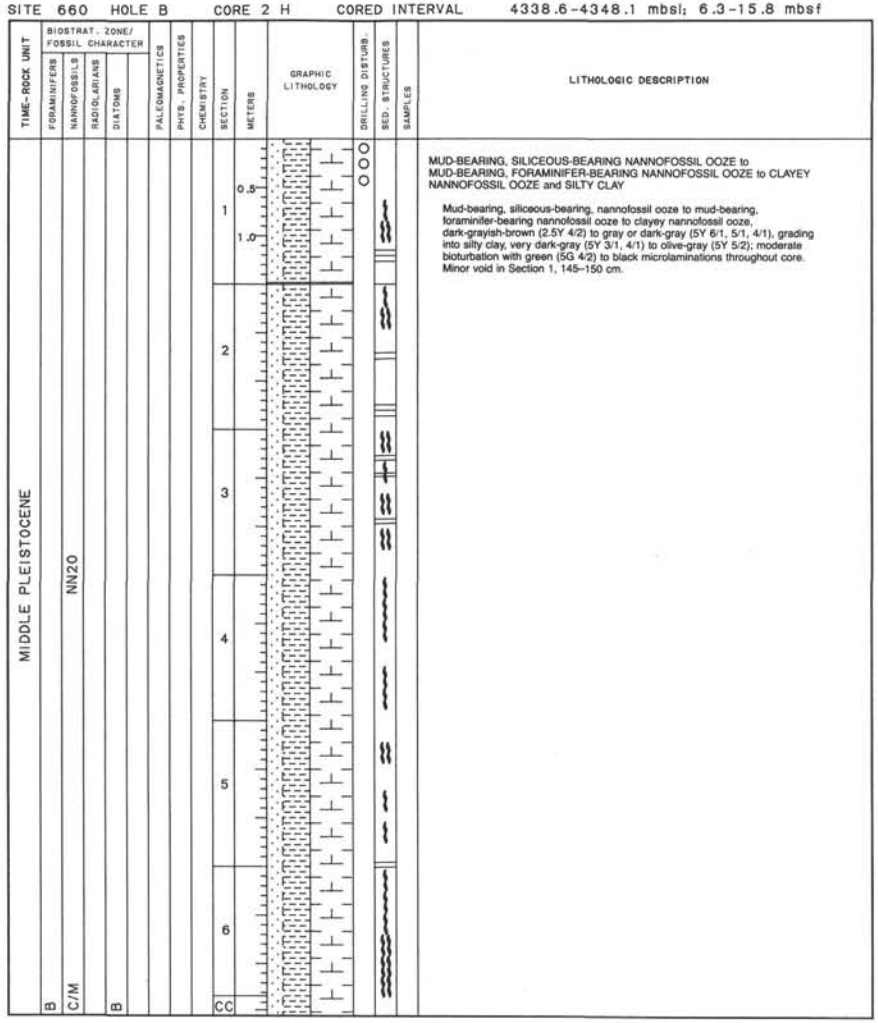

LITHOLOGIC DESCRIPTION

MUD-BEARING, SILICEOUS-BEARING NANNOFOSSIL OOZE to MUD-BEARING, FORAMINIFER-BEARING NANNOFOSSIL OOZE to CLAYEY NANNOFOSSIL OOZE and SILTY CLAY

Mud-bearing, siliceous-bearing, nannofossil ooze to mud-bearing, foraminifer-bearing nannofossil ooze to clayey nannofossil ooze, dark-grayish-brown (2.5Y 4/2) to gray or dark-gray (5Y 6/1, 5/1, 4/1), grading into silty clay, very dark-gray (5Y 3/1, 4/1) to olive-gray (5Y 5/2); moderate bioturbation with green (5G 4/2) to black microlaminations throughout core. Minor void in Section 1, 145–150 cm.

SITE 660 HOLE B CORE 3 H CORED INTERVAL 4348.1-4357.6 mbsl; 15.8-25.3 mbsf

LITHOLOGIC DESCRIPTION

MUD-BEARING, SILICEOUS-BEARING NANNOFOSSIL OOZE to MUD-BEARING, FORAMINIFER-BEARING NANNOFOSSIL OOZE to CLAYEY NANNOFOSSIL OOZE and SILTY CLAY

Mud-bearing, siliceous-bearing, nannofossil ooze to mud-bearing, foraminifer-bearing nannofossil ooze to clayey nannofossil ooze, dark-grayish-brown (2.5Y 4/2) to gray or dark-gray (5Y 6/1, 5/1, 4/1), grading into silty clay, very dark-gray (5Y 3/1, 4/1) to olive-gray (5Y 5/2); moderate bioturbation with green (5G 4/2) to black microlaminations throughout core.

SMEAR SLIDE SUMMARY (%):

	3, 14 D	3, 45 D	6, 26 D
TEXTURE:			
Sand	5	—	5
Silt	25	25	15
Clay	70	75	80
COMPOSITION:			
Quartz	30	20	5
Rock fragments	—	5	—
Clay	70	60	40
Accessory Minerals	—	5	—
Foraminifers	—	—	10
Nannofossils	—	—	45
Other	—	10	—

SITE 660 HOLE B CORE 4 H CORED INTERVAL 4357.6-4367.1 mbsl; 25.3-34.8 mbsf

LITHOLOGIC DESCRIPTION

MUD-BEARING, SILICEOUS-BEARING NANNOFOSSIL OOZE TO MUD-BEARING, FORAMINIFER-BEARING NANNOFOSSIL OOZE to CLAYEY NANNOFOSSIL OOZE and SILTY CLAY

Mud-bearing, siliceous-bearing nannofossil ooze to mud-bearing, foraminifer-bearing nannofossil ooze to clayey nannofossil ooze, dark-grayish-brown (2.5Y 4/2) to gray or dark-gray (5Y 6/1, 5/1, 4/1), grading into and alternating with silty clay, very dark-gray (5Y 3/1, 4/1) to olive-gray (5Y 5/2); moderate bioturbation with green (5G 4/2) to black microlaminations throughout core.

SMEAR SLIDE SUMMARY (%):

	3, 10 D	4, 50 D
TEXTURE:		
Sand	—	10
Silt	40	40
Clay	60	50
COMPOSITION:		
Quartz	40	20
Rock Fragments	5	5
Clay	50	30
Accessory Minerals	5	5
Nannofossils	—	40

SITE 660 HOLE B CORE 5 H CORED INTERVAL 4367.1-4376.6 mbsl; 34.8-44.3 mbsf

TIME-ROCK UNIT	BIOSTRAT. ZONE/ FOSSIL CHARACTER: FORAMINIFERS	NANNOFOSSILS	RADIOLARIANS	DIATOMS	PALEOMAGNETICS	PHYS. PROPERTIES	CHEMISTRY	SECTION	METERS	GRAPHIC LITHOLOGY	DRILLING DISTURB.	SED. STRUCTURES	SAMPLES
UPPER PLIOCENE / LOWER PLEISTOCENE	PL6	NN19						1	0.5				*
									1.0				
	A/M	NN18			○			2					
	A/M				○								
				B	●								
					●			3					
					●●								
					●●●			4					*
								5					
								6					
								7					

LITHOLOGIC DESCRIPTION

MUD-BEARING, SILICEOUS-BEARING NANNOFOSSIL OOZE to MUD-BEARING, FORAMINIFER-BEARING NANNOFOSSIL OOZE to CLAYEY NANNOFOSSIL OOZE and SILTY CLAY

Mud-bearing, siliceous-bearing nannofossil ooze to mud-bearing, foraminifer-bearing nannofossil ooze to clayey nannofossil ooze, dark-grayish-brown (2.5Y 4/2), gray or dark-gray (5Y 6/1, 5/1, 4/1) to light-gray (5Y 7/1), and grading into silty clay, very dark-gray (5Y 3/1, 4/1) to olive-gray (5Y 5/2); moderate bioturbation with green (5G 4/2) to black microlaminations throughout core.

SMEAR SLIDE SUMMARY (%):

	1, 100 D	4, 120 D
TEXTURE:		
Sand	10	—
Silt	30	30
Clay	60	70
COMPOSITION:		
Quartz	15	30
Rock Fragments	5	5
Clay	25	60
Accessory Minerals	5	—
Foraminifers	15	—
Nannofossils	35	5

SITE 660 HOLE B CORE 6 H CORED INTERVAL 4376.6-4386.1 mbsl; 44.3-53.8 mbsf

TIME-ROCK UNIT	BIOSTRAT. ZONE/ FOSSIL CHARACTER: FORAMINIFERS	NANNOFOSSILS	RADIOLARIANS	DIATOMS	PALEOMAGNETICS	PHYS. PROPERTIES	CHEMISTRY	SECTION	METERS	GRAPHIC LITHOLOGY	DRILLING DISTURB.	SED. STRUCTURES	SAMPLES
UPPER PLIOCENE	PL4	NN18						1	0.5				
									1.0				
	A/M	NN17						2		Void			*
	A/G	NN16						3					*
				B				4					
								5					
								6					
								CC					

LITHOLOGIC DESCRIPTION

MUD-BEARING, SILICEOUS-BEARING NANNOFOSSIL OOZE to MUD-BEARING, FORAMINIFER-BEARING NANNOFOSSIL OOZE to CLAYEY NANNOFOSSIL OOZE and SILTY CLAY

Mud-bearing, siliceous-bearing nannofossil ooze to mud-bearing, foraminifer-bearing nannofossil ooze to clayey nannofossil ooze, dark-grayish-brown (2.5Y 4/2), gray or dark-gray (5Y 6/1, 5/1, 4/1) to light-gray (5Y 7/1), and grading into silty clay, very dark-gray (5Y 3/1, 4/1) to olive-gray (5Y 5/2); moderate bioturbation. Minor void in Section 1, 141–150 cm.

SMEAR SLIDE SUMMARY (%):

	2, 120 D	3, 70 D
TEXTURE:		
Sand	—	10
Silt	30	20
Clay	70	70
COMPOSITION:		
Quartz	30	10
Rock Fragments	5	—
Clay	60	35
Accessory Minerals	5	—
Foraminifers	—	10
Nannofossils	—	45

SITE 660 HOLE B CORE 7 H CORED INTERVAL 4386.1-4395.6 mbsl; 53.8-63.3 mbsf

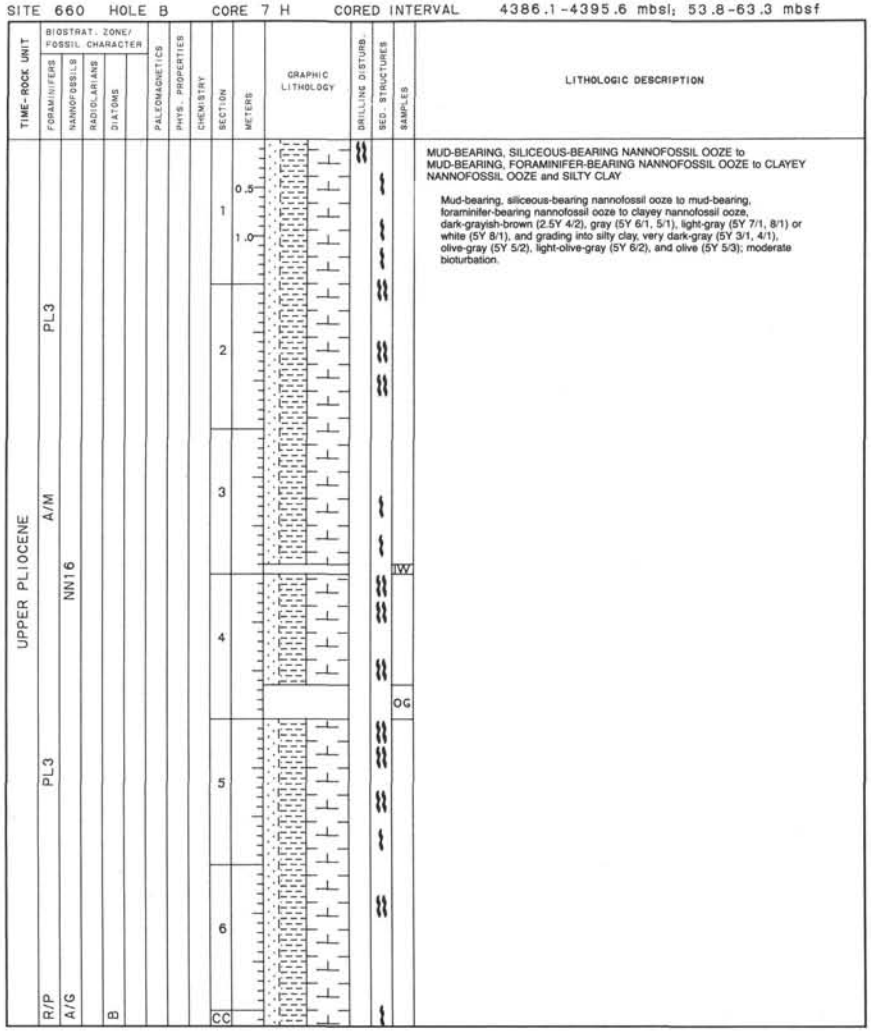

LITHOLOGIC DESCRIPTION

MUD-BEARING, SILICEOUS-BEARING NANNOFOSSIL OOZE to MUD-BEARING, FORAMINIFER-BEARING NANNOFOSSIL OOZE to CLAYEY NANNOFOSSIL OOZE and SILTY CLAY

Mud-bearing, siliceous-bearing nannofossil ooze to mud-bearing, foraminifer-bearing nannofossil ooze to clayey nannofossil ooze, dark-grayish-brown (2.5Y 4/2), gray (5Y 6/1, 5/1), light-gray (5Y 7/1, 8/1) or white (5Y 8/1), and grading into silty clay, very dark-gray (5Y 3/1, 4/1), olive-gray (5Y 5/2), light-olive-gray (5Y 6/2), and olive (5Y 5/3); moderate bioturbation.

SITE 660 HOLE B CORE 8 H CORED INTERVAL 4395.6-4405.1 mbsl; 63.3-72.8 mbsf

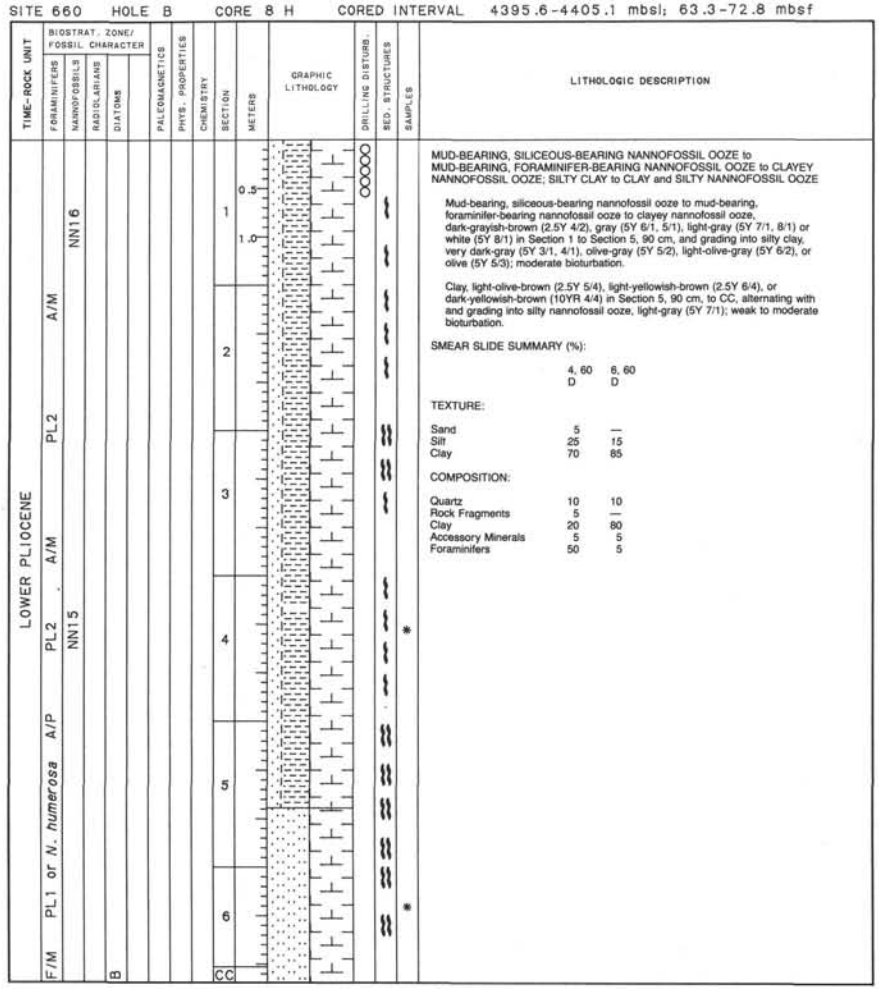

LITHOLOGIC DESCRIPTION

MUD-BEARING, SILICEOUS-BEARING NANNOFOSSIL OOZE to MUD-BEARING, FORAMINIFER-BEARING NANNOFOSSIL OOZE to CLAYEY NANNOFOSSIL OOZE; SILTY CLAY to CLAY and SILTY NANNOFOSSIL OOZE

Mud-bearing, siliceous-bearing nannofossil ooze to mud-bearing, foraminifer-bearing nannofossil ooze to clayey nannofossil ooze, dark-grayish-brown (2.5Y 4/2), gray (5Y 6/1, 5/1), light-gray (5Y 7/1, 8/1) or white (5Y 8/1) in Section 1 to Section 5, 90 cm, and grading into silty clay, very dark-gray (5Y 3/1, 4/1), olive-gray (5Y 5/2), light-olive-gray (5Y 6/2), or olive (5Y 5/3); moderate bioturbation.

Clay, light-olive-brown (2.5Y 5/4), light-yellowish-brown (2.5Y 6/4), or dark-yellowish-brown (10YR 4/4) in Section 5, 90 cm, to CC, alternating with and grading into silty nannofossil ooze, light-gray (5Y 7/1); weak to moderate bioturbation.

SMEAR SLIDE SUMMARY (%):

	4, 60 D	6, 60 D
TEXTURE:		
Sand	5	—
Silt	25	15
Clay	70	85
COMPOSITION:		
Quartz	10	10
Rock Fragments	5	—
Clay	20	80
Accessory Minerals	5	5
Foraminifers	50	5

SITE 660 HOLE B CORE 9 H CORED INTERVAL 4405.1-4414.6 mbsl; 72.8-82.3 mbsf

TIME-ROCK UNIT: UPPER MIOCENE / LOWER PLIOCENE

BIOSTRAT. ZONE/ FOSSIL CHARACTER: FORAMINIFERS: B; NANNOFOSSILS: NN11 A/G NN12 NN13-14; RADIOLARIANS: B; DIATOMS: B

PALEOMAGNETICS

PHYS. PROPERTIES

CHEMISTRY

SECTION: 1 2 3 4 5 6 7 CC

METERS: 0.5, 1.0

GRAPHIC LITHOLOGY

DRILLING DISTURB.

SED. STRUCTURES

SAMPLES

LITHOLOGIC DESCRIPTION

CLAY

Clay, pale-olive (5Y 6/3) to light-yellowish-brown (10YR 5/4); weak to moderate bioturbation.

SITE 660 HOLE B CORE 10 H CORED INTERVAL 4414.6-4424.1 mbsl; 82.3-91.8 mbsf

TIME-ROCK UNIT

BIOSTRAT. ZONE/ FOSSIL CHARACTER: FORAMINIFERS: B; NANNOFOSSILS: B; RADIOLARIANS: B; DIATOMS: B

PALEOMAGNETICS

PHYS. PROPERTIES

CHEMISTRY

SECTION: 1 2 3 4 5 6 CC

METERS: 0.5, 1.0

GRAPHIC LITHOLOGY

DRILLING DISTURB.

SED. STRUCTURES

SAMPLES: OC

LITHOLOGIC DESCRIPTION

CLAY

Clay, reddish-brown (5YR 5/4), light-reddish-brown (5YR 6/3), to light-yellowish-brown (10YR 5/4); weak to moderate bioturbation.

SITE 660 HOLE B CORE 11 H CORED INTERVAL 4424.1-4433.6 mbsl; 91.8-101.30 mbsf

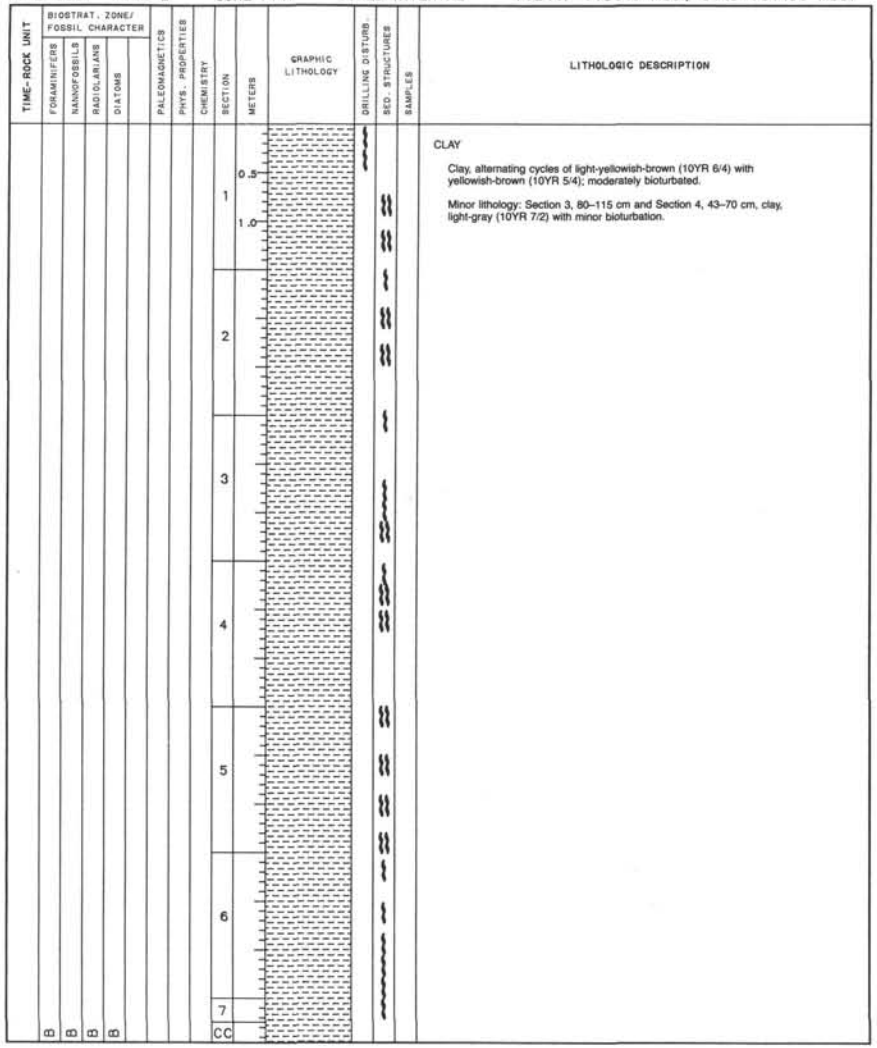

CLAY

Clay, alternating cycles of light-yellowish-brown (10YR 6/4) with yellowish-brown (10YR 5/4); moderately bioturbated.

Minor lithology: Section 3, 80–115 cm and Section 4, 43–70 cm, clay, light-gray (10YR 7/2) with minor bioturbation.

SITE 660 HOLE B CORE 12 H CORED INTERVAL 4433.6-4443.1 mbsl; 701.3-110.8 mbsf

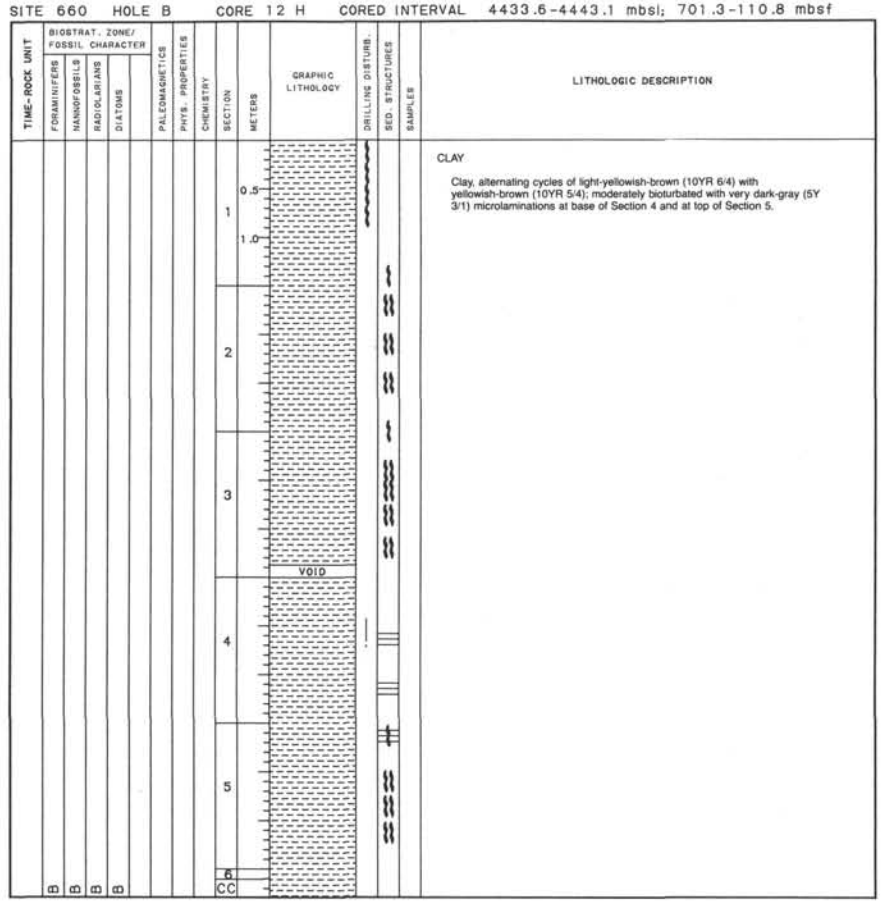

CLAY

Clay, alternating cycles of light-yellowish-brown (10YR 6/4) with yellowish-brown (10YR 5/4); moderately bioturbated with very dark-gray (5Y 3/1) microlaminations at base of Section 4 and at top of Section 5.

SITE 660 HOLE B CORE 13 H CORED INTERVAL 4443.1–4452.6 mbsl; 110.8–120.3 mbsf

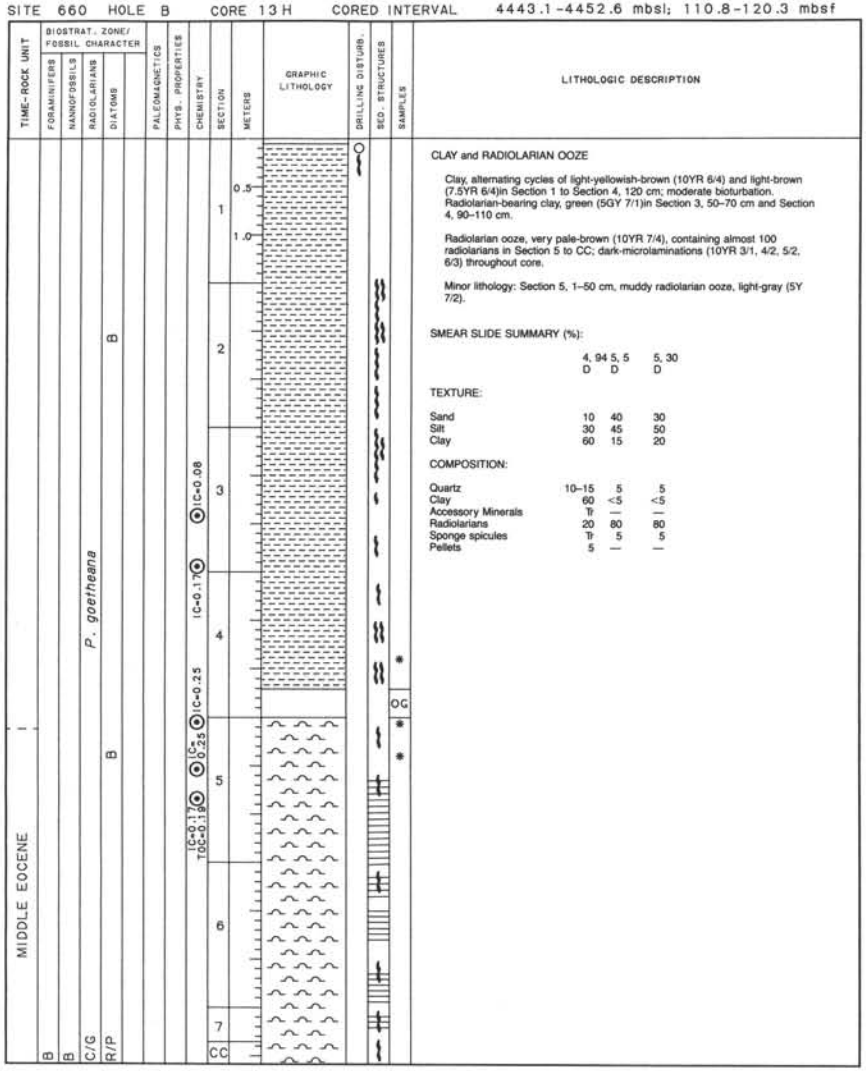

CLAY and RADIOLARIAN OOZE

Clay, alternating cycles of light-yellowish-brown (10YR 6/4) and light-brown (7.5YR 6/4)in Section 1 to Section 4, 120 cm; moderate bioturbation. Radiolarian-bearing clay, green (5GY 7/1)in Section 3, 50–70 cm and Section 4, 90–110 cm.

Radiolarian ooze, very pale-brown (10YR 7/4), containing almost 100 radiolarians in Section 5 to CC; dark-microlaminations (10YR 3/1, 4/2, 5/2, 6/3) throughout core.

Minor lithology: Section 5, 1–50 cm, muddy radiolarian ooze, light-gray (5Y 7/2).

SMEAR SLIDE SUMMARY (%):

	4, 94 D	5, 5 D	5, 30 D
TEXTURE:			
Sand	10	40	30
Silt	30	45	50
Clay	60	15	20
COMPOSITION:			
Quartz	10–15	5	5
Clay	60	<5	<5
Accessory Minerals	Tr	—	—
Radiolarians	20	80	80
Sponge spicules	Tr	5	5
Pellets	5	—	—

SITE 660 HOLE B CORE 14 H CORED INTERVAL 4452.6–4462.1 mbsl; 120.3–129.8 mbsf

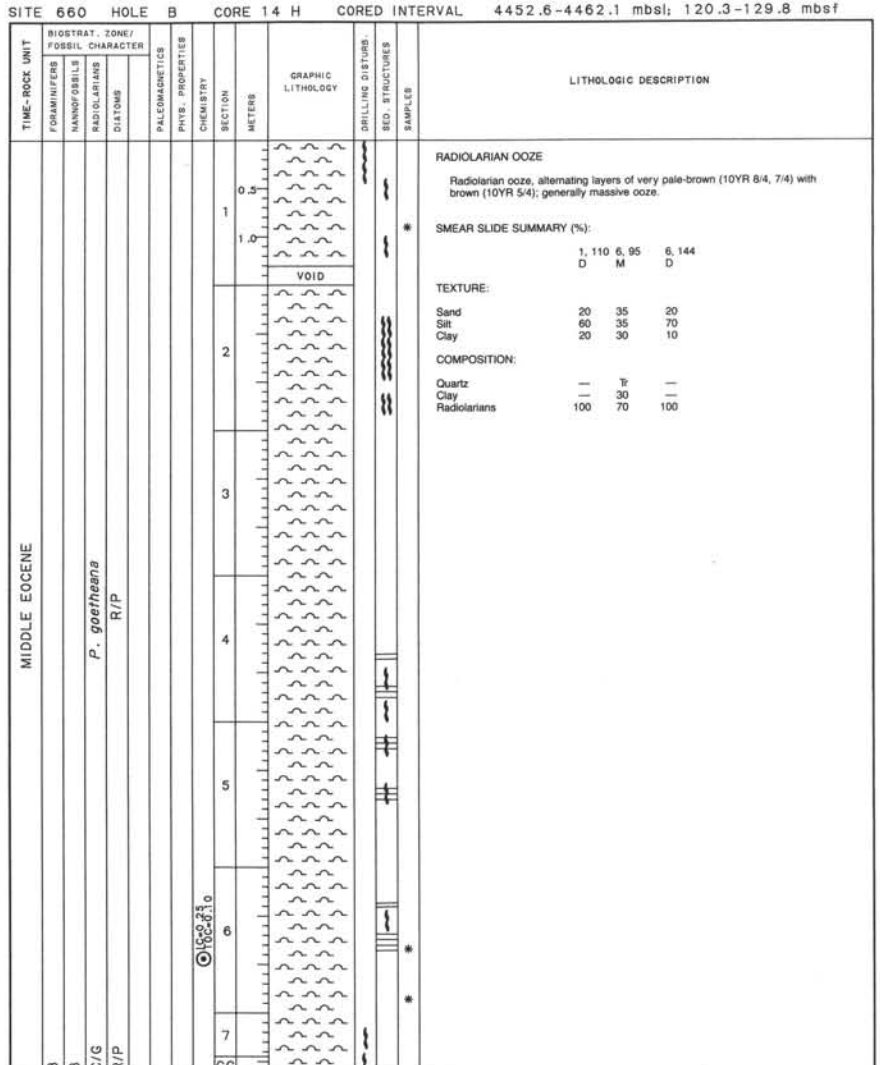

RADIOLARIAN OOZE

Radiolarian ooze, alternating layers of very pale-brown (10YR 8/4, 7/4) with brown (10YR 5/4); generally massive ooze.

SMEAR SLIDE SUMMARY (%):

	1, 110 D	6, 95 M	6, 144 D
TEXTURE:			
Sand	20	35	20
Silt	60	35	70
Clay	20	30	10
COMPOSITION:			
Quartz	—	Tr	—
Clay	—	30	—
Radiolarians	100	70	100

SITE 660 HOLE B CORE 15 X CORED INTERVAL 4462.1-4471.6 mbsl; 129.8-139.3 mbsf

SITE 660 HOLE B CORE 16 X CORED INTERVAL 4471.6-4481.1 mbsl; 139.3-148.8 mbsf

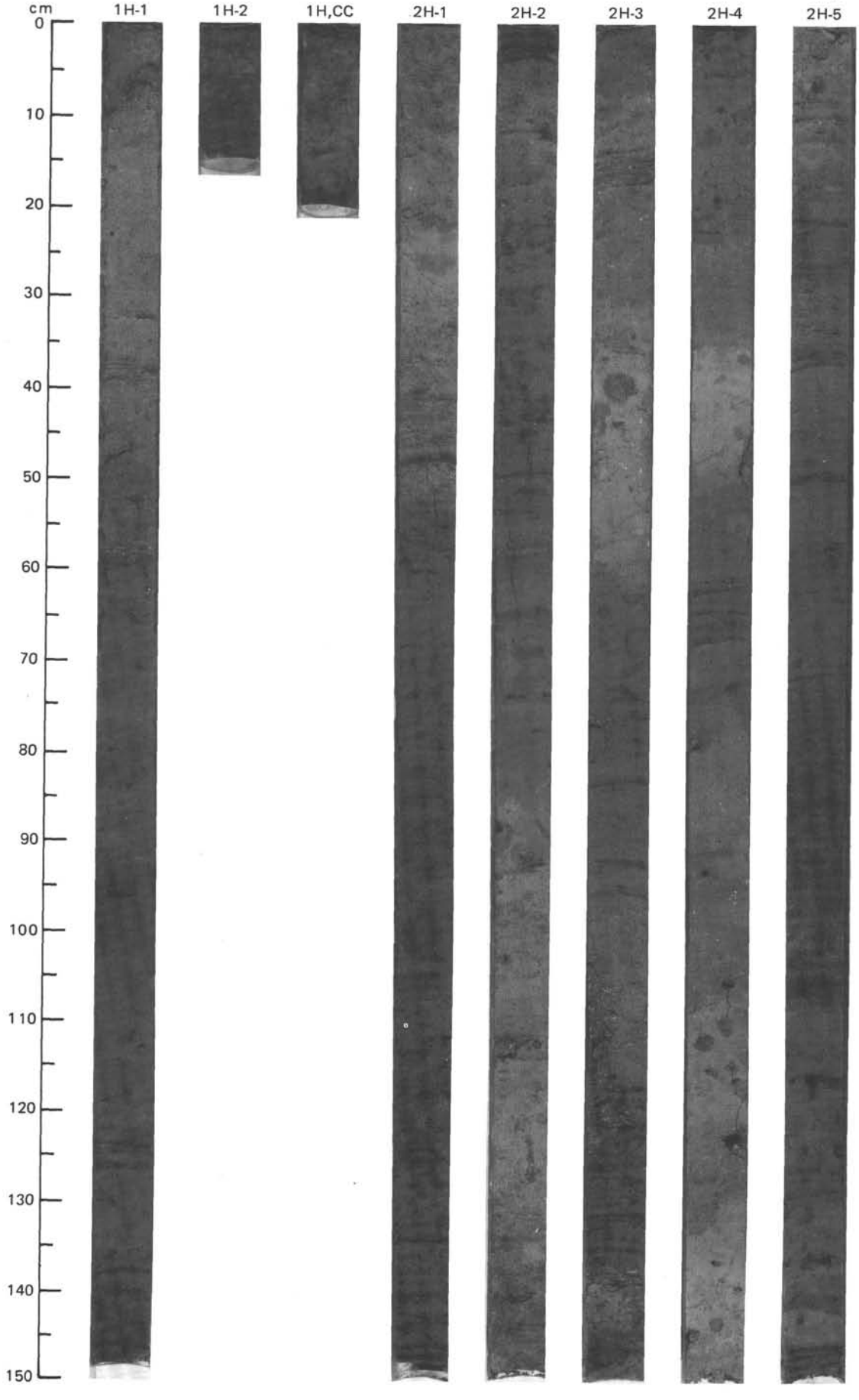
cm
0
10
20
30
40
50
60
70
80
90
100
110
120
130
140
150
1H-1
1H-2
1H,CC
2H-1
2H-2
2H-3
2H-4
2H-5

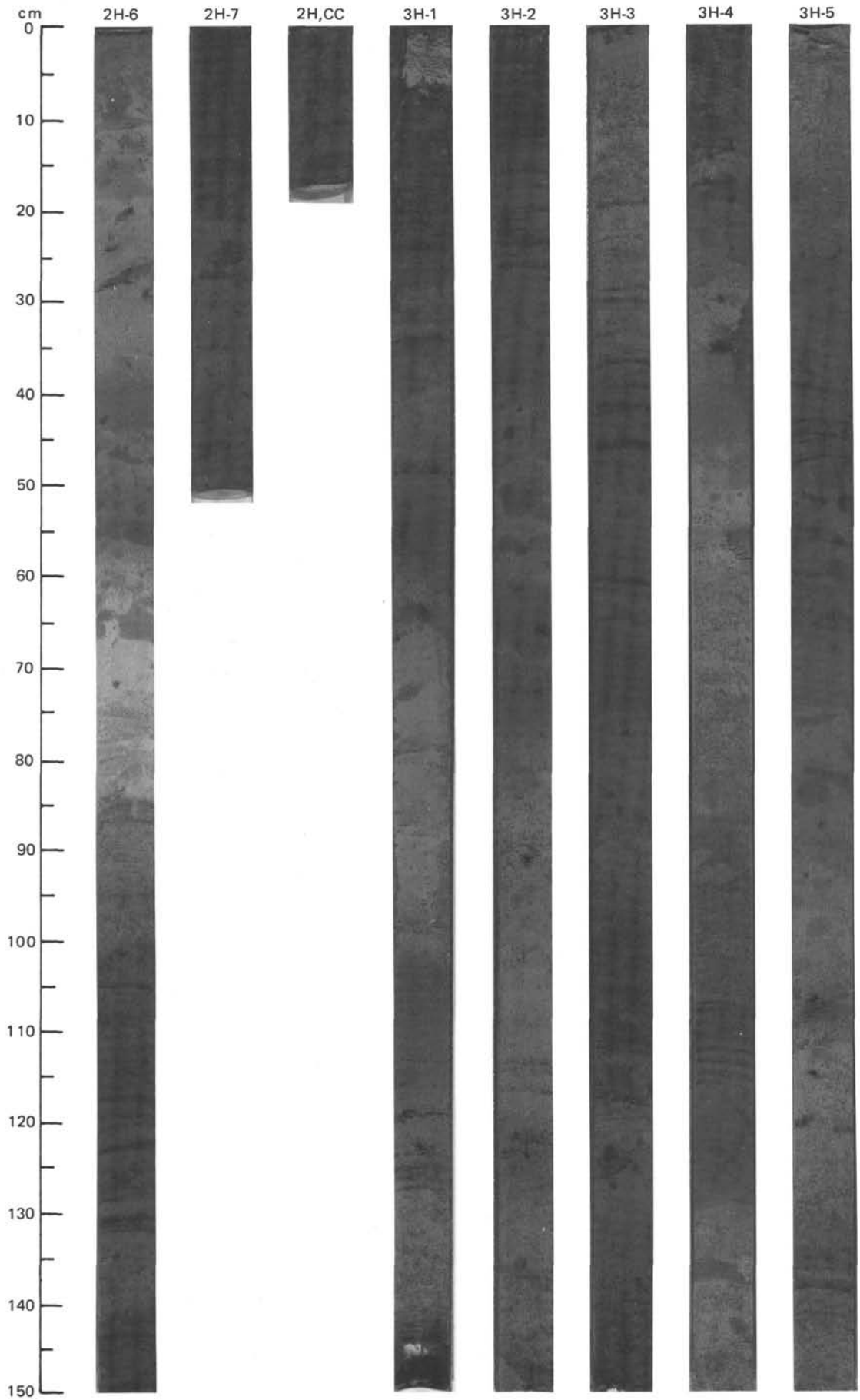
cm
2H-6
2H-7
2H,CC
3H-1
3H-2
3H-3
3H-4
3H-5
0
10
20
30
40
50
60
70
80
90
100
110
120
130
140
150

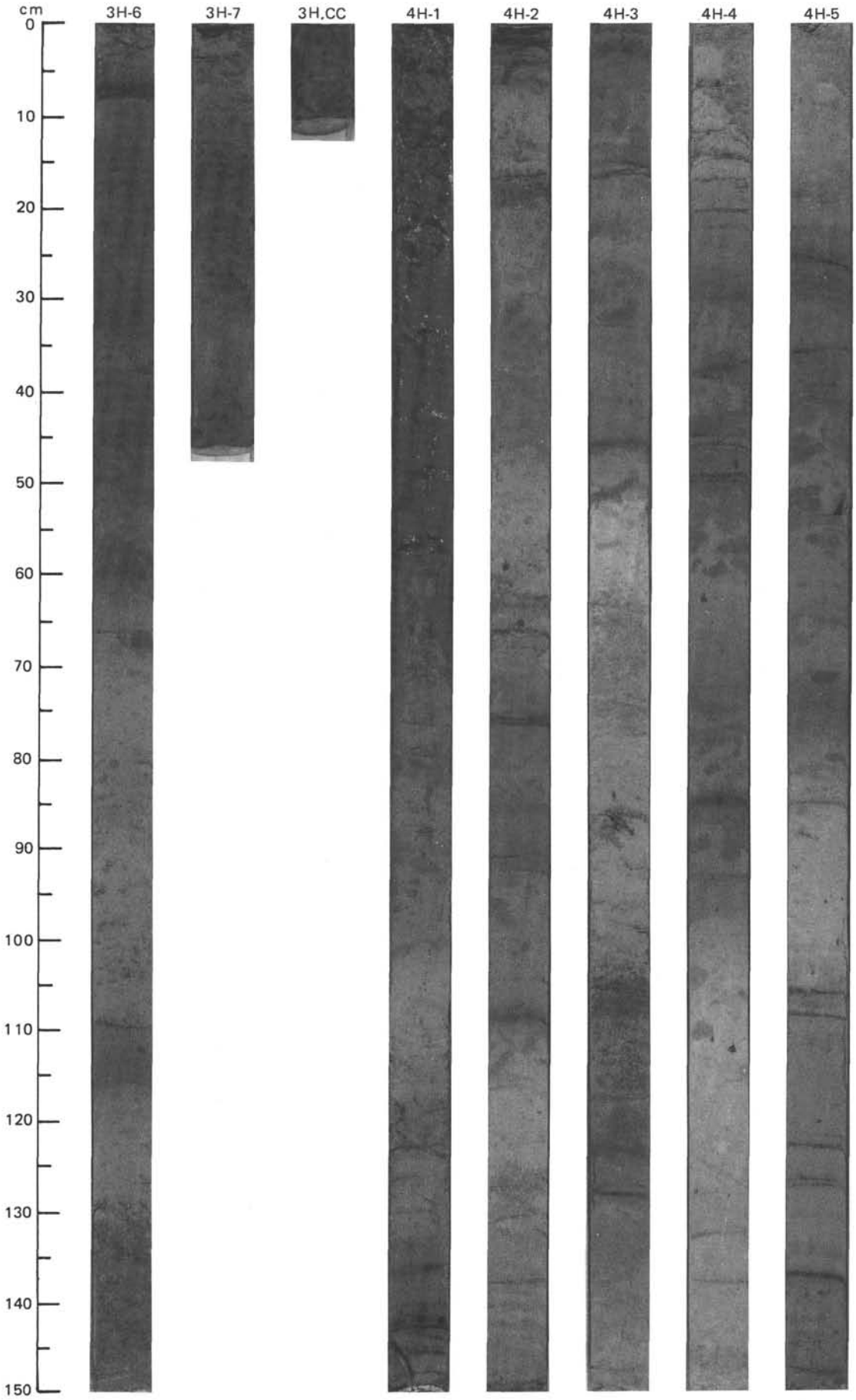
cm
0
10
20
30
40
50
60
70
80
90
100
110
120
130
140
150
3H-6
3H-7
3H,CC
4H-1
4H-2
4H-3
4H-4
4H-5

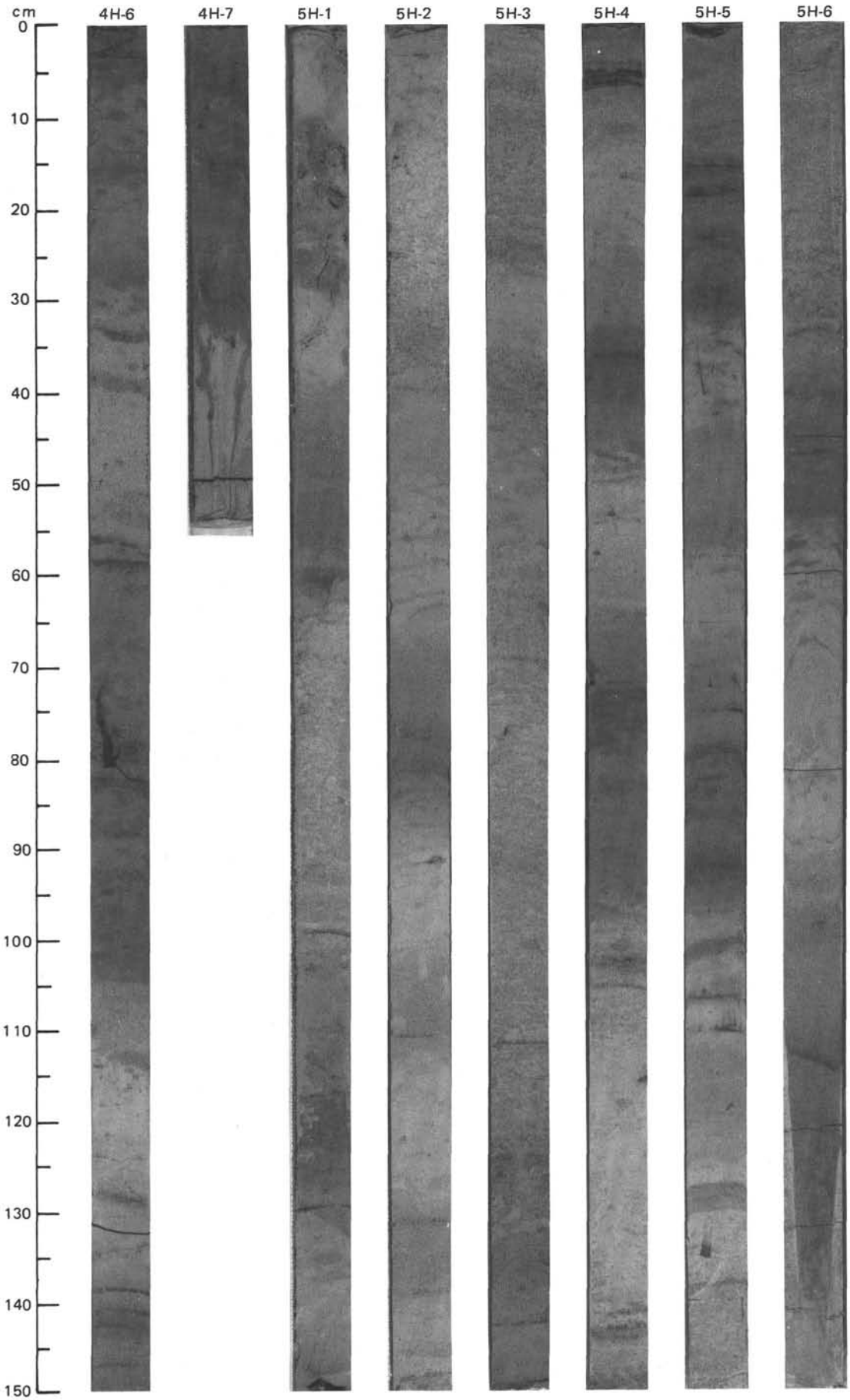
cm
0
10
20
30
40
50
60
70
80
90
100
110
120
130
140
150
4H-6
4H-7
5H-1
5H-2
5H-3
5H-4
5H-5
5H-6

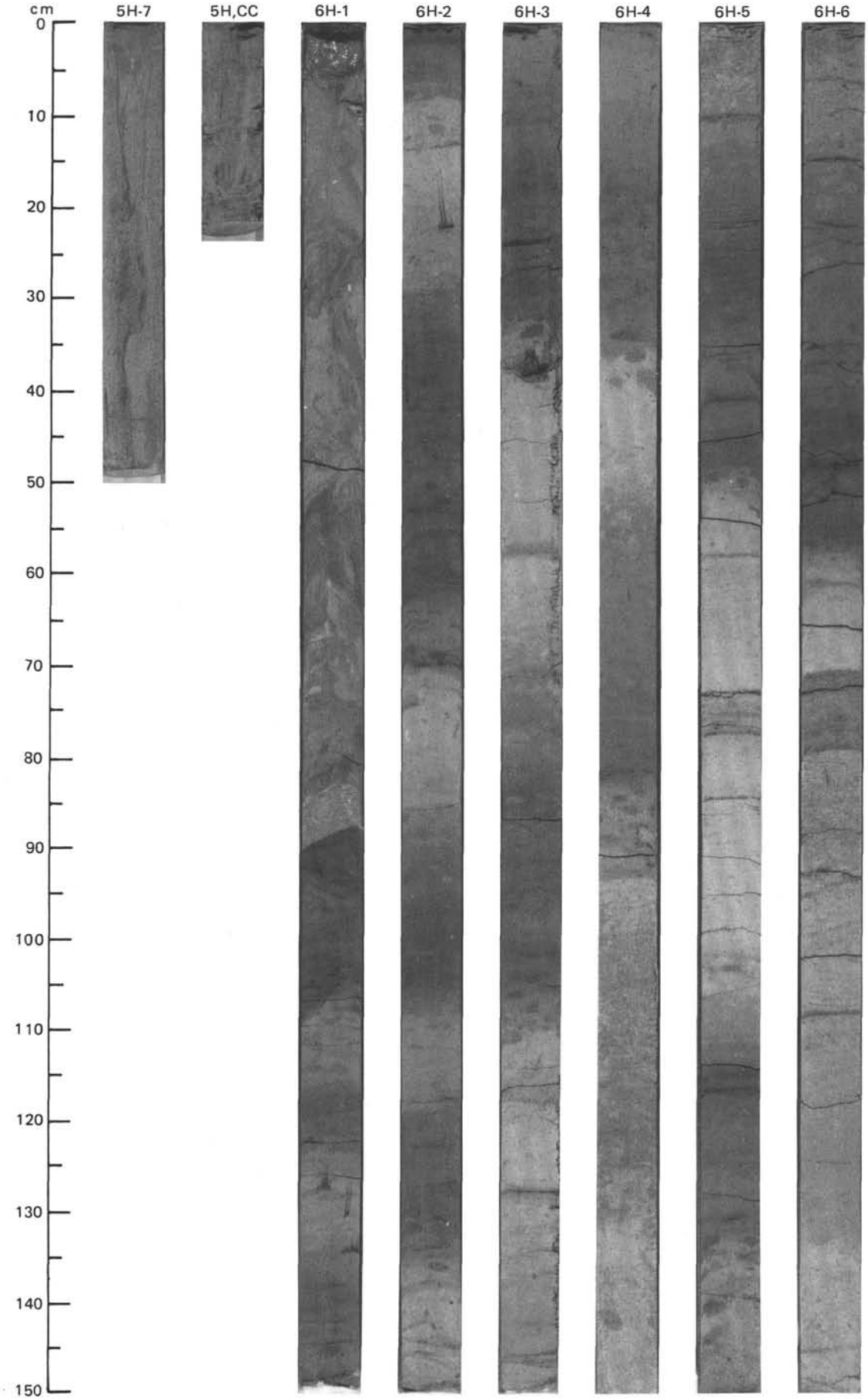
cm
0
10
20
30
40
50
60
70
80
90
100
110
120
130
140
150
5H-7
5H,CC
6H-1
6H-2
6H-3
6H-4
6H-5
6H-6

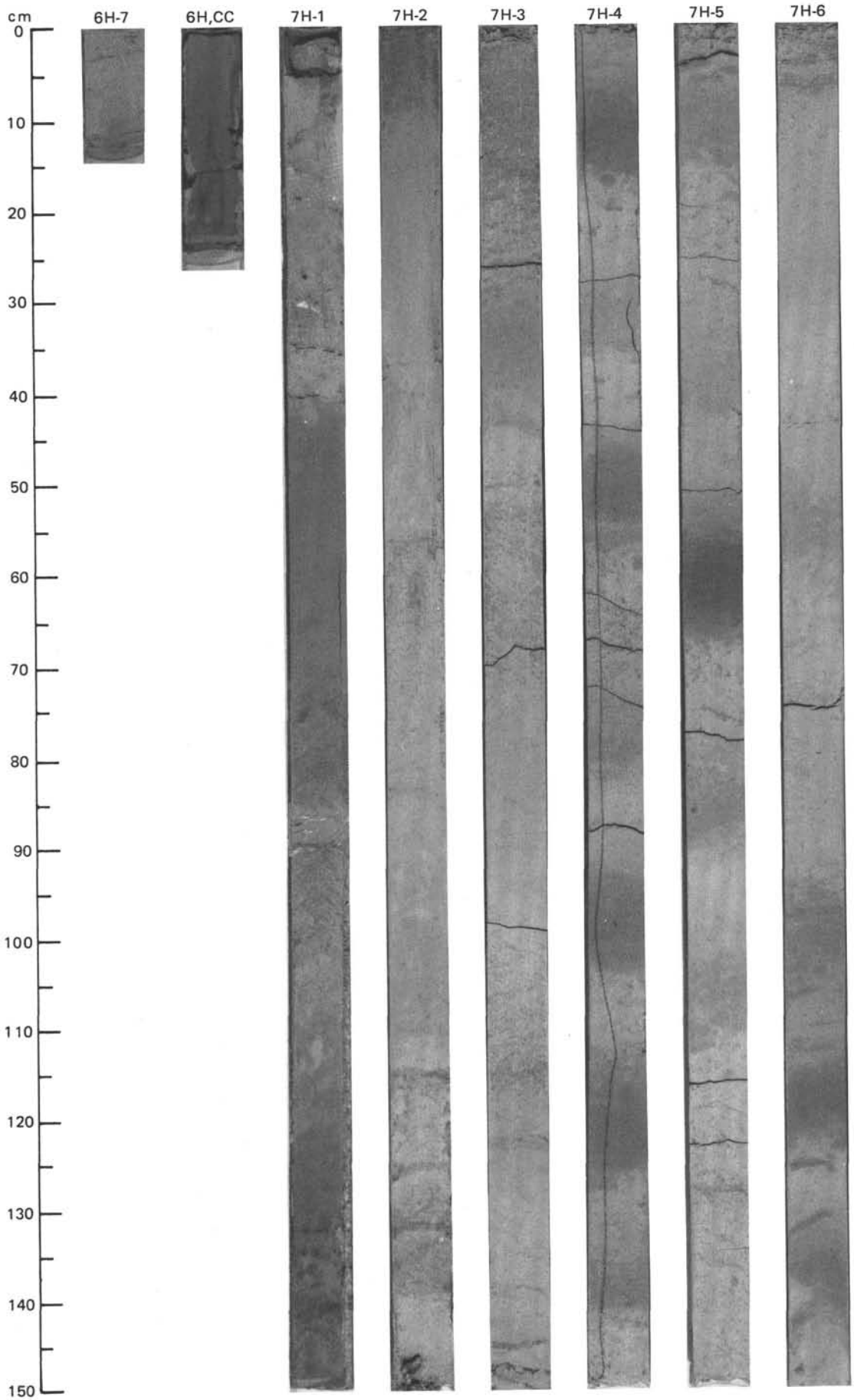
cm
0
10
20
30
40
50
60
70
80
90
100
110
120
130
140
150
6H-7
6H,CC
7H-1
7H-2
7H-3
7H-4
7H-5
7H-6

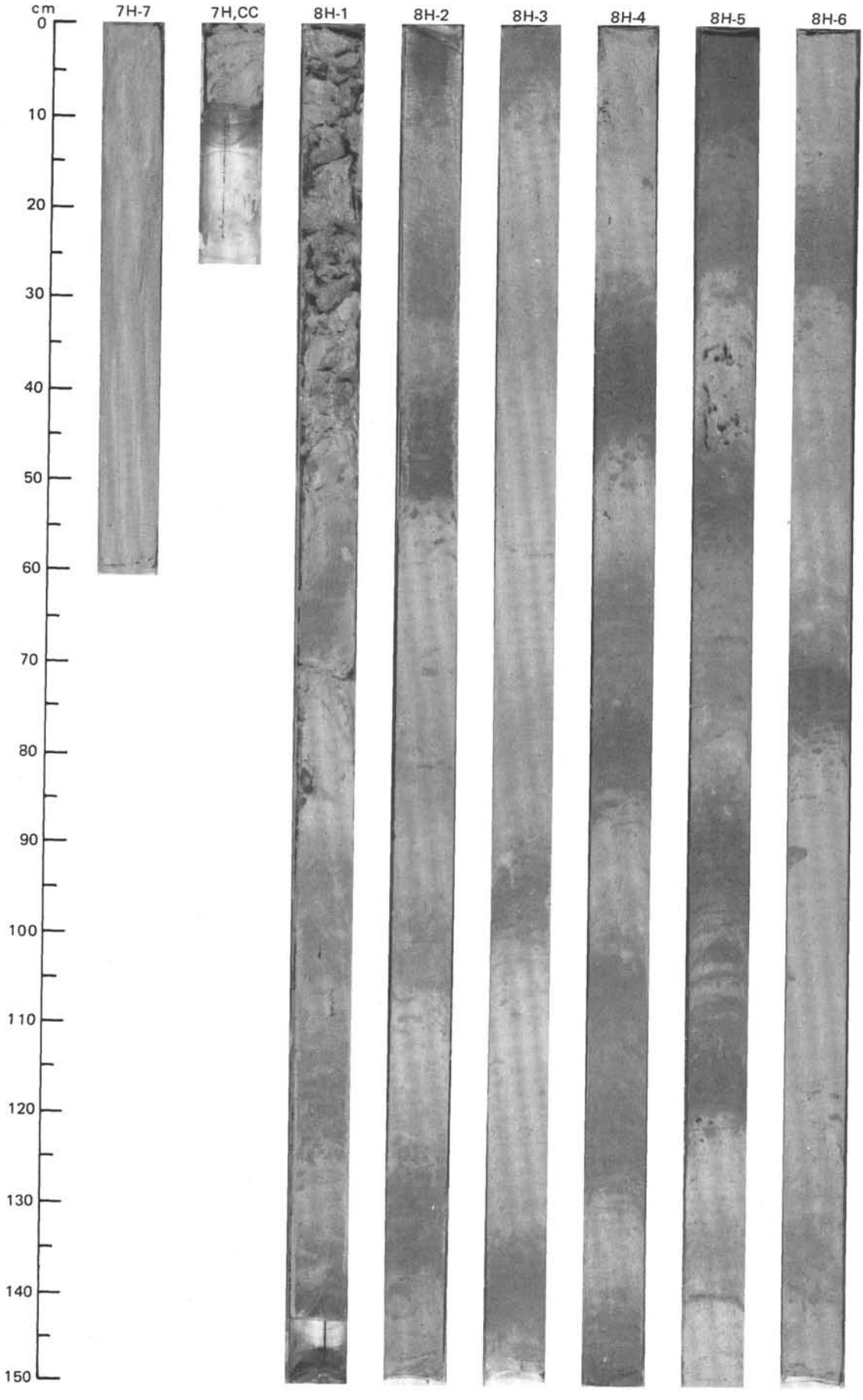
cm
0
10
20
30
40
50
60
70
80
90
100
110
120
130
140
150
7H-7
7H,CC
8H-1
8H-2
8H-3
8H-4
8H-5
8H-6

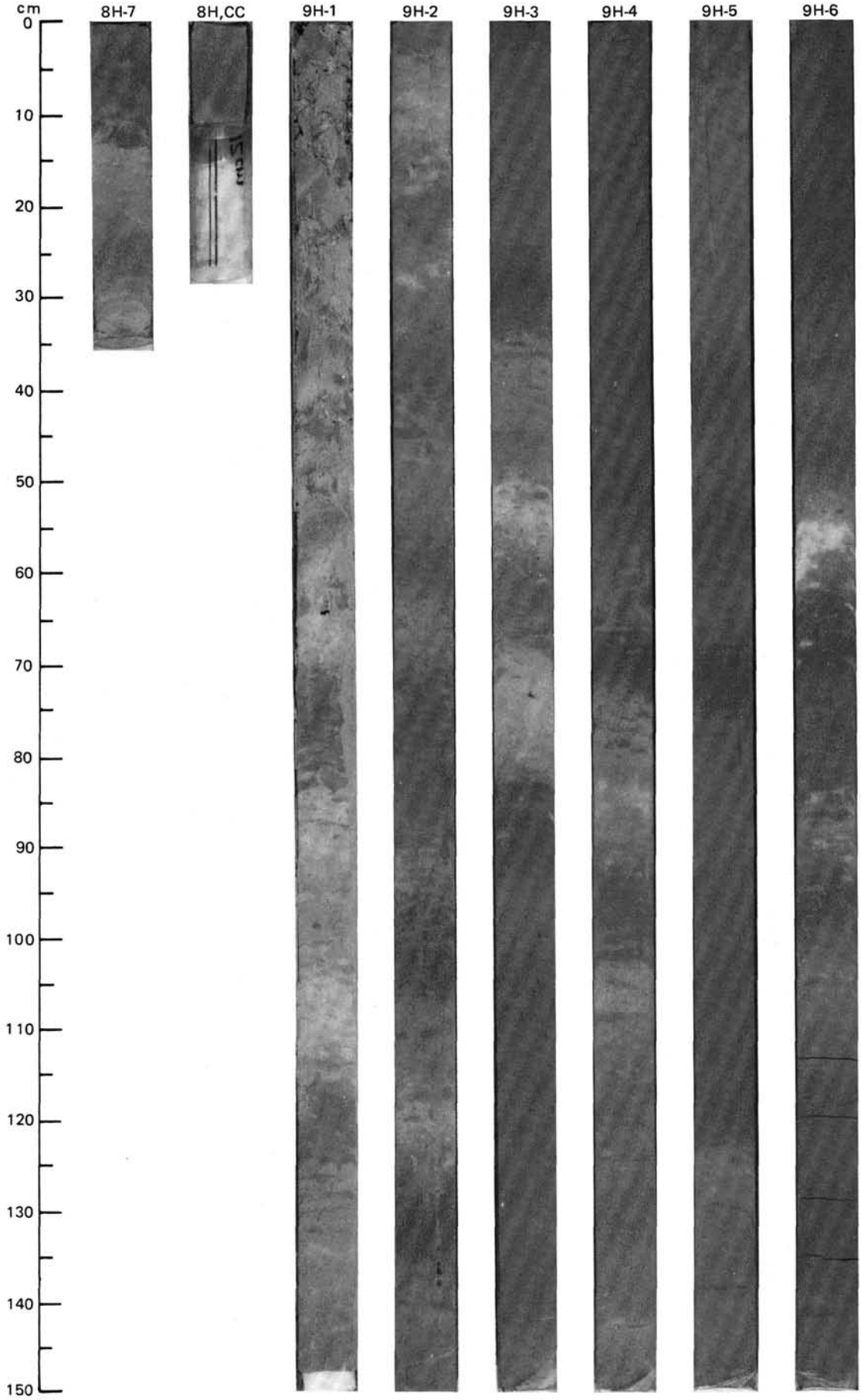
cm
8H-7
8H,CC
9H-1
9H-2
9H-3
9H-4
9H-5
9H-6
0
10
20
30
40
50
60
70
80
90
100
110
120
130
140
150

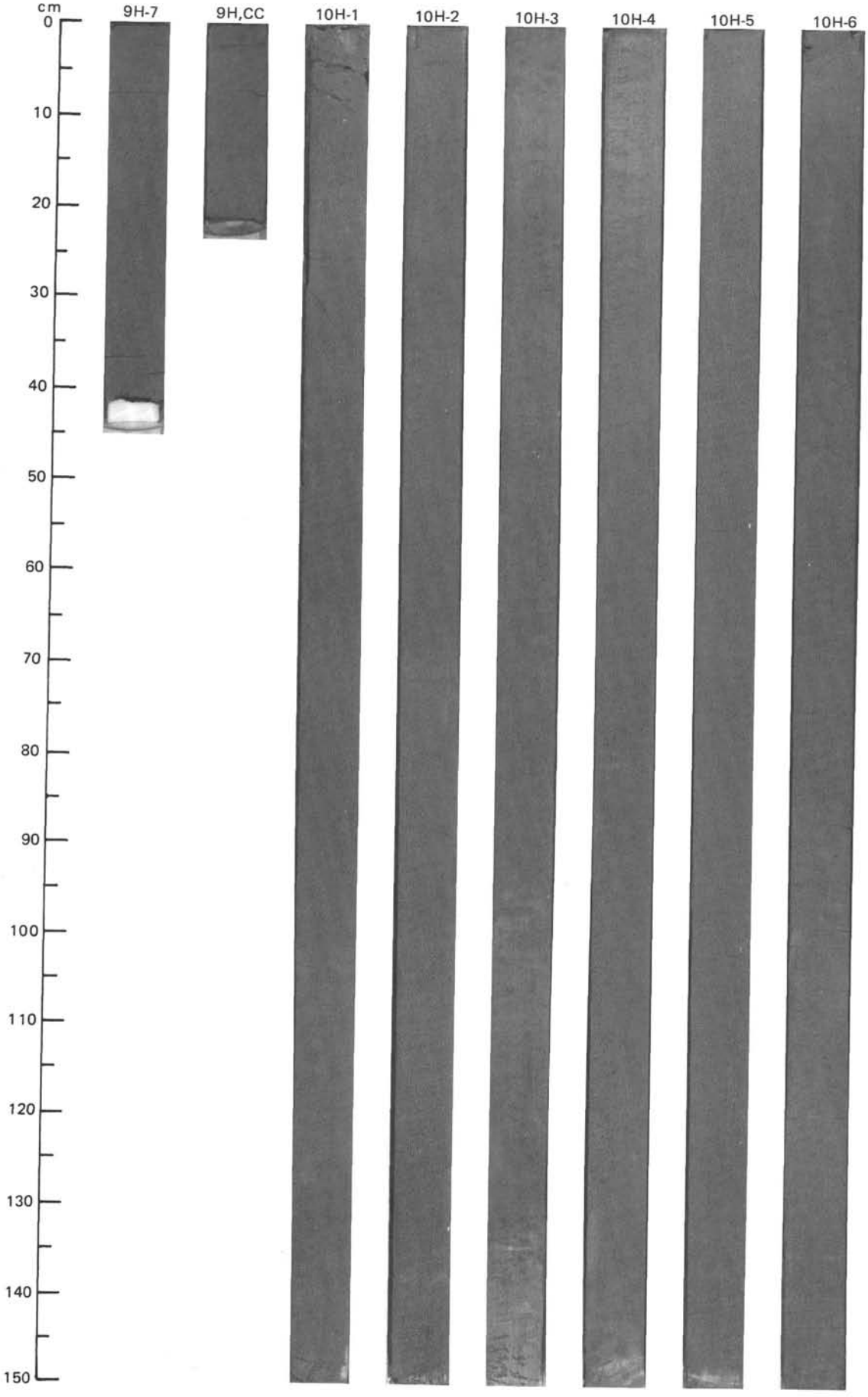
cm
0
10
20
30
40
50
60
70
80
90
100
110
120
130
140
150
9H-7
9H,CC
10H-1
10H-2
10H-3
10H-4
10H-5
10H-6

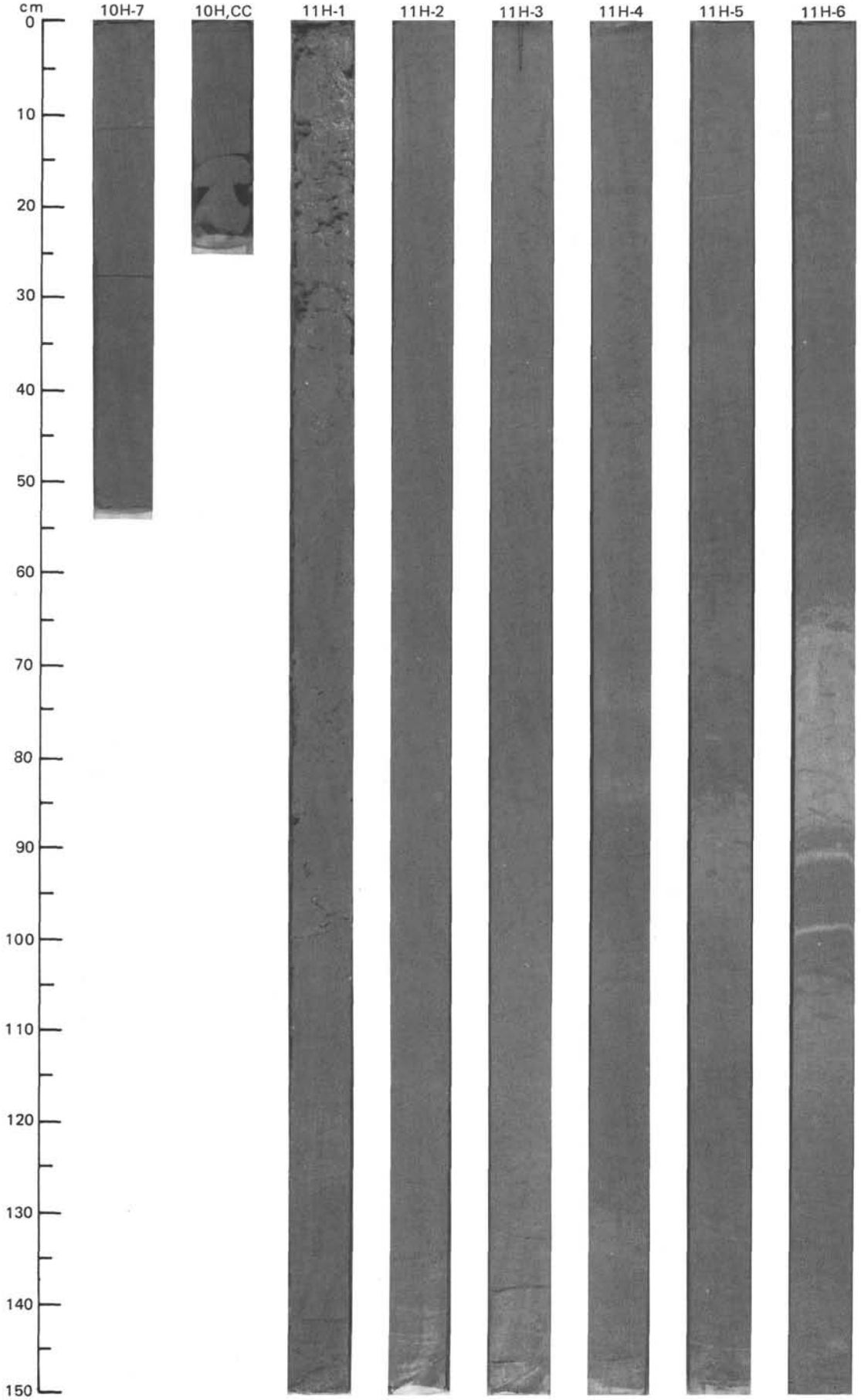
cm
0
10
20
30
40
50
60
70
80
90
100
110
120
130
140
150
10H-7
10H,CC
11H-1
11H-2
11H-3
11H-4
11H-5
11H-6

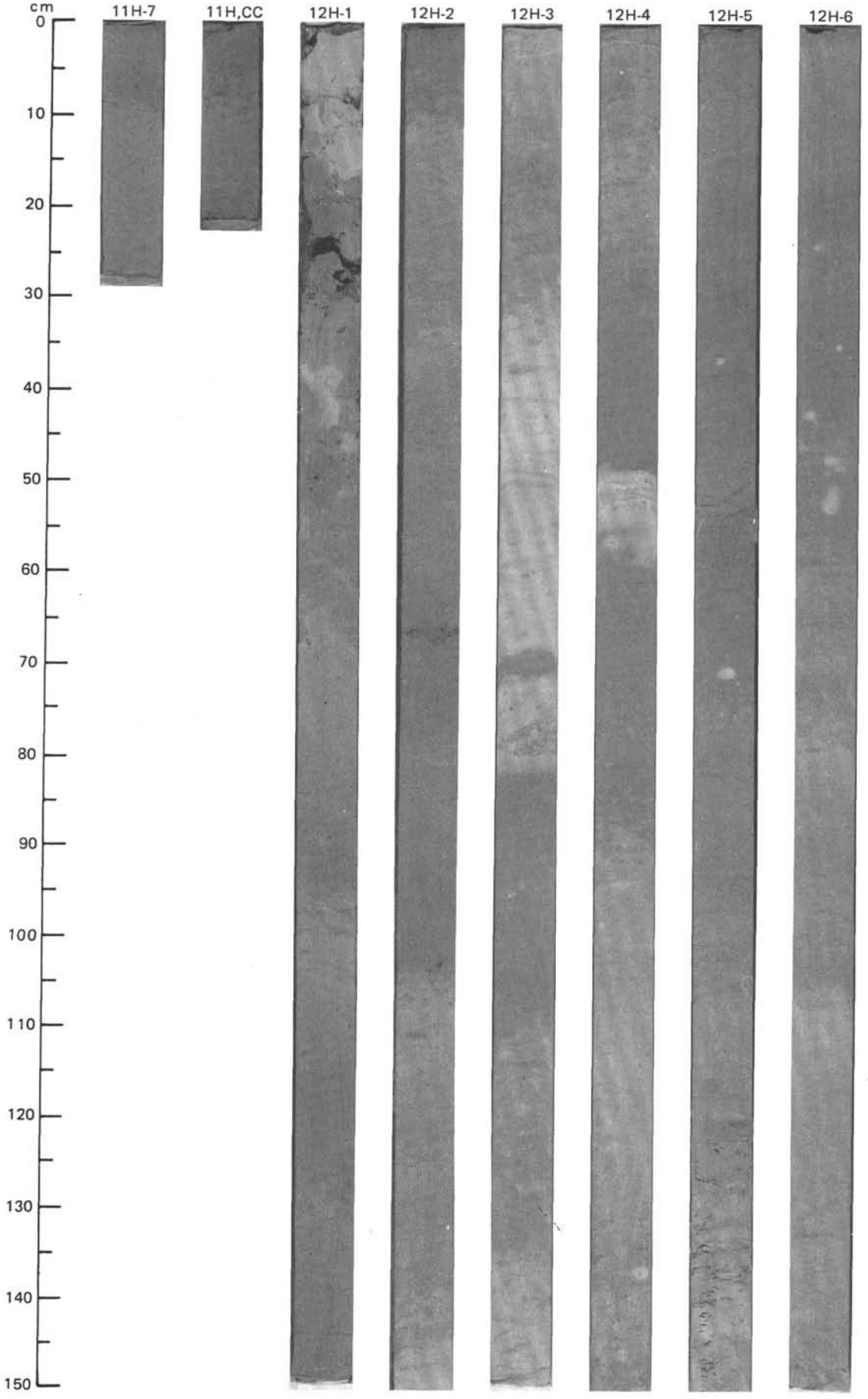
cm
0
10
20
30
40
50
60
70
80
90
100
110
120
130
140
150
11H-7
11H,CC
12H-1
12H-2
12H-3
12H-4
12H-5
12H-6

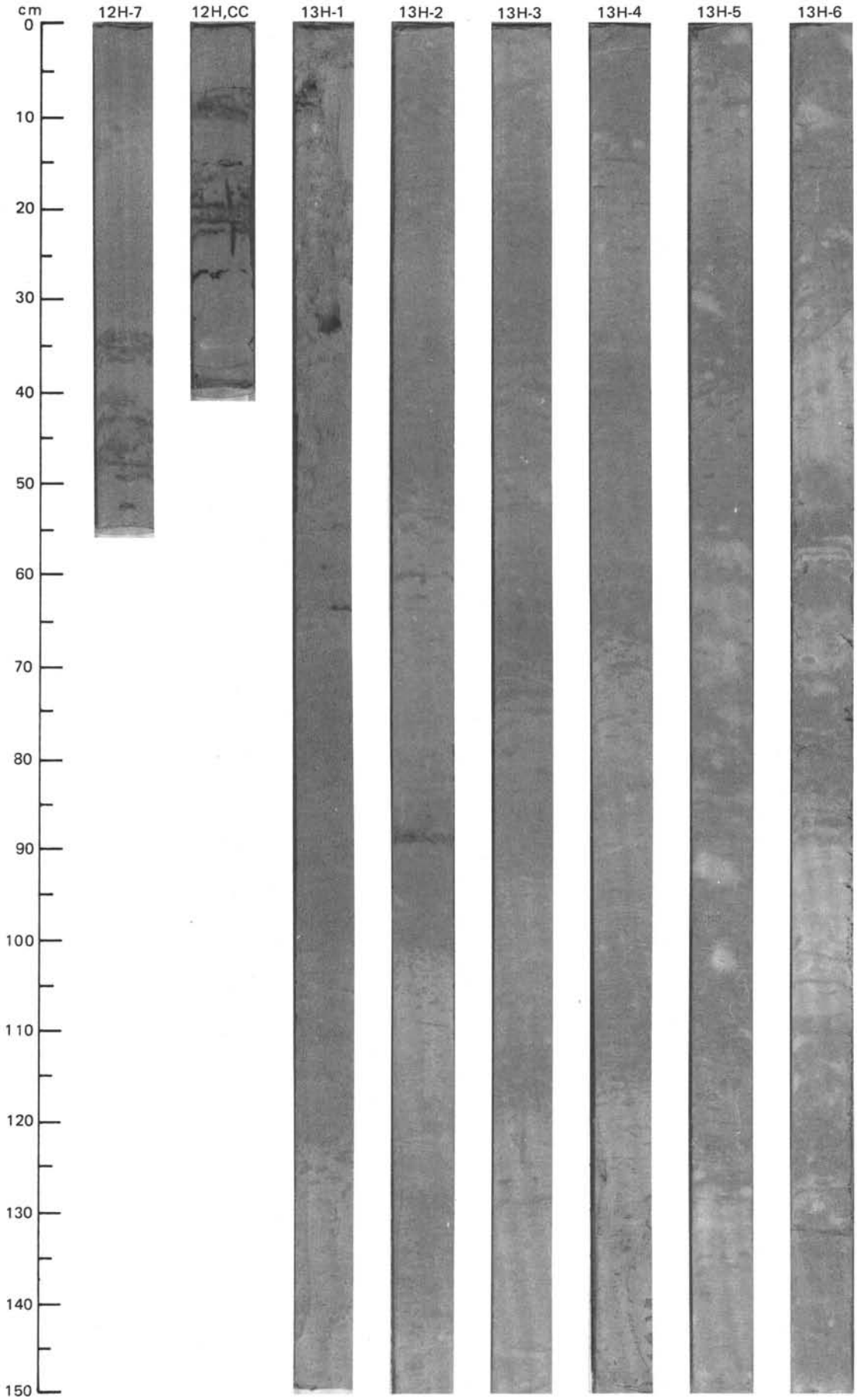
cm
0
10
20
30
40
50
60
70
80
90
100
110
120
130
140
150
12H-7
12H,CC
13H-1
13H-2
13H-3
13H-4
13H-5
13H-6

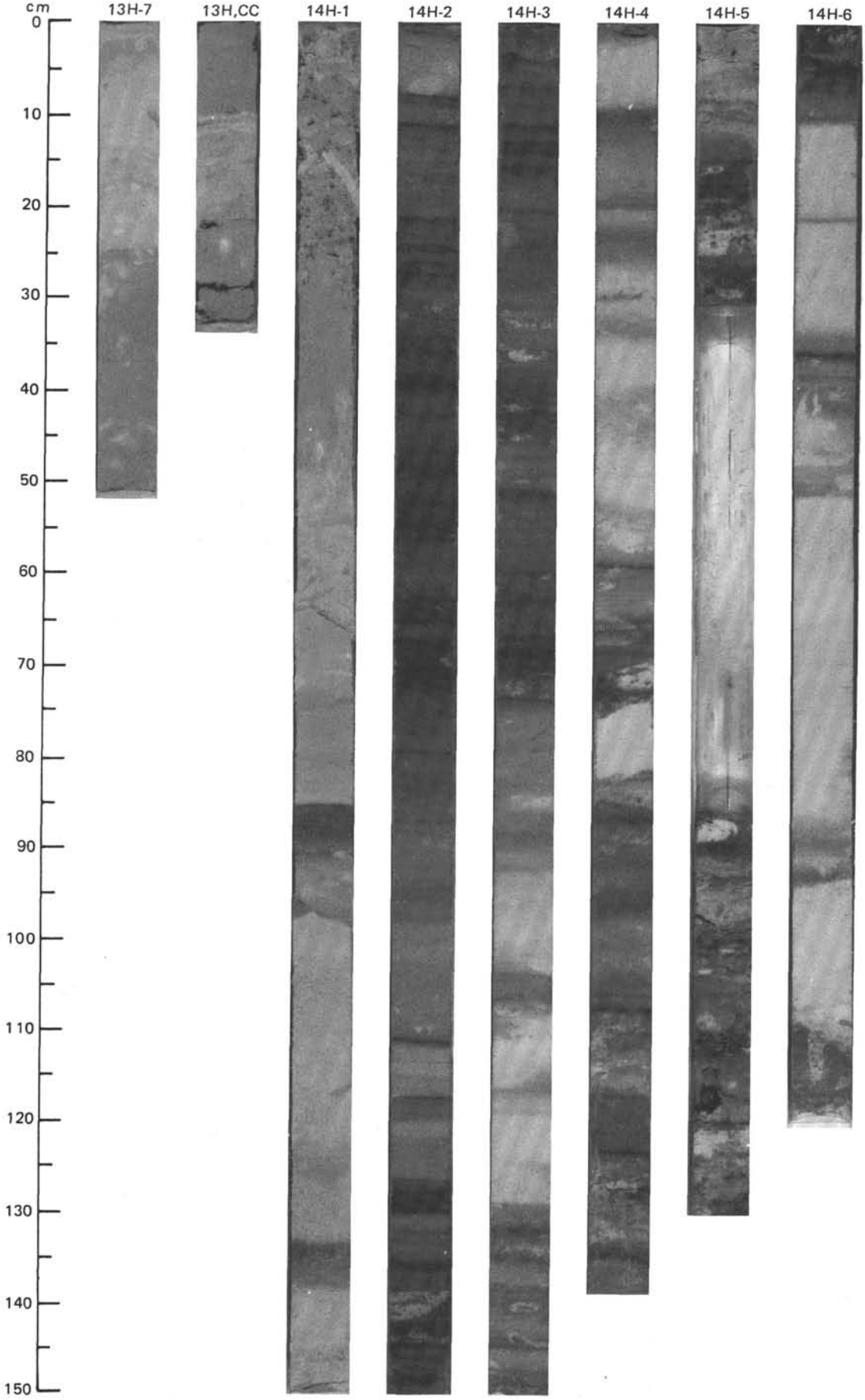
cm
0
10
20
30
40
50
60
70
80
90
100
110
120
130
140
150
13H-7
13H,CC
14H-1
14H-2
14H-3
14H-4
14H-5
14H-6

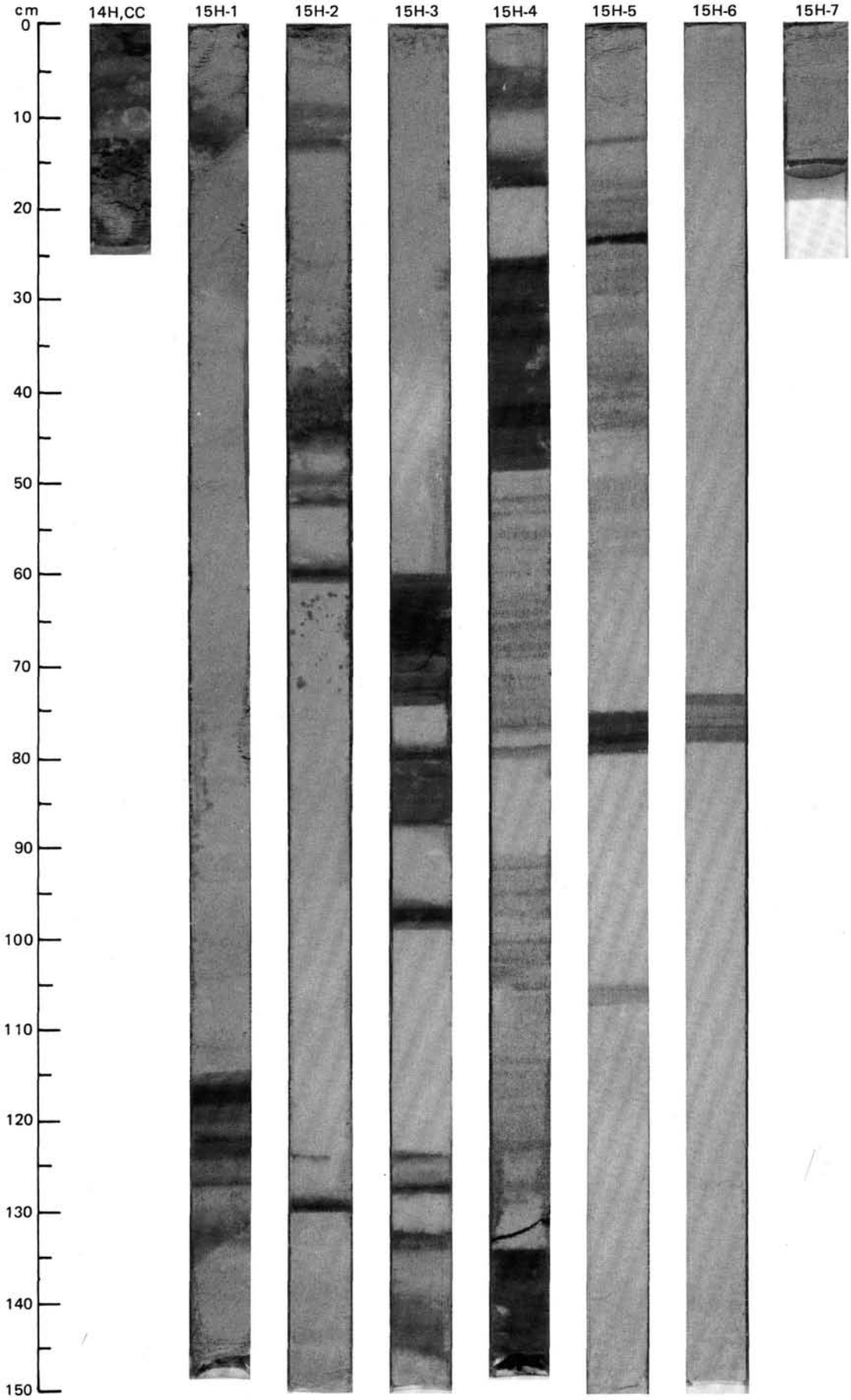
cm
0
10
20
30
40
50
60
70
80
90
100
110
120
130
140
150
14H,CC
15H-1
15H-2
15H-3
15H-4
15H-5
15H-6
15H-7

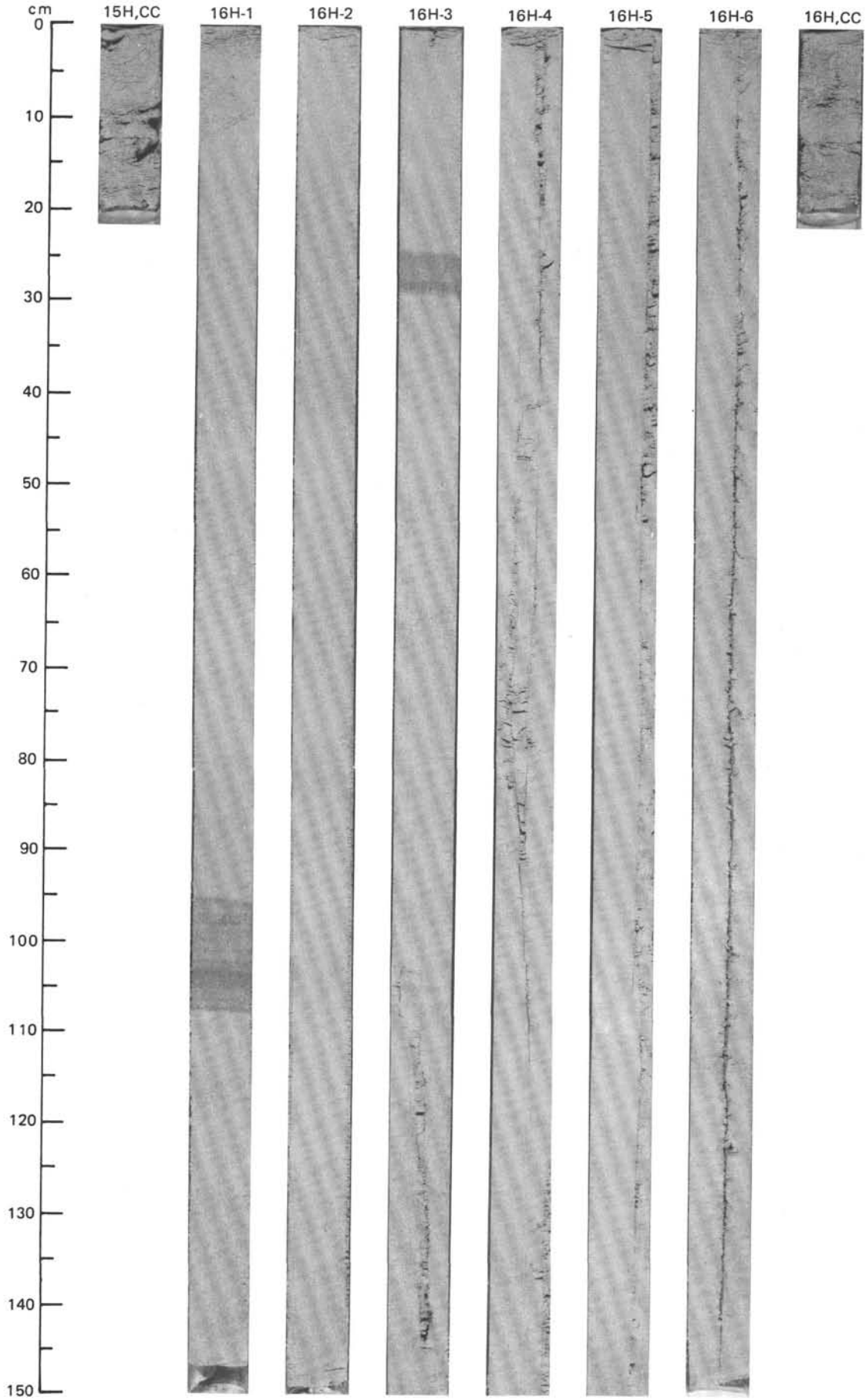
cm
0
10
20
30
40
50
60
70
80
90
100
110
120
130
140
150
15H,CC
16H-1
16H-2
16H-3
16H-4
16H-5
16H-6
16H,CC

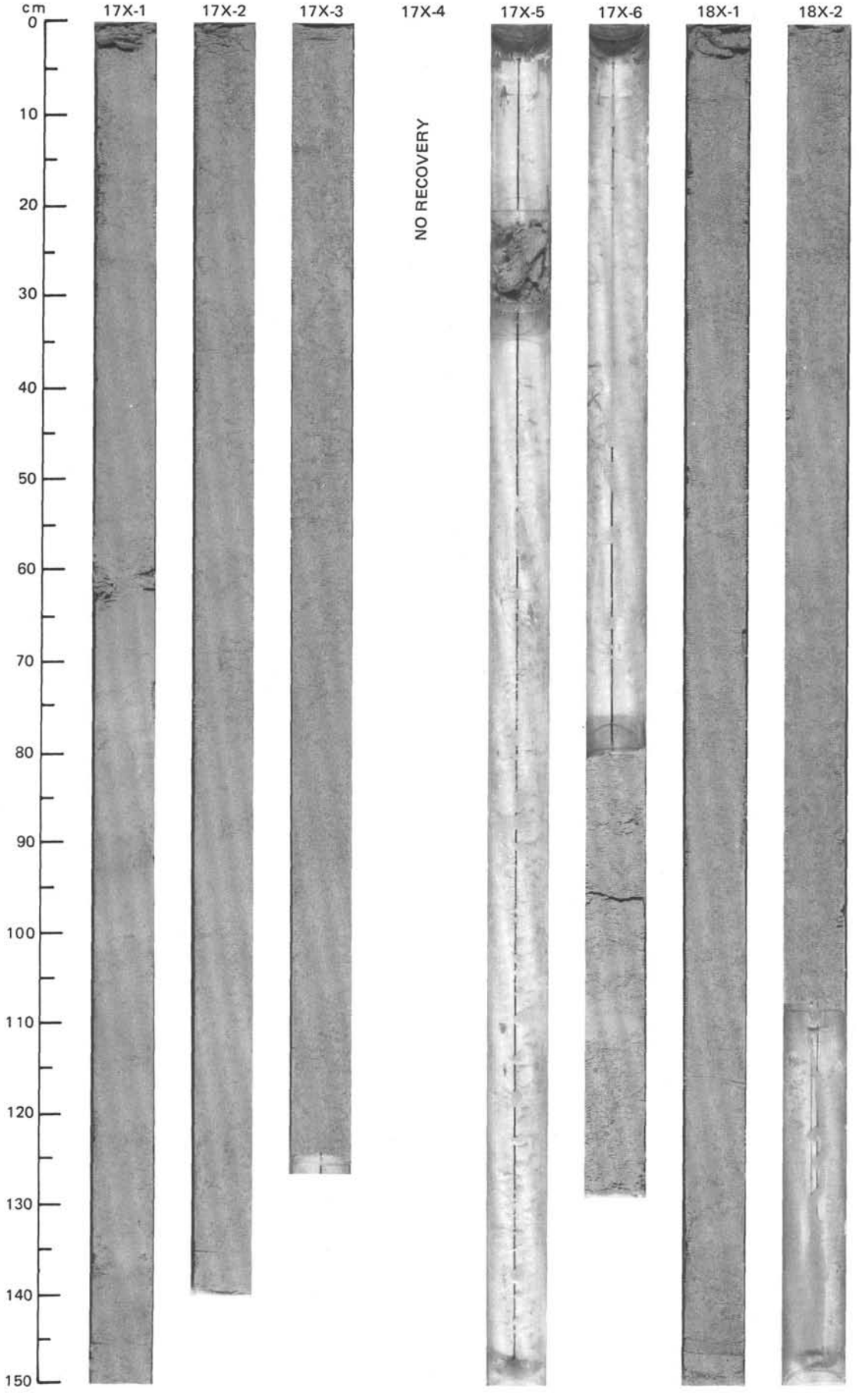
cm
0
10
20
30
40
50
60
70
80
90
100
110
120
130
140
150
17X-1
17X-2
17X-3
17X-4
NO RECOVERY
17X-5
17X-6
18X-1
18X-2

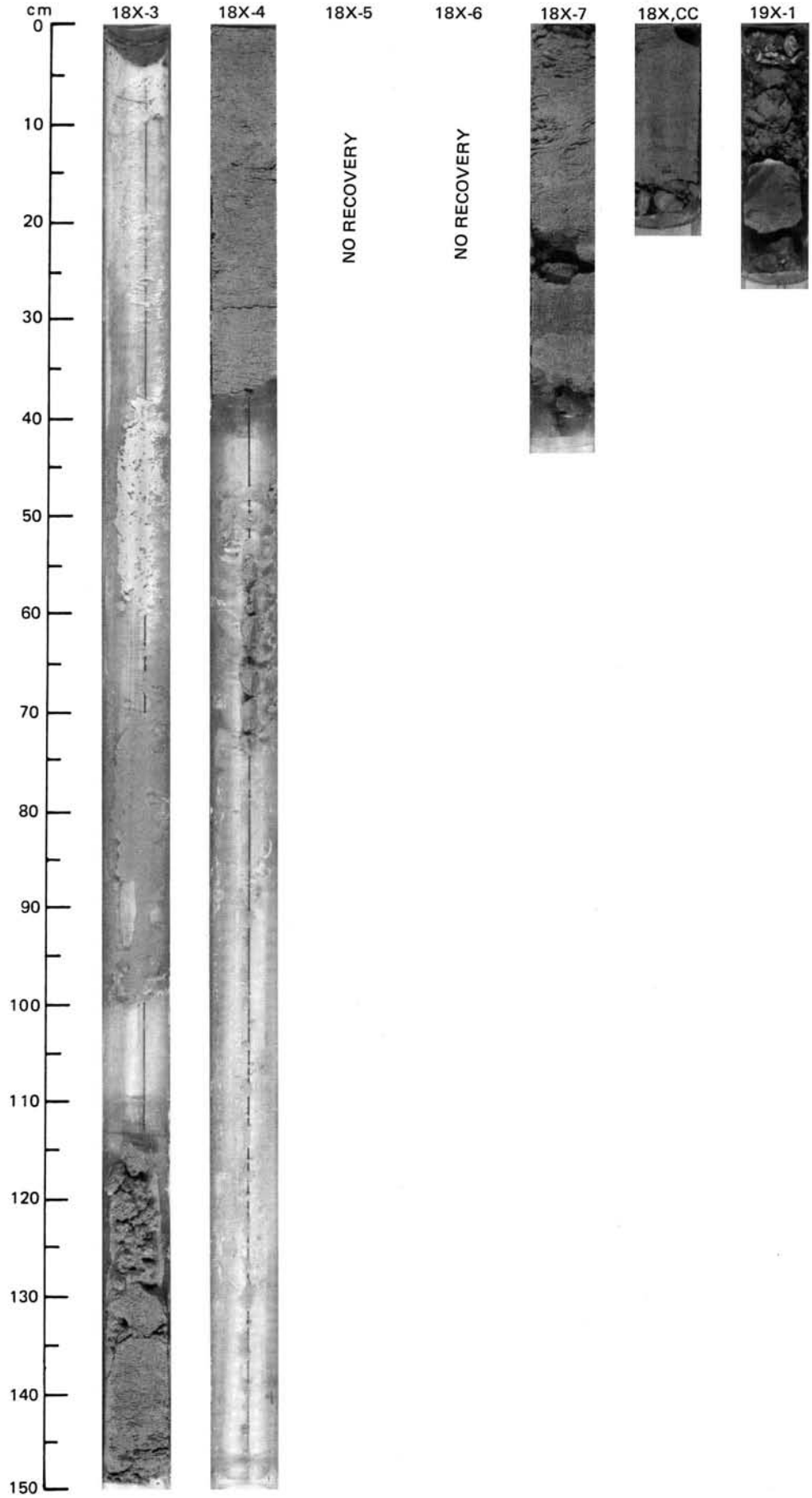
cm
0
10
20
30
40
50
60
70
80
90
100
110
120
130
140
150
18X-3
18X-4
18X-5
NO RECOVERY
18X-6
NO RECOVERY
18X-7
18X,CC
19X-1

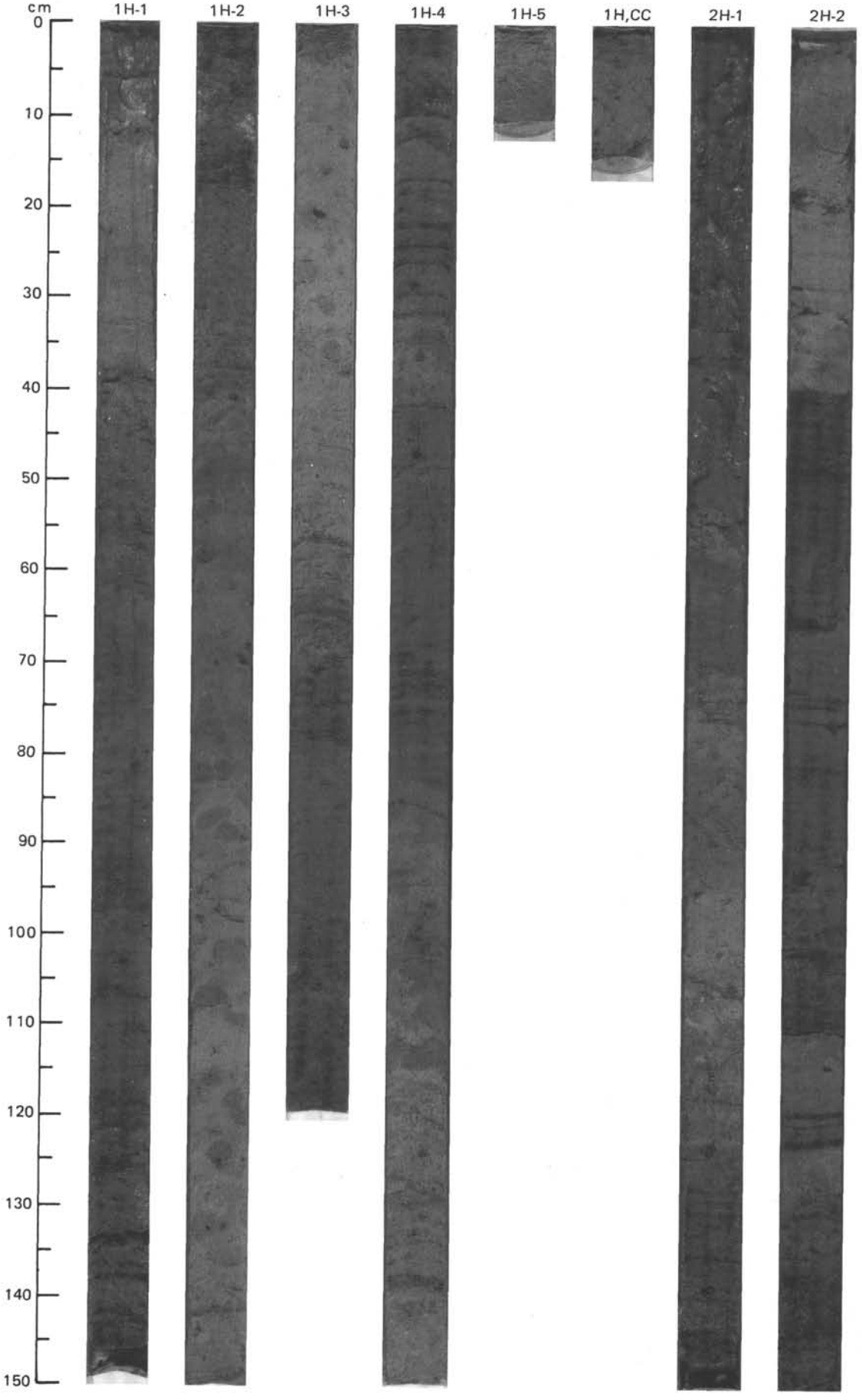
cm
1H-1
1H-2
1H-3
1H-4
1H-5
1H,CC
2H-1
2H-2
0
10
20
30
40
50
60
70
80
90
100
110
120
130
140
150

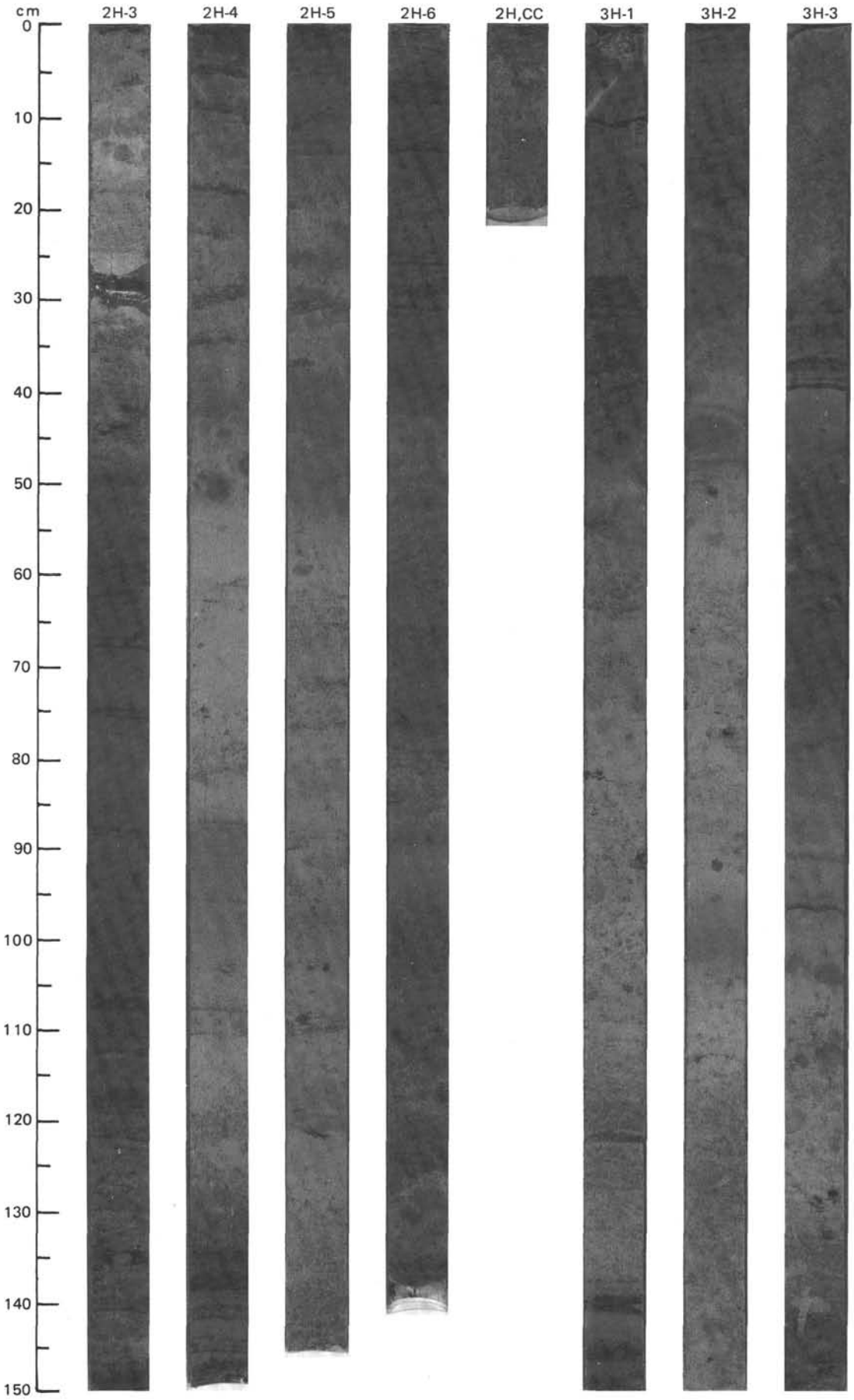
cm
2H-3
2H-4
2H-5
2H-6
2H,CC
3H-1
3H-2
3H-3
0
10
20
30
40
50
60
70
80
90
100
110
120
130
140
150

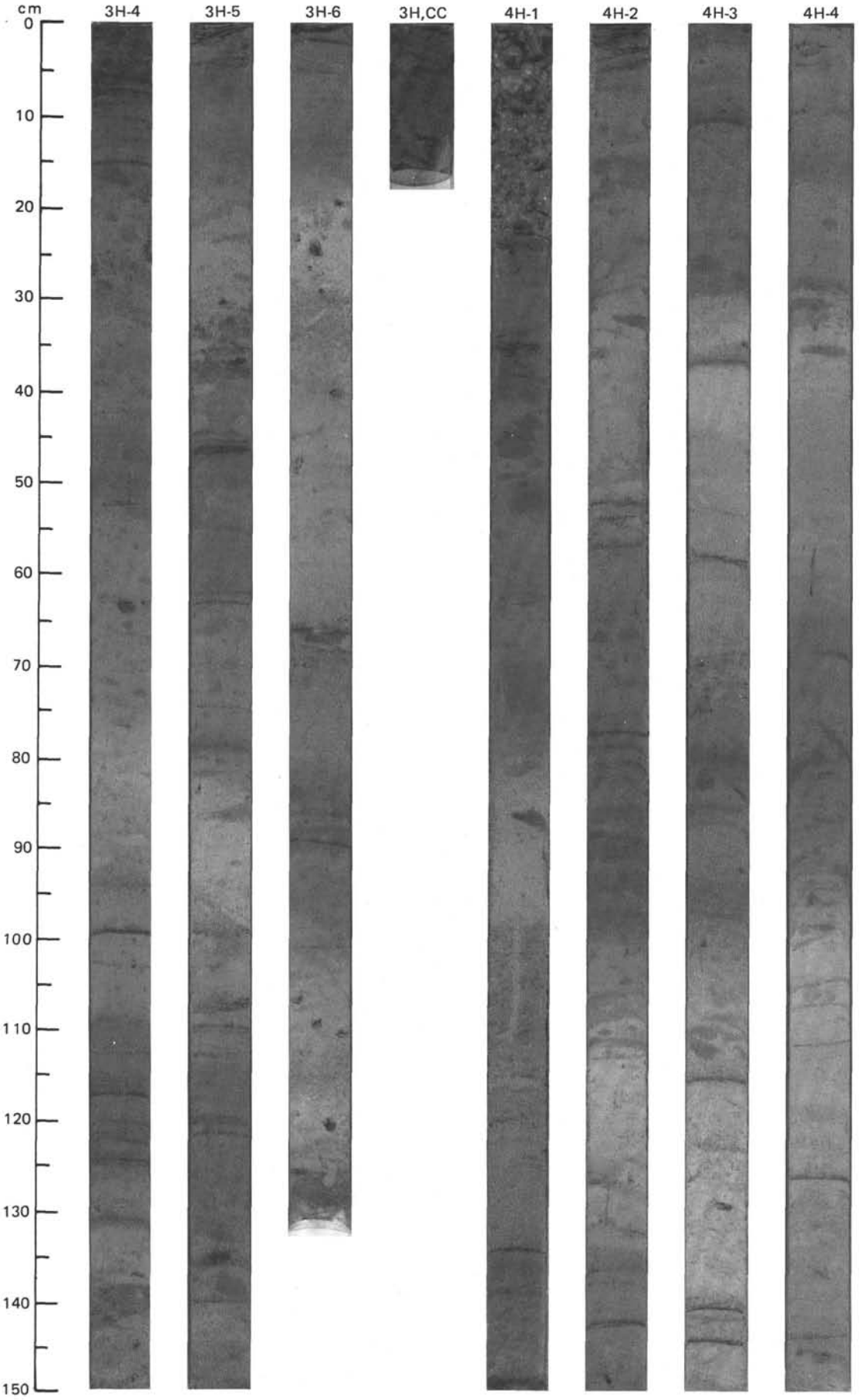
cm
0
10
20
30
40
50
60
70
80
90
100
110
120
130
140
150
3H-4
3H-5
3H-6
3H,CC
4H-1
4H-2
4H-3
4H-4

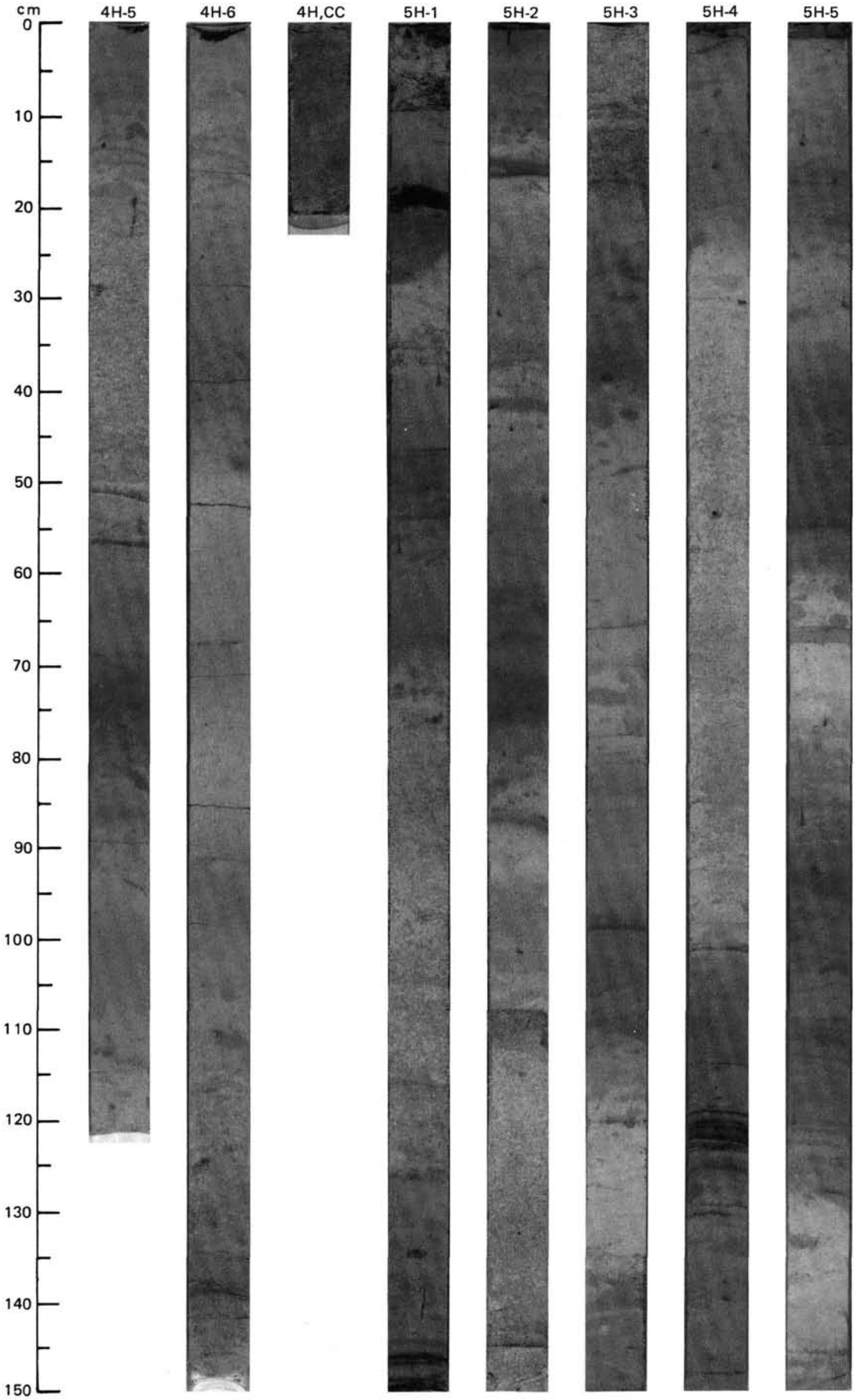
cm
4H-5
4H-6
4H,CC
5H-1
5H-2
5H-3
5H-4
5H-5
0
10
20
30
40
50
60
70
80
90
100
110
120
130
140
150

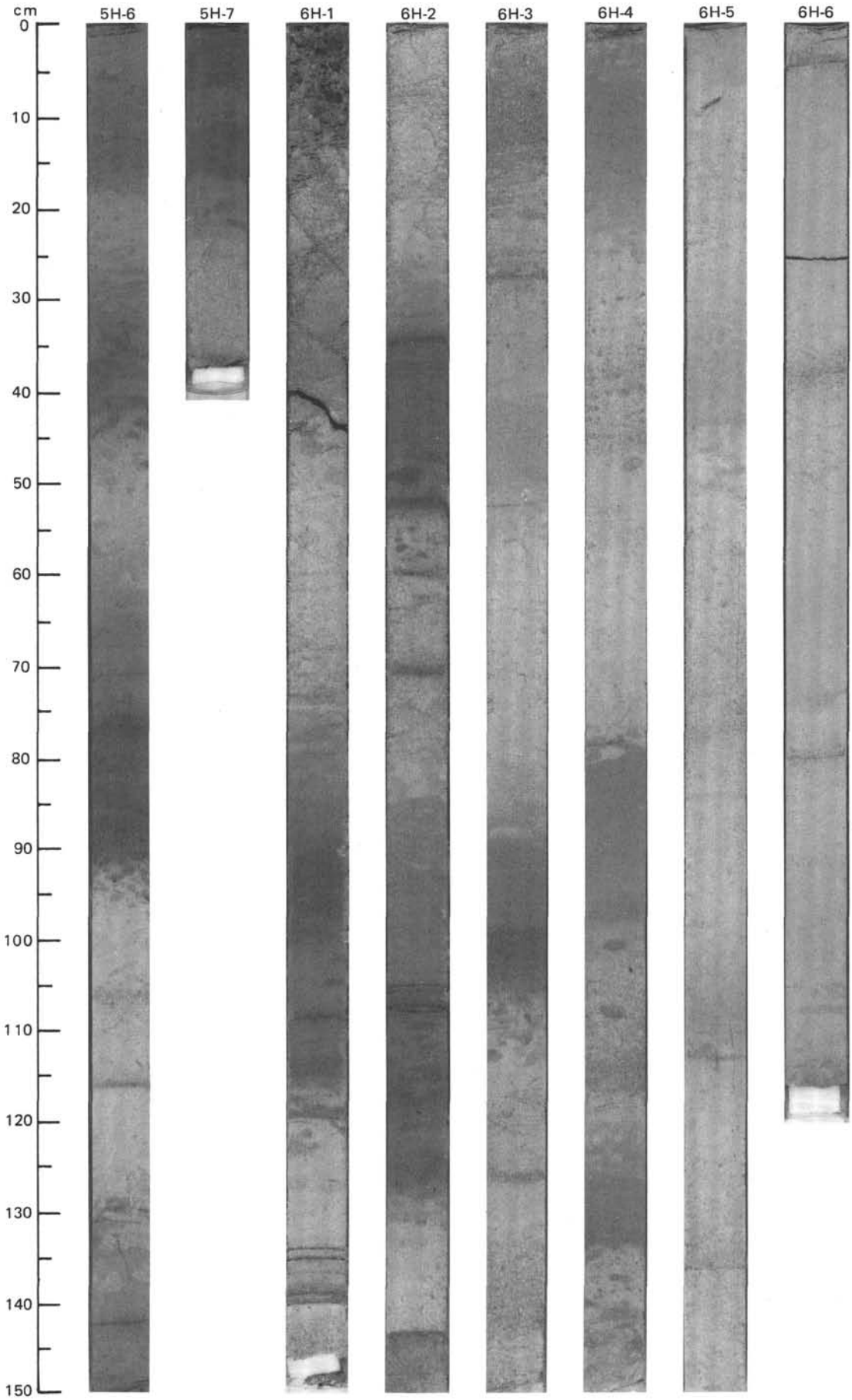
cm
5H-6
5H-7
6H-1
6H-2
6H-3
6H-4
6H-5
6H-6
0
10
20
30
40
50
60
70
80
90
100
110
120
130
140
150

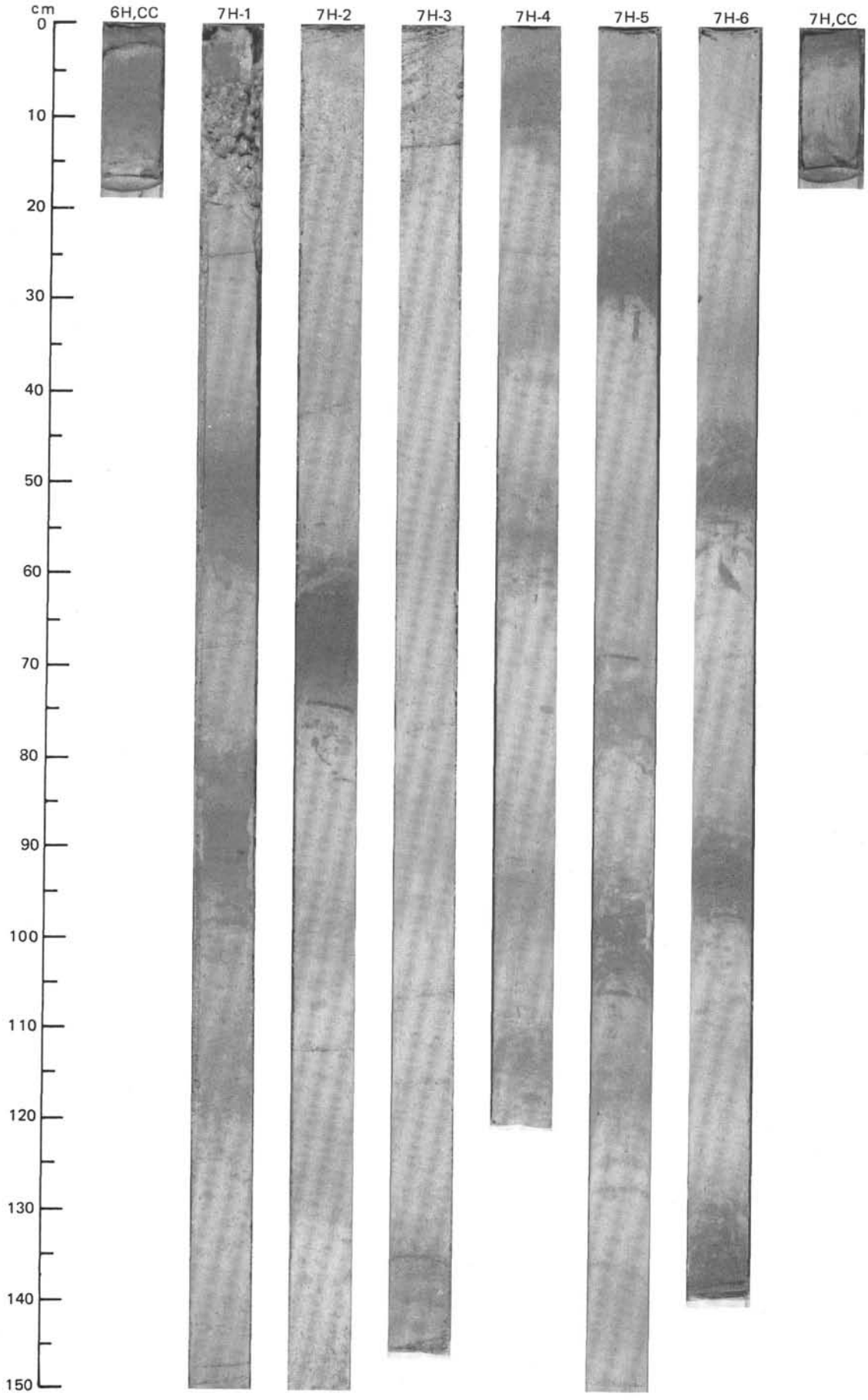
cm
0
10
20
30
40
50
60
70
80
90
100
110
120
130
140
150
6H,CC
7H-1
7H-2
7H-3
7H-4
7H-5
7H-6
7H,CC

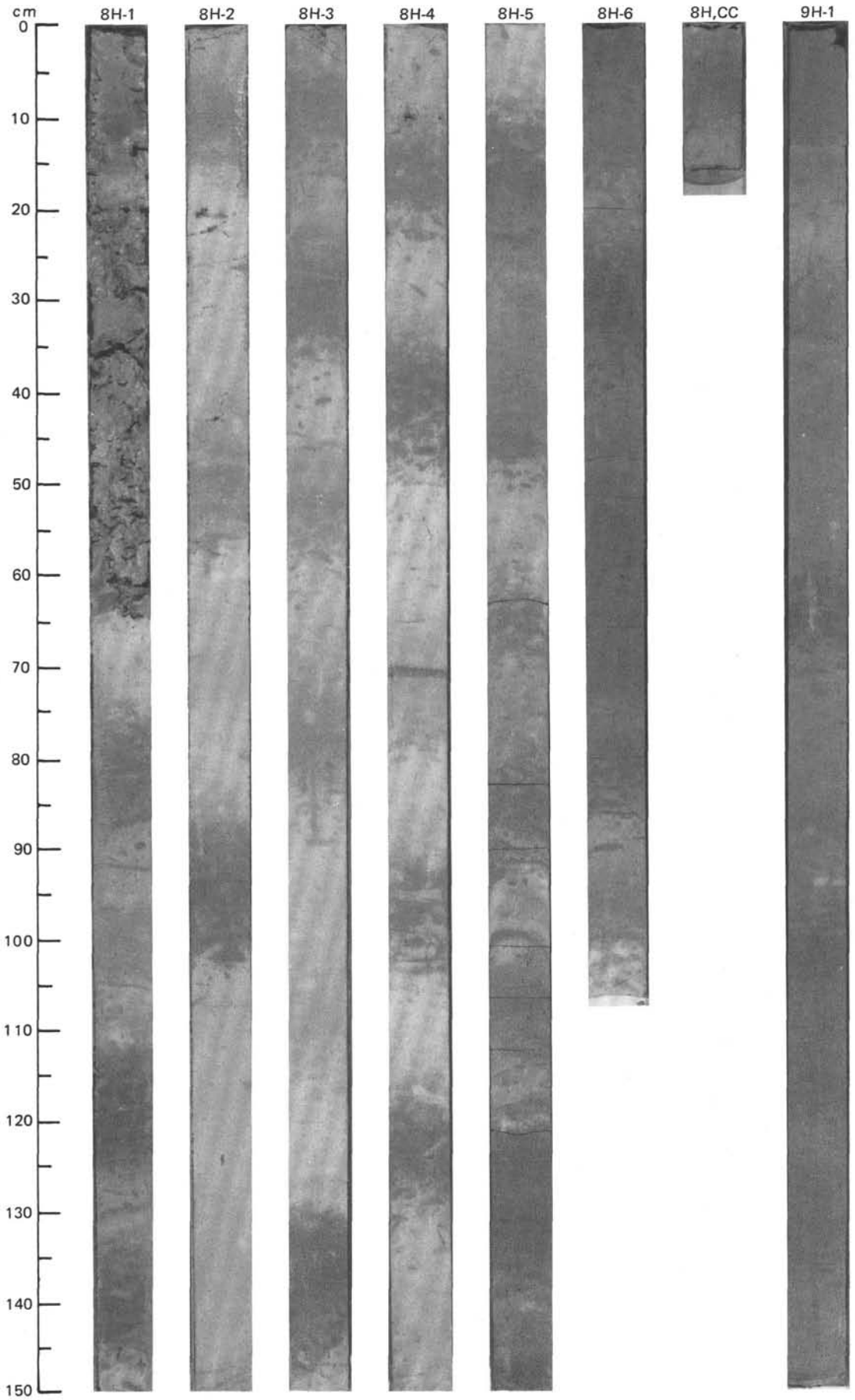
cm
0
10
20
30
40
50
60
70
80
90
100
110
120
130
140
150
8H-1
8H-2
8H-3
8H-4
8H-5
8H-6
8H,CC
9H-1

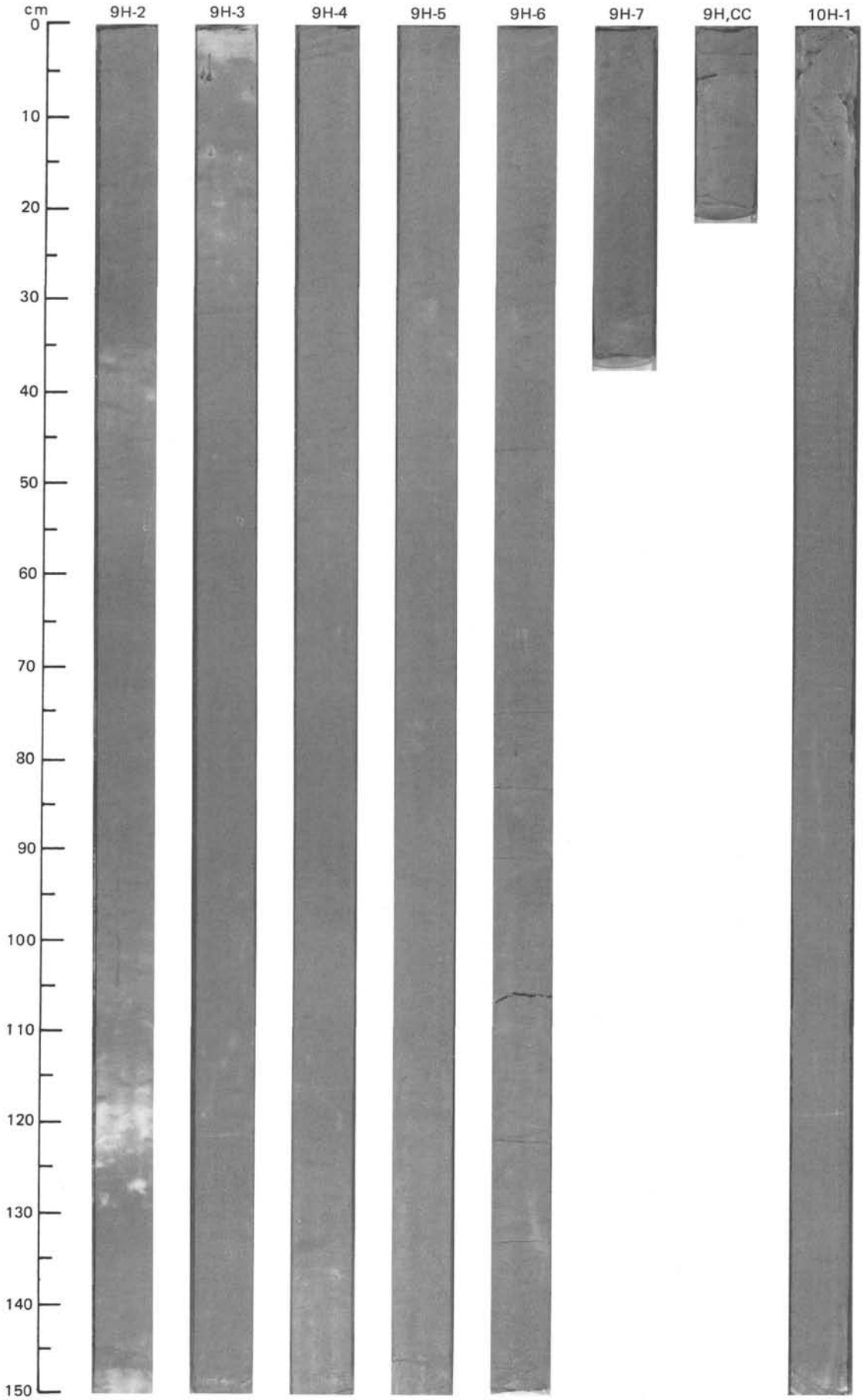
cm
9H-2
9H-3
9H-4
9H-5
9H-6
9H-7
9H,CC
10H-1
0
10
20
30
40
50
60
70
80
90
100
110
120
130
140
150

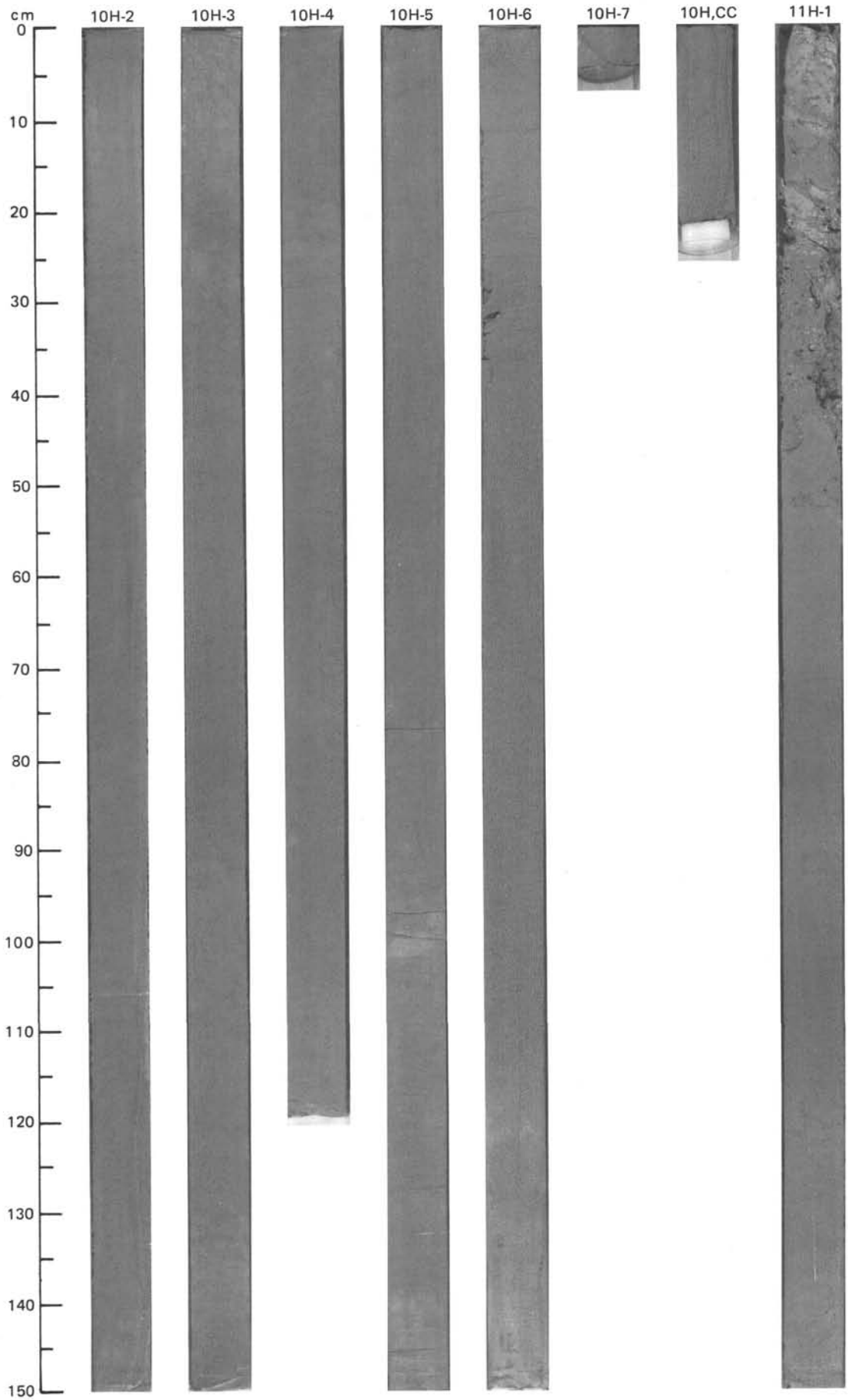
cm
0
10
20
30
40
50
60
70
80
90
100
110
120
130
140
150
10H-2
10H-3
10H-4
10H-5
10H-6
10H-7
10H,CC
11H-1

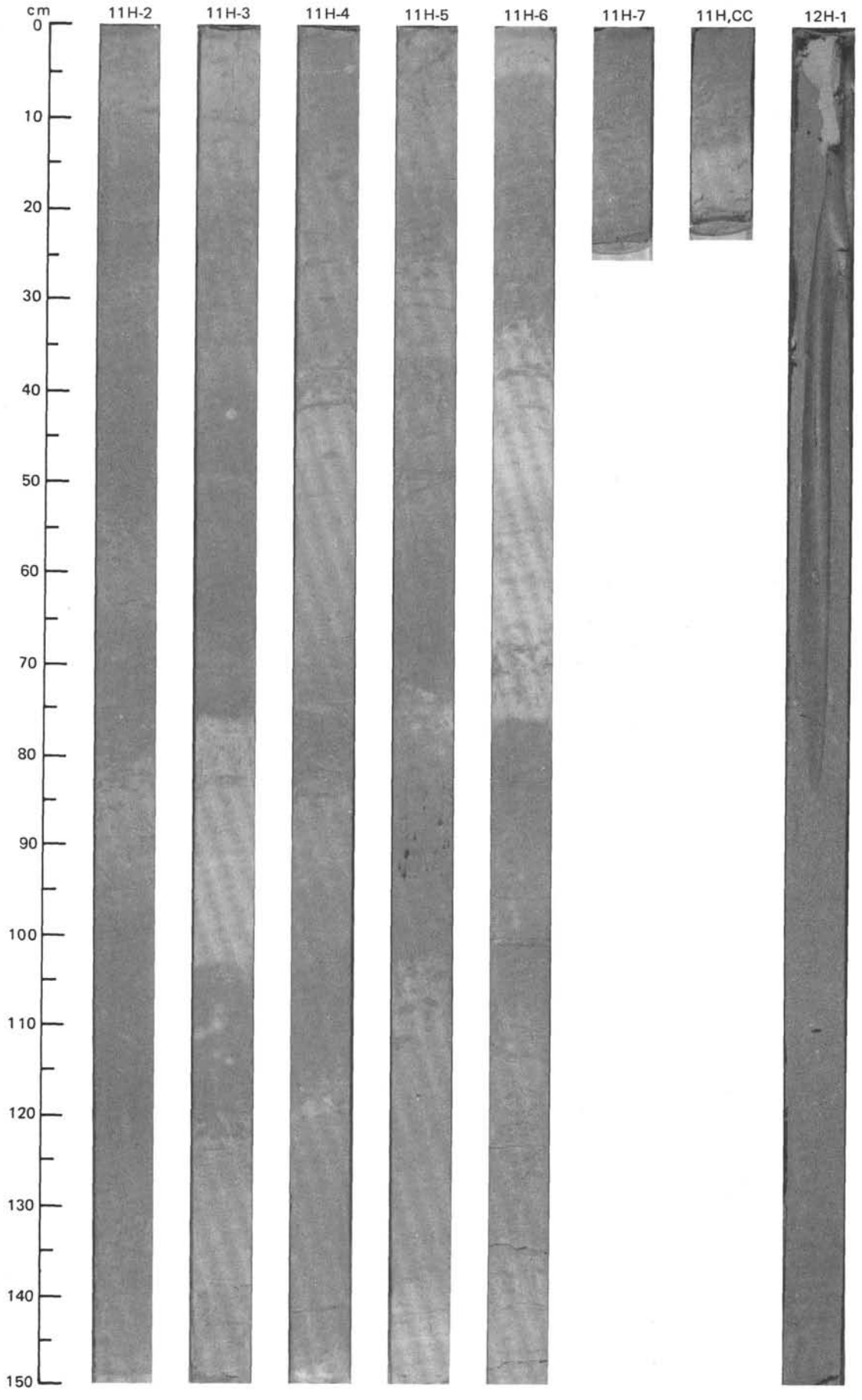
cm
0
10
20
30
40
50
60
70
80
90
100
110
120
130
140
150
11H-2
11H-3
11H-4
11H-5
11H-6
11H-7
11H,CC
12H-1

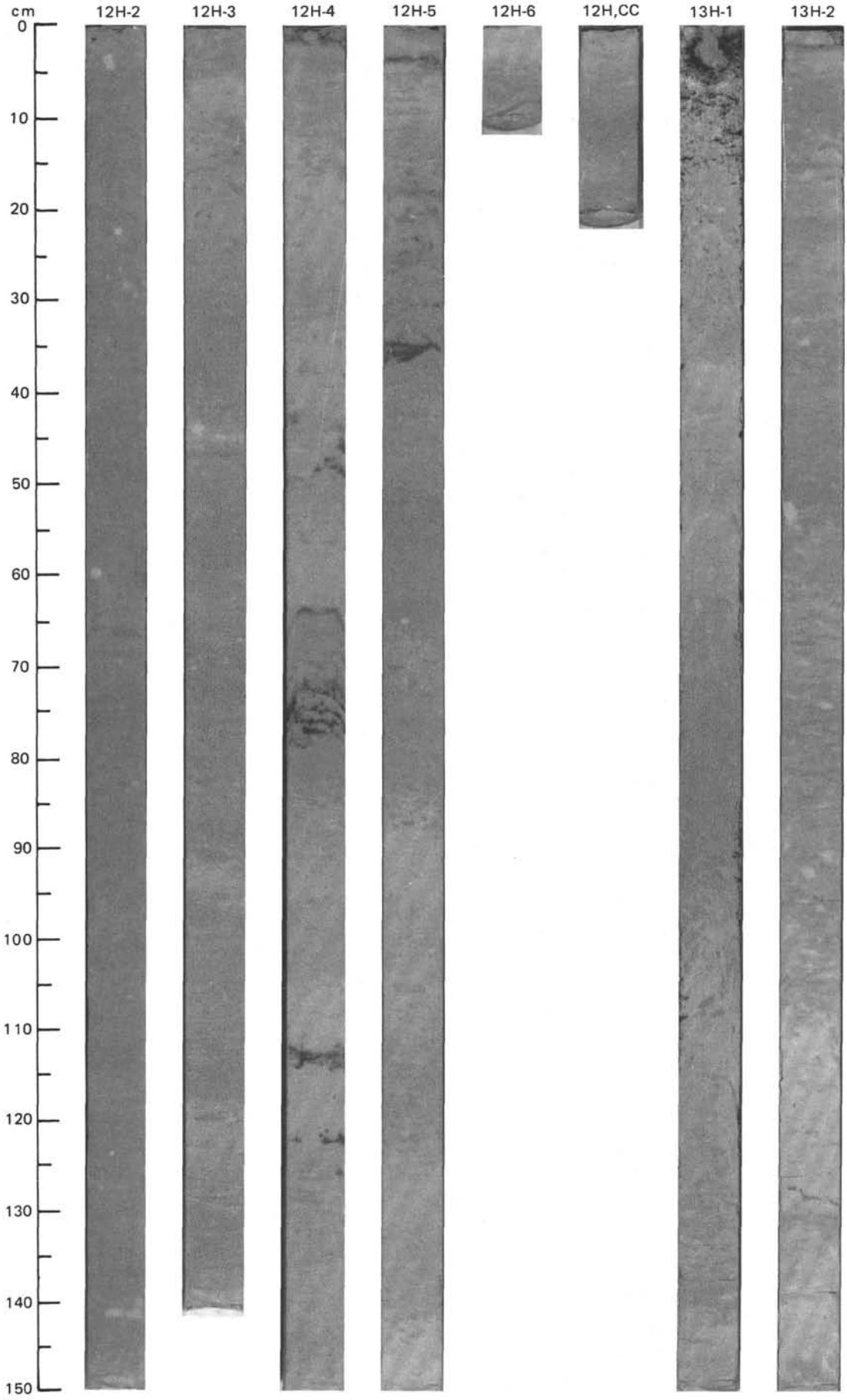
cm
12H-2
12H-3
12H-4
12H-5
12H-6
12H,CC
13H-1
13H-2
0
10
20
30
40
50
60
70
80
90
100
110
120
130
140
150

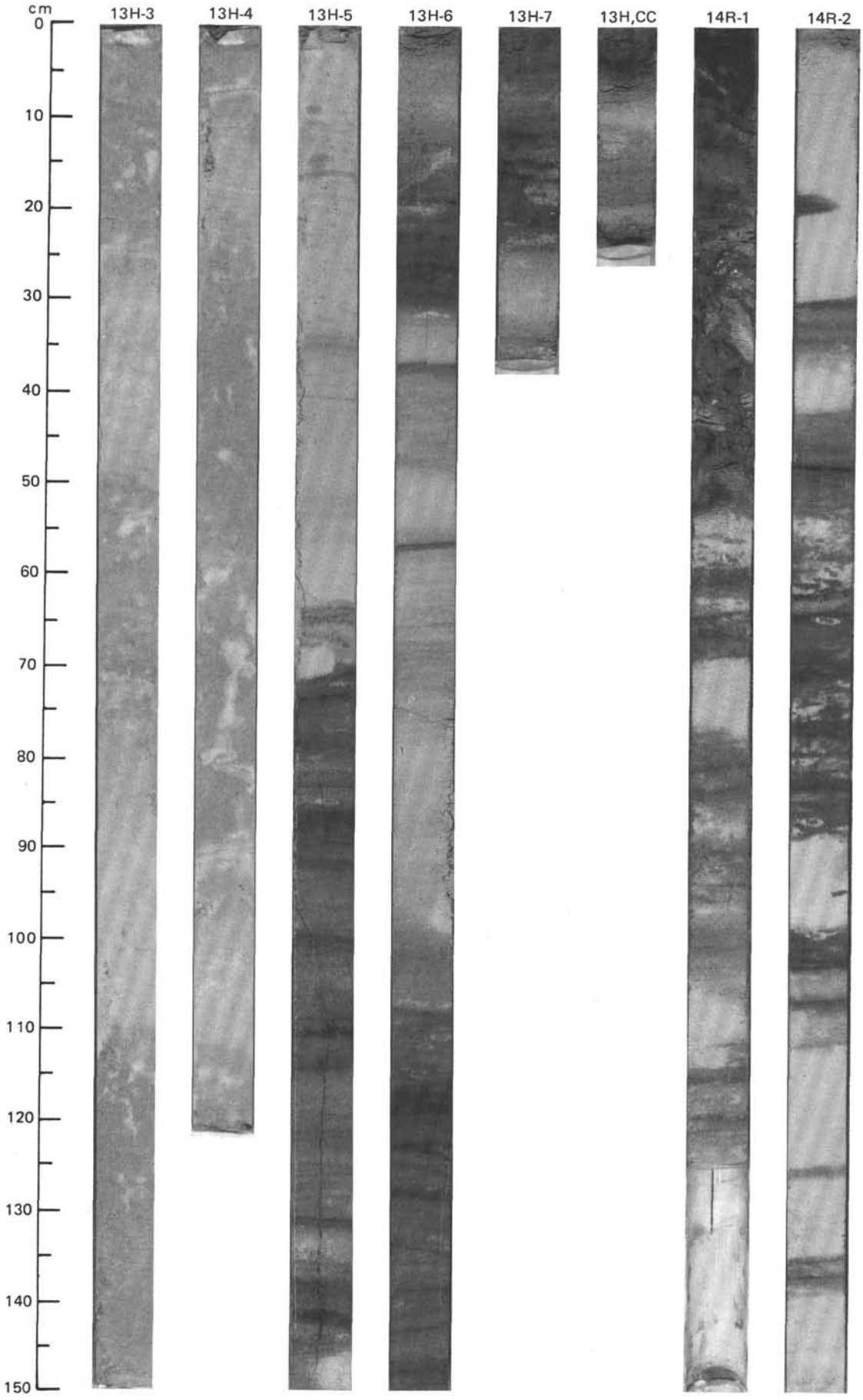
cm
0
10
20
30
40
50
60
70
80
90
100
110
120
130
140
150
13H-3
13H-4
13H-5
13H-6
13H-7
13H,CC
14R-1
14R-2

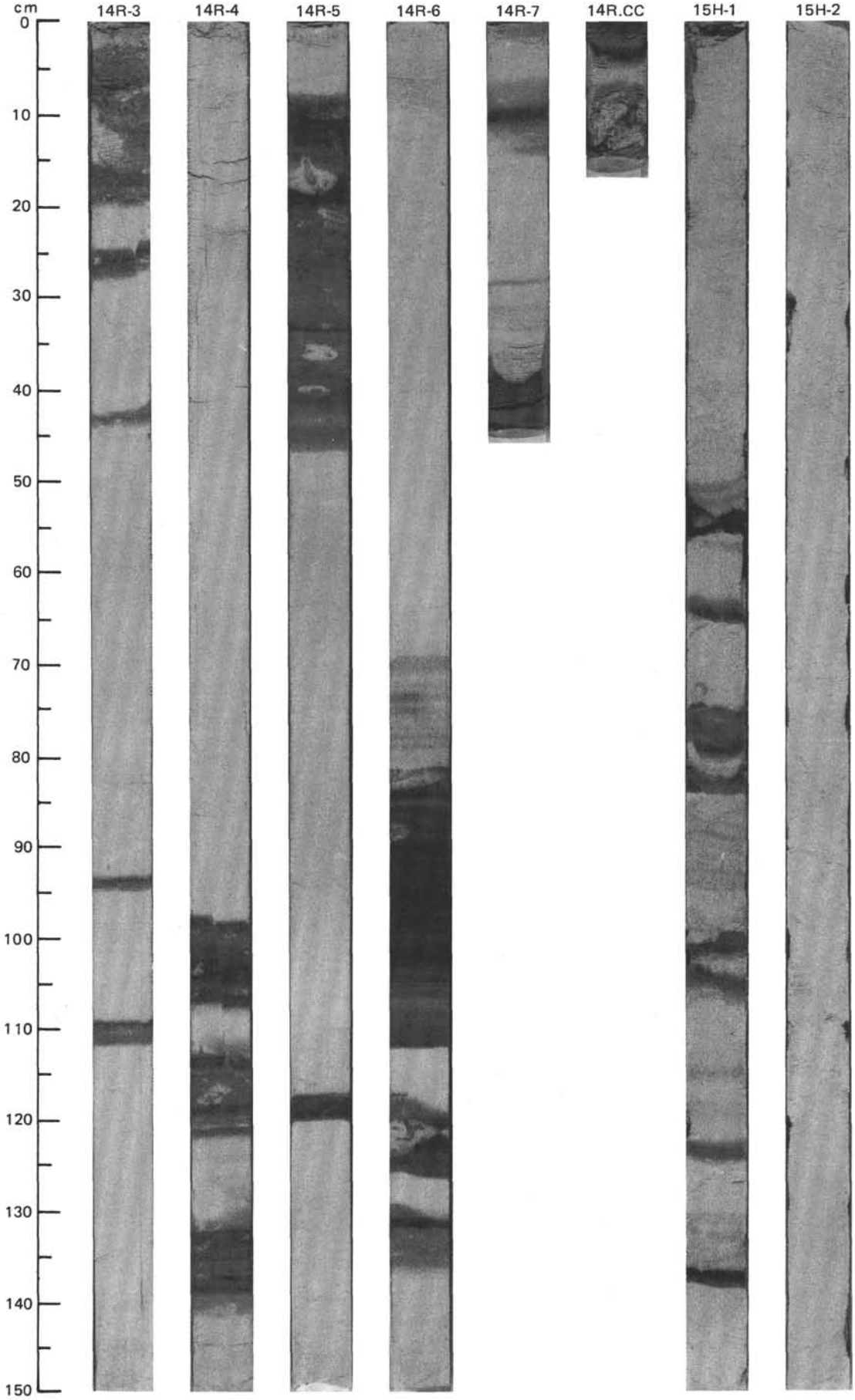
cm
14R-3
14R-4
14R-5
14R-6
14R-7
14R.CC
15H-1
15H-2
0
10
20
30
40
50
60
70
80
90
100
110
120
130
140
150

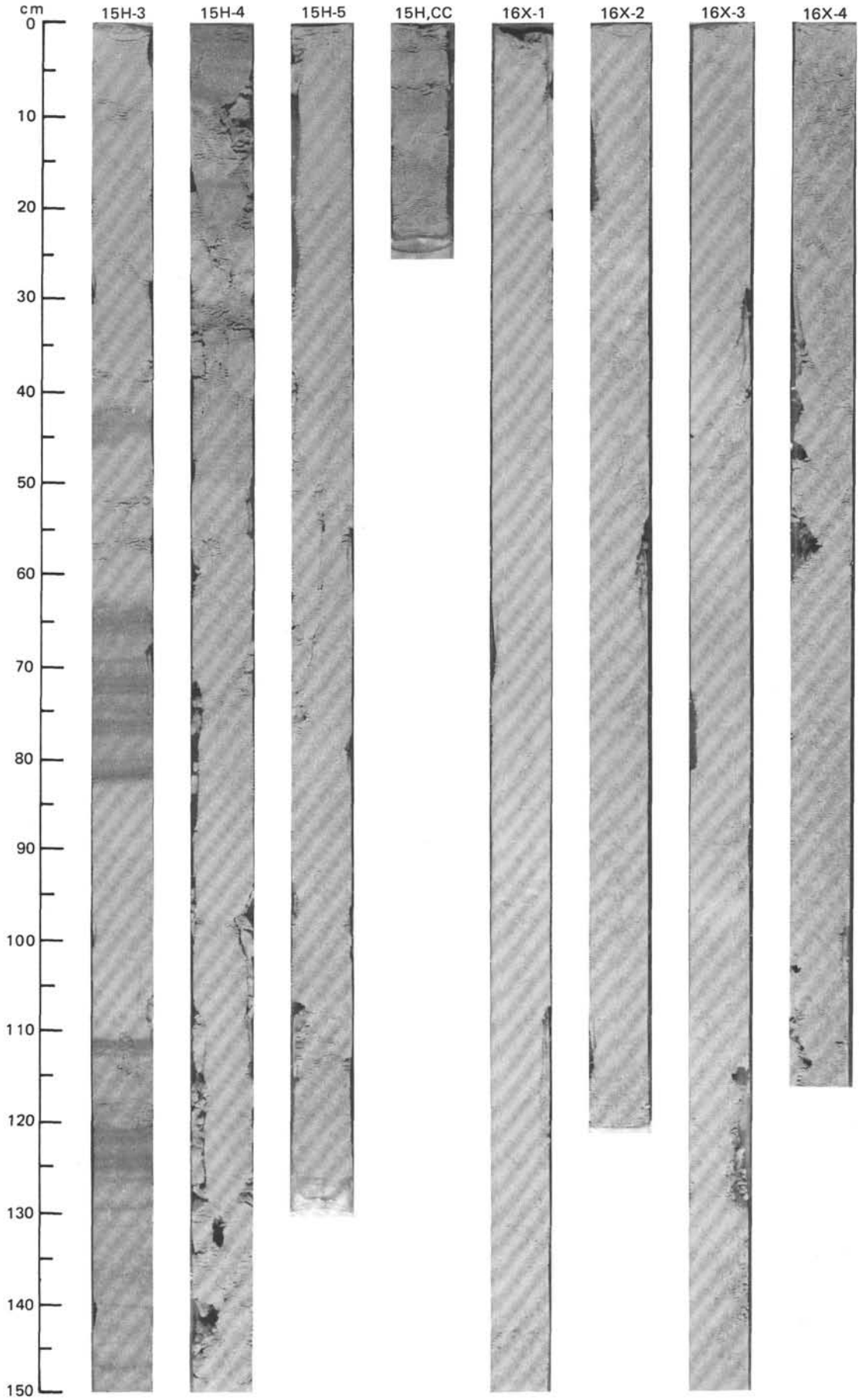
cm
0
10
20
30
40
50
60
70
80
90
100
110
120
130
140
150
15H-3
15H-4
15H-5
15H,CC
16X-1
16X-2
16X-3
16X-4

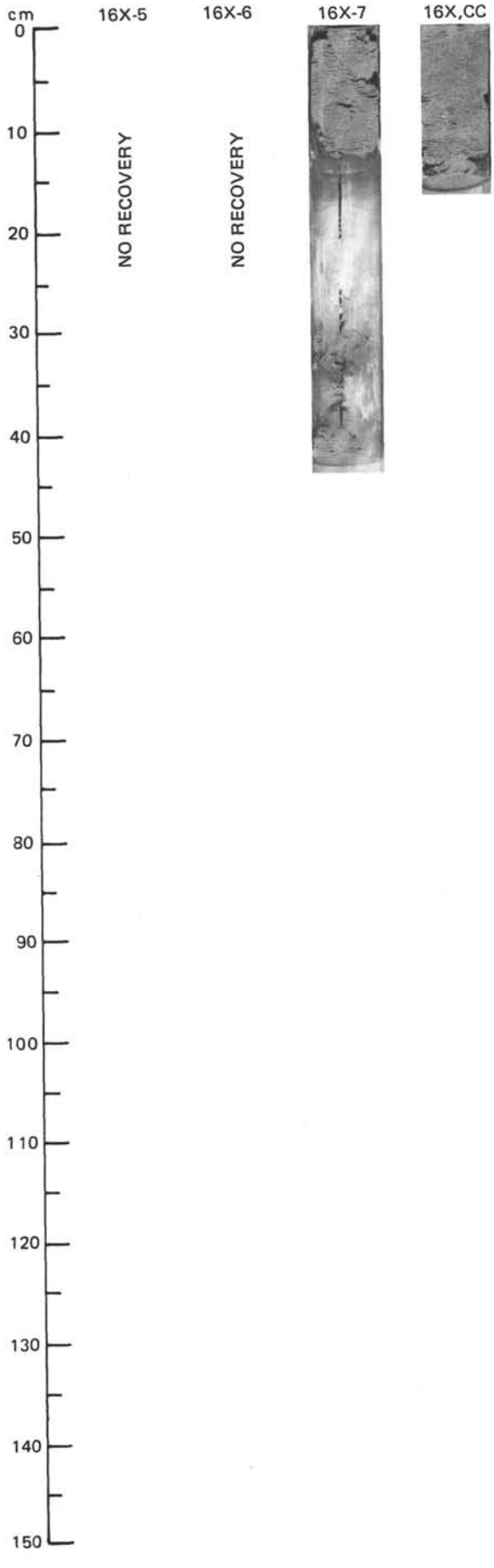
cm
16X-5
16X-6
16X-7
16X,CC
0
10
20
30
40
50
60
70
80
90
100
110
120
130
140
150
NO RECOVERY
NO RECOVERY